ACOUSTICALLY EXCITED VIBRATIONS OF SANDWICH PLATES

by

A.J. Pretlove, B.Sc.

Thesis submitted for the degree

of Doctor of Philosophy

April, 1963

University of Southampton
Department of Aeronautics and Astronautics

SUMMARY

A study is made of the bond stress in a honeycomb sandwich panel excited by random noise pressures.

The bond stresses (normal to the plate stress and bending stress), as the most important response quantities, are assumed to consist of a sum of stresses in the principal modes. These two stresses are found to be similar in magnitude. A Fourier analysis is used to evaluate the mean square stresses. Large stresses are seen to occur when the panel is excited at the double resonance known as 'acoustical coincidence'.

Principal modes and natural frequencies are evaluated for flat and cylindrically curved sandwich panels by a consideration of the dynamic equilibrium of the three components of the sandwich. An expected anomalous frequency variation with circumferential wavelength is found for the curved panels for certain wavelength regions.

Experiments which have confirmed the theory for bond stress by verifying a similar theory for surface strain using strain gauges on a simply supported sandwich panel excited in a random siren tunnel are described.

Experiments which have been carried out to determine the fatigue characteristics of Redux bonding are also described.

CONTENTS

		Page
Introduction		1
Chapter One: A Natural Mode Analysis for the Vibrations of Cylindrically Curved Elastic Sandwich Plates		7
1.1 Introduction		8
1.2 The Nature of the Possible First-Order Modes of Vibration of a Flat Finite Rectangular Elastic Sandwich Plate, Simply-Supported at its Edges ...		13
1.2.1	Anti-Symmetric Modes	13
1.2.1.1	The Flexural Mode	13
1.2.1.2	Thickness-Shear Modes	14
1.2.2	Symmetric Modes	14
1.2.2.1	The Bubbling Mode	15
1.2.2.2	Longitudinal Modes	15
1.2.3	A Note Concerning the Modes of Cylindrically Curved Sandwich Plates ...	16
1.3 A Summary of Assumptions Commonly made in Elastic Sandwich Theories		16
1.3.1	Plane Strain	16
1.3.2	Planar and Linear Deformation	17
1.3.3	Zero Transverse Shear Strain in the Face Plates	18
1.3.4	Zero Rotatory Inertia	18
1.3.5	Zero Flexural Rigidity of the Face-Plates about their own Middle Plane ...	18
1.3.6	Different Modes of Vibration of the same order are not Coupled	19
1.3.7	Homogeneous Core	20
1.3.8	The Assumptions of an Isotropic Core ...	20
1.4 A Review of Previous Work on the Analysis of Elastic Sandwich Plates		21
1.4.1	Bending and Buckling Theories	21
1.4.2	Vibration Theories	22

1.5 The Analysis of the Vibrations of Cylindrically Curved Sandwich Plates 29

1.5.1 Sandwich Plate Core Equations 29
1.5.1.1 Stress-Strain Equations for an Anisotropic Homogeneous Medium 29
1.5.1.2 Equilibrium Relationships 31
1.5.1.3 Strain-Displacement Relationships 32
1.5.1.4 Overall Core Equilibrium Equations ... 32
1.5.2 The Equilibrium of the Face-Plates ... 33
1.5.2.1 Equilibrium Parallel to the Face Surface 33
1.5.2.2 Equilibrium Normal to the Face Surface 36
1.5.3 The Differential Equations of Harmonic Vibration of Cylindrically Curved Honeycomb Cored Elastic Sandwich Plates 39

1.6 Solutions of the Equations Listed in § 1.5.3 ... 40

1.6.1 A Separable Form of Solution for Curved Panels 40
1.6.2 A Solution for Flat Panels 42
1.6.2.1 A Solution for Flexural Modes of Flat Panels Ignoring Rotatory Inertia 44
1.6.2.2 A Solution for Bubbling Modes of Flat Panels 48
1.6.2.3 Flat Panel Thickness Shear and Longitudinal Modes 51
1.6.3 A Solution for Cylindrically Curved Panels 51

1.7 Conclusions 59

Chapter Two: The Acoustic Excitation of Flat Rectangular Sandwich Plates 64

2.1 Introduction 64

2.2 Mathematical Analyses of the Problem 69

2.2.1 The Possibility of Excitation of Flat Finite Sandwich Panels by the Acoustical Coincidence Effect 69
2.2.2 An Analysis of the Bond Normal Stress (σ_z) for a Sandwich Panel Excited by a General Acoustic Pressure Field 73
2.2.2.1 Derivation of the Power Spectrum of Bond Normal Stress 75
2.2.2.2 Derivation of the Mean Square Value of Bond Normal Stress 85
2.2.3 A Restriction of the General Acoustic Field to Random Plane Waves of a Fixed Incidence 93

2.2.3.1 A Comment on the 'Joint Magnification Factor', L_{ℓ} ... 101
2.2.4 A Restriction of the General Acoustic Field to Normal Incidence Random Plane Waves ... 105
2.2.5 An Analysis of the Mean Square Bending Stress in the Bond of a Simply Supported Sandwich Panel when under Excitation by Normal Acoustic Plane Waves ... 109

2.3 General Remarks ... 116

A.2.1 A Magnitude Comparison of the Normal Direct Stress and the Bending Stress in the Bond of a Sandwich Beam Vibrating Freely in a Single Flexural Mode 121

A.2.2 Two Codes of Fourier Transform Notation used in the Analysis of Random Processes ... 123

A.2.3 A Note on Acoustic Radiation and Reaction Forces (Damping and Virtual Mass) ... 125

A.2.4 Evaluation of the Integral of Equation 2.33 for Random Plane Waves at a Fixed Incidence ... 132

A.2.5 The Integrals $I_{c_{rr}}$, $I_{s_{rr}}$, $I_{c_{r\theta r}}$ and $I_{s_{r\theta r}}$ ... 132

Chapter Three: Some Experiments with a Honeycomb Sandwich Panel ... 134

3.1 Introduction ... 134

3.2 The Experimental Equipment ... 135

3.2.1 The Sandwich Panel ... 135
3.2.2 The Panel Simple Supports: Their Development ... 136
3.2.3 The Siren Tunnel ... 138
3.2.4 The Siren Driving Equipment ... 139
3.2.5 Instrumentation ... 139

3.3 Harmonic Excitation of the Panel ... 140

3.3.1 The First Series of Tests ... 140
3.3.2 The Second Series of Tests: Vector Analysis 141

3.4 Random Excitation of the Panel ... 142

3.5 Experimental Results 142

3.5.1 Direct Results 142
3.5.2 Derived Results 143

3.6 The Derivation of Results Given in § 3.5.2 143

3.6.1 Derivation of Plate Modal Characteristics from the Vector Response Diagram 143
3.6.2 Derivation of the Theoretical Values of r.m.s. Strain 145

3.7 Discussion of Results 146

A.3.1 An Analysis of the Surface Strain of a Sandwich Panel Excited by Grazing Incidence Random Plane Waves 152

Chapter Four: Fatigue Tests on the Bond of Honeycomb Sandwich Plates 155

4.1 Introduction 155

4.2 The Experimental Equipment 157

4.2.1 The Test Specimens 157
4.2.2 The Test Rig 158
4.2.3 Vibrator Driving Equipment 158
4.2.4 Instrumentation 158

4.3 The Experimental Procedure 159

4.3.1 Detection of the Bubbling Mode Resonance and other Preliminary Tests 159
4.3.2 Calibration of the Gramophone Pick-up 160
4.3.3 Fatigue Testing 162

4.4 Experimental Results 163

4.5 Concluding Remarks 165

A.4.1 Calculation of the Natural Frequency of the Zero-Order Bubbling Mode of the Sandwich Under Test ... 167

Chapter Five: A Summary of Conclusions 168

5.1 Theoretical Work (Chapters One and Two) 168

5.2 Experimental Work (Chapters Three and Four 170

References 176

TABLES

Table 1 — Simplified Form of the Non-Dimensionalised Characteristic Determinant for Curved Plate Natural Frequencies

Table 2 — Curved Honeycomb Sandwich Plate Non-Dimensional Natural Frequencies for Flexural Type Modes

Table 3 — Curved Honeycomb Sandwich Plate Non-Dimensional Natural Frequencies for Bubbling Type Modes

Table 4 — Values of the Parameter $C(\omega,s)$ (ft^4/lb^2) at the Various Strain Gauge Positions

Table 5 — Showing the Development of $W_\varepsilon(\omega)$ and $\overline{\varepsilon^2(t)}$ for the Face at Strain Gauge 1 $(x/a = 0.5)$. Overall Noise Pressure Intensity = 143.5 dB

FIGURES

Figure 1 — First Order Mode Shapes of a Simply Supported Sandwich Plate

Figure 2 — Sketch Showing Plate and Skin Conventions

Figure 3 — Flat Plate Flexural Mode Frequencies (non-dimensional)

Figure 4 — Non-Dimensional Frequency vs. Frequency in Kc/s

Figure 5 — Flat Plate Flexural Mode Mass Ratio Frequency Correction

Figure 6 — Flat Plate Bubbling Mode Frequencies (non-dimensional)

Figure 7 — Flat Plate Bubbling Mode Mass Ratio Frequency Correction

Figure 8 — Flat Plate Flexural Mode Frequencies with Incidence Angles for the Coincidence Effect

Figure 9 — Curved Plate Flexural Mode Frequencies vs. Circumferential Wavelength

Figure 10 — Curved Plate Flexural Mode Frequencies vs. Axial Wavelength

Figure 11 — Curved Plate Flexural Mode Frequency vs. μ

Figure 12 — Curved Plate Flexural Mode Frequencies vs. Curvature $(\hat{r})$

Figure 13 Curved Plate Bubbling Mode Frequencies vs. μ

Figure 14 Parameter $\beta(\omega)$ vs. Frequency; for Rolls-Royce Avon R.A.26 with 20.8" Dia. Conical Nozzle (after Ref. 21)

Figure 15 Joint Magnification Factor L_5 vs λ_m/λ_t

Figure 16 Photograph of the Sandwich Panel of Chapter Three Showing the Strain Gauges

Figure 17 Sketch of Panel Support System and Sandwich Panel in the Siren Tunnel Showing Axis System and Strain Gauge Positions.

Figure 18 Harmonic Response Curve for Strain Gauge 3 at an Input Pressure Intensity of 133.5 dB

Figure 19 Phase Diagram of the Response of Strain Gauge 3 in the Region of the Fourth Natural Frequency (937 c/s)

Figure 20 A More Detailed Phase Diagram, as Figure 19, Showing the Derivation of ω_4 and δ_4

Figure 21 A Sketch of the Experimental Sandwich Viewed from Above

Figure 22 Photographs of Typical Bond Failures and of the Strain-Gauged Specimen

Figure 23 The Calibration of the Gramophone Pick-up. Core Stress per Volt vs. Frequency

Figure 24 An S-n Curve for the Uniaxial Fatigue of Honeycomb Sandwich Bond Type Redux 775R

NOTATION

a, b	plate lengths in the x and y directions
$A, B, C, E, F, G, H, L, M, N$	elastic moduli
B_r	generalised damping coefficient
C	the speed of sound in air
$C(\omega, s')$	defined by equation 3.11
D	the plate flexural rigidity ($D = E_m h_2^3 / 12(1-\nu^2)$ for one face about its own middle plane $D = E_m h_2 h_1^2/(1-\nu^2)$ for a sandwich plate as a whole)
e	strain
$F(t)$	generalised force
$\Im(\omega)$	Fourier transform
f	face-plate body force per unit volume
$f_r(s')$	normalised modal deflection function
g	gravity
$2h$	sandwich plate depth
$2h_1$	sandwich core depth
h_2	face plate thickness
K	$= N(1-\nu^2)/E_m h_2$
K^*	$= M(1-\nu^2)/E_m h_2$
K_r	generalised stiffness coefficient
ℓ^2	$=\left(\frac{n\pi}{a}\right)^2 + \left(\frac{m\pi}{b}\right)^2$
L_r	the joint magnification factor (See Appendix A.2.4)
M_r	generalised mass

m, n	number of half-waves in the y and x directions
m	(Chapter 2), plate component masses - see after equation 2.15
$p(t)$	noise pressure
p	core body force per unit volume
$q_r(t)$	generalised displacement
$N_i\ M_j\ Q_k$	force and moment resultants as shown in Figure 2
R	(Chapter 1), cylindrical radius of the plate
$\mathcal{R}$	(Chapter 2), "the real part of"
t	time
$x, y, z - u, v, w\ (U, V, W)$	cylindrical orthogonal co-ordinates, as shown in Figure 2 and their respective displacements
X	see equation 2.23
Y	see equation 2.28
$W(\omega)$	power spectrum
$z_r(\omega)$	generalised impedance
β^2	(Chapter 1) = $\frac{\rho_1 \omega^2}{g}$
δ	(Chapter 1) = $\frac{d}{dz}$
δ	(elsewhere) damping ratio
ε	$\left(\frac{n\pi}{a}\right)^2 + \frac{1-\nu}{2}\left(\frac{m\pi}{b}\right)^2$, (strain, in Chapter 3)
ε^*	$\left(\frac{m\pi}{b}\right)^2 + \frac{1-\nu}{2}\left(\frac{n\pi}{a}\right)^2$
ζ	z-wise co-ordinate with origin at the middle plane of the face-plate
θ	incidence angle of plane waves on a plate
λ_s	wavelength of sound

λ_t	trace wavelength of sound on a plate
ρ_1	core density
ρ_2	face plate density
ρ_f	$= \rho_2 + \tau/h_2$
σ	stress
τ	bonding weight per unit area
$\psi(\tau)$	correlation function
$\bar{\psi}(\tau)$	normalised correlation function or 'correlation coefficient'
$\bar{\psi}^{x}(\varsigma,\varsigma';\tau)$	cross correlation coefficient
ω	frequency of vibration
∇^2	Laplace's operator, $\frac{\partial^2}{\partial x^2} + \frac{\partial^2}{\partial y^2}$
Ч, Ш, Й, Д, Я, Ю	mode arbitrary constants

<u>Non-dimensionalised quantities</u>

A_n	$= a/h_1 n$
A_m	$= b/h_1 m$
a_r	defined by equation 2.61
C_r	defined immediately prior to equation 2.56
$\hat{\gamma}$	$= h_1/R$
α	$= E_m/E_{bond}$ (In Appendix A.2.4, $\alpha = \lambda_m/\lambda_{tr}$)
β	(Chapter 2), $= (2m+m_1)/m$ (see after equation 2.15)
γ	$= N/C$
$3\gamma/2$	$= M/C$ (for British honeycombs)
$\bar{\varepsilon}$	$= h_1^2 \varepsilon$
$\bar{\varepsilon}^*$	$= h_1^2 \varepsilon^*$

λ	$= E_m/C = \rho_2/\rho_1$ called the 'area-ratio' of the honeycomb. See the footnote on page 92
μ	$= h_2/h_1$
ν	Poisson's ratio
ϕ	(Chapter 1), $= \beta h_1$
ϕ_r	(Chapter 2), see equation 2.50
$\bar{\psi}$	(Chapter 1), $= h_1^2 \ell^2$

Note: (i) The incidence of a $\pm$ sign or $\mp$ sign does not indicate a choice. This is simply a shorthand method of writing two equations as one. The upper sign gives the equation connected with the upper face plate and vice-versa.

(ii) All noise levels are quoted in dB with reference to a pressure of 0.0002 dynes/cm^2.

Acknowledgements

The author would especially like to thank his supervisor Mr. D.J. Mead for countless hours spent discussing the work contained herein and for his ready assistance with miscellaneous problems at all times.

He would like to thank D.O.N. James for many useful discussions concerning certain mathematical problems encountered.

Thanks is also due to the technical staff of the Department of Aeronautics and Astronautics for their help with building experimental equipment and instrumentation.

Lastly, thanks is due to the Ministry of Aviation through Mr. Howard for the financial support for this work on sandwich structures.

Introduction

In recent years the engines of jet aircraft have become so powerful that the problem of acoustic fatigue failure of the aircraft structure has become a pressing one. With the engines mounted in the wing, the wing trailing edges and the whole of the rear fuselage including the tail surfaces have become subject to high noise pressures. The recent advent of rear-mounted engines has reduced the vulnerable area to the tail surfaces only. With noise levels which may reach 160 to 170 dB (re. 0.0002 dynes/cm^2), however, precautions have had to be taken to improve the resistance of the structure to noise in these zones. This improvement can be obtained by making a stiffer structure with higher damping (desirably without an increase in weight), by eliminating stress-raising discontinuities, and by designing panels to minimise the effects of the physical properties of the noise field. In some cases an improvement has been obtained by using sandwich panels. The sandwich panel is much stiffer than its conventional 'skin-stringer' counterpart of the same weight and there are not so many stress-raising rivets in the structure.

A sandwich panel consists essentially of two thin face-plates separated by a light core to which the faces are bonded. The high flexural stiffness of such a combination compared with an ordinary panel of similar weight is dependent on the correct functioning of all the three components of the sandwich. The core must be rigid enough in the plate normal direction to keep the faces separated so that the bending stiffness due to the wide separation of the faces is unimpaired.

The core shear stiffness must also be sufficient to prevent any appreciable reduction in plate bending stiffness due to shear deflection effects. If a core can be found which satisfies these requirements then the bending stiffness becomes merely a function of the properties of the face plates and their separation, provided that each component fulfils only its own duty. The sort of core currently being used for sandwich panels by the aircraft industry is the metal honeycomb which is light in weight and adequately conforms to the above specification. It is clear therefore that a sandwich panel can fulfil a flexural role much more efficiently than an ordinary panel if efficiency is defined as the flexural stiffness for a given weight.

Other factors do arise, however, in the practical use of sandwich panels, which limit their use in the modern aircraft. One of these factors is the exceptional difficulty experienced in manufacturing honeycomb sandwich panels which are curved either singly or doubly. This is because curved panels cannot be formed from flat panels, unless curvature is slight, without failure of one sort or another (usually buckling of the inner face). Thus the three components must be formed before adhesion. This poses considerable production difficulties in the case of the core. In America manufacture of double curvature sandwich panels with corrugated cores has been achieved by a pressure welding by hot rolling process. Other factors which give rise to difficulties in manufacture include the joining of sandwich panels to other structural elements, shedding of concentrated loads and non-destructive inspection. All of these

factors make the production of sandwich panels very costly.

The use of sandwich panels in severe acoustic environments is however becoming a normal practice, where it is feasible to do so, in spite of the disadvantages mentioned above, because experience has shown that these panels stand up to this sort of dynamic loading so much better than ordinary panels do. A sandwich panel has a flexural stiffness very much higher than a conventional stringer-stiffened panel of the same weight, so that its natural frequencies are much higher. This is one of the main factors which gives a sandwich panel a better resistance to noise. Another factor is the comparative absence of stress-raising rivets giving a more homogeneous stress distribution.

Fatigue failures of sandwich panels being excited by intense noise pressures have occurred in different ways, as shown below:

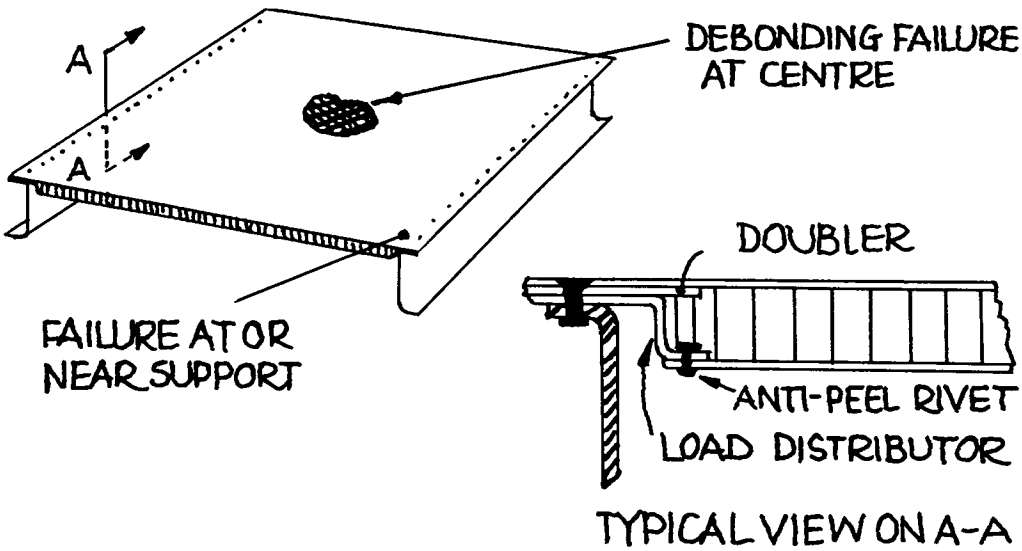

FAILURE AREAS & TYPICAL EDGE FIXING

Often the panels fail in some way near the supports and sometimes the support itself fails. However, the edge fixing of sandwich panels is receiving much attention to eliminate these failures. A failure can also occur at the centre of the panel which is known as 'debonding'. One of the faces of the sandwich becomes separated from the core due to a fatigue failure of the bond. It is this sort of failure with which chapters two and three of this work are concerned. Failures of sandwich panels are very sensitive to the characteristics of the exciting noise field and to the acoustic environment. As with conventional skin-stringer panels the designer must be aware of not only the relation between the panel natural frequencies and the noise field frequency spectrum but also the relation between modal wavelength and the narrow band spatial pressure correlation. As is shown in chapter two, it is quite likely that the acoustical coincidence effect can occur and if it does so then a large response occurs, limited of course by the condition that the surface velocity cannot exceed the incident particle velocity. Designers should also be aware of the effects which acoustic cavities can have on panel responses. It is almost certain that some form of resonant vibration causes fatigue failures of the 'debonding' type. For this reason attention should be paid to damping the sandwich in order to reduce the risk of failure.

Sandwich panels have been used in aircraft in a static load carrying capacity for some twenty years. Originally, birch faces were used with a balsa core on the D.H. Mosquito. Since then much development has taken place. Recently, the VC-10, with metal

honeycomb sandwich panels on most of its control surfaces, made its maiden flight. Sandwich panels incorporated in the elevators and rudder of the VC-10 are situated in a region of intense noise from the rear-mounted engines and it is obvious that their function is to carry the dynamic loading provided by the engine noise field. Consideration has also been given in America to the use of sandwich structures for the main structural elements of rockets because of their low weight with high inherent stability, reducing the need for pressurisation. The problem of the acoustic excitation of sandwich plates has therefore become important and in this thesis an attempt to analyse the problem has been made.

An analysis of the natural vibrations of cylindrically curved sandwich panels is made in chapter one as a preliminary to an analysis of the stresses in sandwich panel bonds. A discussion of assumptions commonly made in work on sandwich panels and a review of past work on the topic precedes the vibration analysis. The modes of vibration are divisible into two groups for flat panels, namely 'symmetric' and 'anti-symmetric'. These groups are not coupled to each other at all. The well-known flexural mode is an anti-symmetric mode. The lesser-known bubbling mode (analagous to the wrinkling mode of honeycomb plate instability) is its symmetric counterpart. Solutions to the equations of motion are found comparatively easily for flat plates, but for curved plates a solution is more difficult to obtain.

The possibility of the excitation of sandwich panels by the powerful 'acoustical coincidence' effect is discussed at the beginning of chapter two. The most important area of attention in the sandwich

is the bonding between core and faces because it is here that failures have occurred in practice. Expressions are therefore derived for the stresses in the bond when the panel is excited by acoustic noise pressures. A preliminary investigation (included in the Introduction to chapter two) of the normal stress and the bending stress in the bond of a sandwich beam shows that these stresses are of the same order of magnitude. A theory is developed for the normal stress in the bond of a panel excited by a general noise pressure field, assuming the response to be an infinite sum of principal modes. The generalised impedance of each mode is assumed to contain a damping term which derives from structural and acoustic effects. An appendix to chapter two discusses acoustic forces on the plate due to the motion of the plate itself. The general analysis for the plate normal stress is restricted successively to plane waves of any incidence and then to waves of normal incidence. A bending stress analysis is carried out for random normal plane waves.

Chapter three contains a description of some tests which have been carried out on a simply supported honeycomb sandwich panel in a siren tunnel. The purpose of these tests was to confirm the theories of chapter two by verifying a similar theory for panel surface strain. This method was resorted to because of the difficulty of measuring bond strain. A method of simply supporting a panel has been developed and shown to work well for sandwich panels. Some simple tests have been made to determine the fatigue characteristics (S-N curve) of Redux bonding by exciting a loaded specimen in a zero-order bubbling mode.

CHAPTER ONE

A Natural Mode Analysis for the Vibrations of Cylindrically Curved Elastic Sandwich Plates

Summary

Consideration of the equilibrium of the anisotropic core of a cylindrically curved sandwich plate leads to the three simultaneous differential equations for the three orthogonal deformations. Boundary conditions on two sides are found by considering the equilibrium at the core-face plate interface. A separable solution leads to the two sets (symmetric and anti-symmetric) of three homogeneous equations for the flat sandwich plate with a honeycomb core. These two sets lead to non-dimensional determinantal frequency equations for the flexural and bubbling modes. The calculation of mode shapes is indicated and the non-dimensional frequency is plotted against other variables for all likely aircraft panel configurations.

A solution is also found for curved sandwich plates by assuming that a flat plate core solution bounded by curved plate edge conditions holds true. An indication, though not a proof, of the validity of this assumption is given. A determinantal frequency equation is thus found for curved plates and an expected anomalous frequency variation with circumferential wavelength becomes evident.

The variation of frequency with wavelength for bubbling modes is only very slight for both flat and curved plates.

1.1 Introduction

Much work has been carried out over the last ten or fifteen years on the analysis of elastic sandwich structures. Bending theories were followed by buckling theories and these eventually led to vibration theories, which have only been developed in recent years. Most of the work published to date on the vibrations of elastic sandwich plates has been produced by Professor Yi-Yuan Yu of the Polytechnic Institute of Brooklyn. The aim of this chapter is to analyse the vibrations of single curvature elastic sandwich plates using the exact three-dimensional theory of elasticity with special reference to aircraft structures. Because the usual aircraft sandwich panel cores are neither homogeneous nor isotropic (honeycomb cores) the core has been regarded as anisotropic. However, the core has had to be regarded as homogeneous, and this places limitations on the size of wavelength which can be considered (see § 1.3.7).

The value of this natural mode analysis lies in its extension to the analysis of the response of sandwich plates to external forcing. This latter analysis is carried out for excitation by a noise pressure field in chapter two.

Initially, the least number of simplifying assumptions compatible with obtaining an analytical solution is made, so that further simplifications can be made at a later stage and their effect on the solutions can then be judged. It has been found possible to compute almost exact solutions for some of the modes of simply-supported flat plates. Solutions have also been found for simply-supported curved

plates. Only the simply-supported case has been considered here. Although this boundary condition is rather unrealistic, an acoustic fatigue analysis for simply-supported sandwich plates can lead to certain conclusions which will be equally applicable to plates with other boundary conditions.

In § 1.2 the nature of the possible modes of a simply-supported sandwich plate are described in order to define terminology. Also, in order to clarify the position concerning the simplifying assumptions used in this and other theories, § 1.3 is devoted to a description of the various assumptions often made and to their significance. In § 1.4, a concise review of past work on sandwich structures is presented. § 1.4 also indicates the assumptions of the work carried out so far by Yu (and to a lesser extent by Mindlin) in the U.S.A.

The principal differences between this analysis and the work of Yu are as follows: The approach to the problem here is an extension of a buckling theory[5] and starts with basic equilibrium equations, whereas Yu makes use of a variational approach. The application of this work differs also in that it deals rather specifically with honeycomb cores whereas Yu considered isotropic cores. A more basic difference is that, here, no assumption of planar or linear deformation or plane strain of the core is made. However, it is assumed that there is no shear deformation in the face plates (for reasons, see next paragraph) whereas Yu does not make this assumption. A difference between Yu's work on the vibration of cylinders[14] and this work is that this analysis is carried out for the vibrations of

segments of cylinders simply-supported at their edges whilst Yu's analysis was concerned with the axially symmetric and torsional types of modes of complete infinite cylinders. The reason for the solution of this type of vibration problem is that this work is concerned with applications to aircraft whilst Yu's paper is probably concerned with applications to rockets.

The basic approach to the problem here is to obtain the equilibrium equations of the core and faces, and then to apply the boundary conditions given by the equilibrium at the core-face plate interface. A separable solution is assumed for the deformation with harmonic time variation. For the flat plate two uncoupled sets of three homogeneous equations are thus derived in the six arbitrary constants which constitute the mode shapes of the symmetric and anti-symmetric modes (see § 1.2). From these equations the frequency equation is derived and substituting the appropriate frequency back into the homogeneous equations, the appropriate mode shape can be found. For curved plates a flat plate core solution is bounded by curved plate face conditions and this leads to six coupled homogeneous equations in the same way as above. The validity of this operation is discussed in some detail. This work neglects shear effects in the faces of the sandwich because only longer wavelengths can be considered due to the honeycomb core (see § 1.3.7). For longer wavelength modes Fig. 1 of reference 11, indicates that this assumption will be valid even though materials of different mass density and elastic moduli are being considered. The full equations of motion are derived under these assumptions. The anti-symmetric 'flexural' mode and the symmetric

'bubbling' modes are of the most interest. By assuming that the inertia forces in the plane of the plate are zero, solutions are restricted to those which correspond to flexural and bubbling modes. These modes are analysed in detail for the flat plate. For the curved plate the solutions are also found for flexural and bubbling type modes only. In the problem of acoustic excitation of sandwich structures (see chapter 2) the only modes likely to be excited are these flexural and bubbling modes. Non-dimensional forms of solution for frequency are obtained and these are shown in Fig.3 at the end of the thesis.

In the 1940's Arnold and Warburton noticed an unexpected variation of natural frequency with variation of flexural wavelength around the circumference of thin cylinders. It appears that the natural frequency, for a certain configuration, was dropping as the circumferential wavelength decreased. Subsequently, they propounded a theory[19] which showed that this effect could occur, and which agreed remarkably well with their experimental results. A physical explanation of the mechanism of this surprising effect is to be found in the types of strain energy involved in a deflection from the equilibrium state. The type of strain energy associated with the small deflections of thin flat plates (viz. flexural or bending strain energy) is present. Also, however, it is now possible for in-plane direct strain of the mid-surface of the plate to occur involving an energy which is comparable in magnitude to the flexural

strain energy. For a given central deflection and radius of curvature this in-plane stretching energy intrinsically decreases as the wavelength decreases, because the sector angle of the plate is becoming smaller (i.e. nearer the flat-plate condition). Thus, it is this variation of the in-plane mid-surface stretching energy which causes the unusual variation of curved plate natural frequency. This effect has been noticed for some configurations of the curved sandwich plates, and Fig. 9 shows such a variation.

An exact solution of the differential equations of motion with curvature included cannot be obtained analytically. In the early work on this problem a perturbation technique was attempted in order to obtain a solution. In this, the solution for curved plate core deflection was assumed to be a perturbed flat plate deflection. The problem thus formulated was not readily solvable in this form. However, it is argued that the use of a flat-plate core deflection solution together with curved-plate boundary conditions gives sufficiently accurate values for frequencies. Hence, by using the same technique as employed for flat plates, six homogeneous equations are obtained in six variables (arbitrary constants) and the determinant of coefficients is equated to zero to find the natural frequencies. The frequency solutions have been obtained using a numerical technique and a digital computer.

1.2 The Nature of the Possible First-Order Modes of Vibration of a Flat Finite Rectangular Elastic Sandwich Plate, Simply-Supported at its Edges

For a flat sandwich plate with symmetry about its middle plane there are two distinct sets of modes of vibration. The first, and perhaps the more important, is the anti-symmetric set. For this set, the displacements in the plane of one of the face plates are equal, but opposite in direction, to those in the other face. Therefore the middle plane of the plate is a plane of 'anti-symmetry'. Clearly, the classical flexural modes of the plate are anti-symmetric. There is also a set of symmetric modes in which the displacements in the plane of one of the face plates are equal to, and in the same direction as, those in the other face. It is found that there are three anti-symmetric first-order modes and three symmetric first-order modes. However, two of the anti-symmetric modes are of the same type as also are two of the symmetric modes. Thus there are only four types of mode. These modes are now described in some detail and are shown in Fig. 1.

1.2.1 Anti-symmetric Modes

1.2.1.1 The Flexural Mode

In this mode, the displacement normal to the middle plane of the plate (z-direction) varies with x and y (the orthogonal co-ordinates in the plane of the plate), but for most purposes it can

be assumed not to vary with z (Figure 1a). Energies associated with this mode are lower than those associated with other modes when the plate depth is small compared with its length and width, and therefore the first-order flexural mode will have a comparatively low frequency.

1.2.1.2 Thickness-Shear Modes

For the plate described above there are two thickness-shear modes, one associated with the x-direction and the other associated with the y-direction (Figure 1b). The displacements in the zero-order thickness-shear modes are independent of the x and y co-ordinates and are parallel to the plane of the plate. Displacements perpendicular to the plate are zero. The displacements of the first-order thickness-shear modes are also parallel to the plane of the plate but they now vary with x and y . For most purposes the first-order thickness-shear modes can be regarded as a linear variation of u and v with respect to the normal co-ordinate z . There will now be some displacement perpendicular to the plate surface and superficially the mode appears to be of a flexural type. These modes have a higher frequency than the flexural modes for the sandwiches considered here.

1.2.2 Symmetric Modes

For the flat plate described first-order symmetric modes are not coupled in any way with first order anti-symmetric modes.

1.2.2.1 The Bubbling Mode

The motion in this mode produces direct tension and compression of the core in the z-direction, the faces moving in opposite directions (Fig. 1c). Most of the strain energy is in the core. There is a variation of the z-wise displacement, w, with x and y however, and consequently there is some flexure of the faces. This mode usually has a higher natural frequency that its anti-symmetric counterpart, the flexural mode; and the frequencies of the bubbling modes are possibly of the same order as those of the thickness-shear modes. It is probable that this mode is lightly damped, and owing to its high natural frequency it might become important where fatigue is being considered.

1.2.2.2 Longitudinal Modes

These modes are the symmetric counterpart of the thickness-shear modes. Again, two such first-order modes exist for the plate under consideration, one with motion predominantly in the x-direction and the other with motion predominantly in the y-direction. Only displacements of second order of magnitude take place normal to the plate, and so all displacements can be assumed parallel to the middle plate of the plate. In this mode the top and bottom faces move by the same amount in the same direction (whereas in the thickness-shear mode they moved by the same amount in opposite directions). In the first-order mode u and v vary with x and y. The frequency of these modes is comparatively high, and

therefore they are not of much interest acoustically as they would be difficult to excite.

1.2.3 A Note Concerning the Modes of Cylindrically Curved Sandwich Plates

For curved plates, the asymmetry about the neutral axis produces a coupling between what we have called the symmetrical and anti-symmetrical modes and they can no longer use these names. However, there is still a flexural and bubbling mode for curved plates, the difference being that for curved plates these two modes are coupled together, usually only very lightly because of the wide frequency separation.

1.3 A Summary of Assumptions Commonly made in Elastic Sandwich Theories

1.3.1 Plane Strain

A simplification of the exact three-dimensional theory of thin plates is possible when one of the characteristic dimensions is large. It can be assumed that strain in this long dimension direction is zero[16]. Thus for a plate which has a long side, the bending and vibration characteristics will depend almost entirely on the short dimension, and on the boundary conditions on the long edge. Only strains in the plane defined by the normal to the plate and lines parallel to the shorter dimension need be considered, i.e. plane strain analysis is sufficient. It is often found convenient to make this assumption when the effect of other approximations is

to be judged. Most sandwich plate analyses have assumed plane strain and have been called "one-dimensional" even though displacements, strains and stresses occur in two dimensions.

1.3.2 Planar and Linear Deformation

Three-dimensional bending and vibration theories of thin plates often consider the in-plane deflections, u and v, to vary linearly with the co-ordinate z, i.e. straight lines normal to the plane of the plate in the unstrained state remain straight after loading. This is the linear deformation assumption.

In two-dimensional (sometimes known as 'one-dimensional') theories a similar assumption can be made, but in this case, plane sections remain plane after loading. This is a particular case of linear deformation where no deformation takes place with respect to one of the in-plane co-ordinates, and is known as planar deformation.

As far as long wavelength, low frequency, vibration theories of sandwich plates are concerned these assumptions are accurate enough. Exact elasticity theory shows the relationship between in-plate deformation and normal co-ordinate to be: $u = U \sin \beta z$

For long wavelength, low frequency vibrations the maximum value of the argument βz is small, and thus the sine can be replaced approximately by the argument and the assumption of planar deformation is seen to hold true. However, for higher frequency modes of vibration

the argument βz is no longer small, and the planar deformation assumption is likely to give inaccurate results. For thickness-shear modes Yu[10] has had to apply corrections to his planar deformation theory.

1.3.3 Zero Transverse Shear Strain in the Face Plates

Bending theories of thin plates have shown that the effect of transverse shear strains is negligible unless the characteristic length (e.g. the wavelength of vibration) is of the order of the plate depth (see reference 7, for example). Likewise, if the faces of a sandwich plate are thin compared with the characteristic length, then the inclusion of transverse shear effects is unnecessary.

1.3.4 Zero Rotatory Inertia

The kinetic energy of a plate vibrating in flexure is commonly assumed to consist of the transverse translational energy only. Another component of kinetic energy exists due to rotational velocity of plate elements about an axis in the middle plane of the plate. As with transverse shear, this effect becomes important when the characteristic plate dimension becomes of the order of the total plate depth.

1.3.5 Zero Flexural Rigidity of the Face-Plates about their own Middle Plane

In a deformed stiff-cored sandwich most of the strain energy in the faces is extensional energy, i.e. the strain in the face is

almost constant throughout the thickness of the face. This however is not strictly true and the effect of the true variation of strain can be included by superimposing a flexural strain (with the middle plane of the face-plate as origin) upon the extensional strain. Flexural rigidity of the faces about their own middle plane is included in this way. The flexural effect is much smaller than the extensional effect when the face thickness is small compared with the core depth and when the wavelength is large compared with the plate depth. When the face is very thin, its flexural rigidity can be neglected.

1.3.6 Different Modes of Vibration of the Same Order are not Coupled

It can be shown that there is no coupling at any time between the symmetric and anti-symmetric modes of vibration of a symmetrically arranged flat sandwich plate. However, coupling exists between the different symmetric and the different anti-symmetric modes. Ekstein[8] has pointed out that weakly coupled vibrations of two zero-order modes are likely to become strongly coupled when the natural frequencies of the two modes approach each other. A similar effect can be expected for first and higher order modes. Usually the natural frequency of the first-order flexural mode is far removed from the natural frequencies of the first-order thickness-shear modes and also the natural frequency of the first-order bubbling mode is far removed from the natural frequencies of first-order longitudinal modes. In this case, therefore, the four types of mode can be treated separately with a reasonable degree of accuracy. However, as the plate thickness-

wavelength ratio becomes larger and as the thickness of the face becomes larger the coupling will become stronger and it may be necessary to take it into account.

1.3.7 Homogeneous Core

The cores of sandwich plates used by the aircraft industry are often of the honeycomb type. This type of core is certainly not homogeneous as it consists of many small hexagonal cells bounded by metal foil. However, if the cell size is small compared with the characteristic dimension under consideration, the assumption of homogeneity is a reasonable one. Care must be taken, however, when vibrational wavelengths become small.

1.3.8 The Assumption of an Isotropic Core

The cores of composite sandwich plates are often assumed to be isotropic. Where practical applications are concerned this is not usually true and therefore here the differential equations are derived for an anisotropic core. For honeycomb cores, three of the six elastic moduli can be assumed to be zero. These are the direct moduli in the plane of the plate, and the shear modulus G_{xy}. For British honeycombs the two non-zero shear moduli are usually in the ratio of 2 to 3.

1.4 A Review of Previous Work on the Analysis of Elastic Sandwich Plates

1.4.1 Bending and Buckling Theories

Papers concerned with the bending and buckling of elastic sandwich structures started to appear soon after the war. Hemp's theory[1] of sandwich construction was published in 1948, and other papers by Reissner[2], Hoff[3], Eringen[4] and Hunter-Tod[5] appeared soon afterwards.

Reissner's paper was the first to derive the equilibrium equations for the bending deformation of a normal type of sandwich construction shell. He has first derived the equilibrium equations of the core and faces. Then, after finding the appropriate expression for the strain energy of the composite plate, Castigliano's principle has been applied to minimise the complementary energy. The minimum of complementary energy gives the equilibrium stress system. The assumptions made in this work are that the faces are thin and thus behave like membranes (i.e. constant direct stress across the thickness and no shear stresses normal to the face), that the core behaves as a homogeneous elastic material in which only transverse stresses occur (two shear stresses, one direct stress), and that deflections are small. The equations have been obtained from the three-dimensional theory of elasticity, subject to the restrictions above, and for the ordinary type of sandwich plate (in which the skins are thin compared with the total depth of the sandwich) these assumptions held good.

1.4.2 Vibration Theories

If Reissner's paper is to form the basis of work on the vibrations of sandwich plates then the restrictions of his theory, as stated in 1.4.1 above, must be borne in mind. For longer wavelength, low frequency flexural vibrations of sandwich plates, assumptions similar to Reissner's can be made. Mindlin has derived the equations of flexural motion of elastic sandwich plates with thin faces by neglecting the transverse shear deformation and rotatory inertia of the faces. These assumptions are equivalent to those made by Reissner in his bending theory, and they have given accurate results for low order flexural modes of vibration of ordinary sandwich plates.

The analysis of short wavelength flexural vibrations of sandwich plates, with, perhaps, thick skins, becomes very complicated when a solution derived from the exact theory of elasticity is contemplated. The additional factors which must now be included are:-

(i) The effect of transverse shear deformation in the face plates

(ii) The effect of rotatory inertia of the faces

(iii) The coupling which might exist between the three anti-symmetric modes

(iv) For honeycombs, the fact that the cell dimensions are likely to be of the order of size of the wavelength.

For a discussion of these factors and when they become significant see § 1.3.

In a series of six recent papers[9,10,11,12,13,14] Yu has developed a new theory of bending and vibration of elastic sandwich

plates including transverse shear effects in the faces and based on the three-dimensional theory of elasticity.

In his first paper[9] he has considered the bending of an infinite elastic sandwich plate in the so-called one-dimensional case, under the assumption of planar deformation, as described in 1.3.2, in each of the three components of the sandwich, although planar deformation of the cross-section as a whole has not been assumed. Thus he has been able to include the effects of transverse shear deformation in the faces. One advantage of this theory over previous bending theories of sandwich plates is that no restriction has been imposed on the thickness of the faces and the solution therefore is more general. As a result of including transverse shear effects in the faces, subsequent application of the theory of this paper to vibration problems applies up to higher frequency modes than other papers have done. The frequency and wavelength at which departure from planar deformation becomes important is dependent on the skin thickness and density and the core mean density, and the departure becomes larger as the wavelength decreases and the frequency increases. And so at very high frequencies accuracy is gained by including transverse shear effects in the skin but at the same time it is lost by assuming planar deformation. The theory of this paper is only concerned with small deflections, as usual.

The second paper by Yu[10] is a short note on the simple one-dimensional thickness-shear modes of an infinite plate. The modes discussed are the zero-order modes of the type described in § 1.2.1.2. Only free vibrations have been considered. For the case

of infinite homogeneous isotropic plates, such modes have been discussed by Mindlin[15] firstly on the basis of a plate theory which takes account of transverse shear deformation and rotatory inertia but assumes plane strain and planar deformation, and secondly on the basis of exact elasticity theory (plane strain being assumed again but not planar deformation). The discrepancy between the lowest frequency values obtained by the two methods is removed by introducing to the former a factor K whose value is found to be $\pi^2/12$ for an homogeneous isotropic plate. Yu's paper has investigated the one-dimensional zero-order thickness shear modes of sandwich plates in exactly the same manner as Mindlin has done for homogeneous isotropic plates using the theory of reference 9 and matching the approximate frequencies to the frequencies derived from the exact elasticity theory with the factor K. However, for sandwich plates, it is found that K varies between $\pi^2/12$ and 1. $K = \pi^2/12$ corresponds to the case of a sandwich plate with relatively thick faces whereas $K = 1$ corresponds to the case of a sandwich with relatively thin faces. As $K \neq 1$ implies perfect matching of frequencies between the exact and approximate theories, it is seen that the assumption of planar deformation is valid for thin faces. (Note: This is true only in a broad sense because other factors do enter the argument. However, the relative thickness of the faces is the predominant factor). The frequency equation for these modes derived from the theory of reference 9, has been given in this note, as has the equation obtained from exact elasticity theory.

In Yu's third paper[11] the equations of motion of flexural

vibrations of sandwich plates have been developed using the theory of reference 9 (one-dimensional case). All of the usual effects have been included in this analysis, the important assumptions being those of plane strain and planar deformation in each of the plate components. The theory therefore applies to sandwich plates with thick faces because transverse shear effects in the faces have been included, as pointed out previously. In the introduction the need to include transverse shear and rotatory inertia in the theory has been emphasised again so that higher frequency modes may be computed more accurately. The flexural vibrations of sandwich plates have also been analysed using exact elasticity theory which has been restricted to the so-called one-dimensional case at the outset so that results thus obtained can be compared with the results obtained from the approximate analysis. On the basis of these theories the flexural vibrations have been investigated with the emphasis on ordinary sandwich plates. It is shown, by a numerical example, that the two methods described above give almost identical results; which indeed they should, since the assumption of planar deformation holds good for the flexural vibrations of ordinary sandwich plates at the lower frequencies. It is found that the neglect of shear deformation in the core gives rise to inaccurate results and therefore this effect should be included at all times. It is also found that the joint flexural-extensional rigidity of the faces must be included in the analysis if accurate results are to be expected, unless the faces are exceptionally thin, in which case, the flexural rigidity of the faces can be neglected. For plates with very thin faces and vibration modes of a low frequency, the possibility

of some considerable simplification is forecast.

This simplification has been carried out in the next paper to be published by Yu[12]. The flexural vibration equations derived in reference 11 are complicated, and they hold good for a wide frequency range. For the low frequency ranges and ordinary sandwich plates with thin faces a considerable simplification of the problem can be effected. In this paper these simpler equations have been introduced and their accuracy is determined by a comparison with the more complete equations of reference 11.

In the theory developed in references 9 and 11, it has been assumed that the transverse displacement is constant across the depth of the plate, and that the in-plate displacements are proportional to to the plate normal co-ordinate, the derivatives of in-plate displacements in the core and faces, with respect to the normal co-ordinate, being different from each other. In this way all of the deformation energies have been taken into account. For sandwich plates with thin heavy faces the important factors have been found to be shear in the core, rotational and translational inertia of the core, translational inertia of the faces, and the joint effect of flexural and extensional rigidity of the faces. These effects have been included in this simpler analysis[12]. Two sets of equations have been derived.

The derivation of the first set of simplified equations consists of a two-dimensional analysis with transverse shear deformation in the

faces not being taken into account. The equations have been derived from three-dimensional elasticity theory using a variational procedure as in reference 9. This set of equations has been found to yield the same frequency equation as a certain degeneration of equations derived in reference 11.

The form of deformation used for these two simplified sets is as described above except that the in-plate deformation of the faces has been regarded as constant over the face depth. For the first set these displacements have been derived, in the faces, by considering the core as extending to the interface whereas for the second set the core has been considered as extending to the middle plane of the faces. The second set of equations thus obtained has also been found to be a degenerate version of the equations of reference 11, but the restriction necessary for the simplified frequency equation to hold is not as great as the restriction for the first set, and therefore the second set yields more accurate solutions. In this way a simplified analysis for the flexural vibrations of thin skin sandwich plates in the lower frequency range has been found which yields solutions of good accuracy.

In a paper concerned with the forced flexural vibrations of sandwich plates in plane strain[13] Yu has started again with the displacement equations of motion derived in reference 9. Treating the case of a simply-supported plate he has expanded the response as a series of principal modes which had been found previously[11] and

the orthogonality condition of the principal modes has been derived. A method due to Mindlin and Goodman[18] has been used to analyse the response to time dependent boundary conditions and an example has been worked out for this type of forced motion. The assumptions of reference 9 have been made for this work.

Recently, Yu has also written a paper on the vibrations of sandwich cylindrical shells[14]. This analysis is almost identical to the analysis for flat plates in reference 9 except, of course, that the cylindrical quantities are introduced. The equations of motion so obtained have been simplified by making the assumption that the faces of the sandwich are very thin. The assumption of planar deformation has been made, and therefore as described previously in this section, shear coefficients K had to be calculated to match the thickness shear frequencies in order to correct errors brought about by this assumption. The simplified equations have been used to analyse the axially symmetric and torsional vibrations of an infinite cylinder.

Yu's papers are a useful set of works on the vibrations of sandwich structures, especially for one-dimensional analysis of flat plates and two-dimensional analysis for low frequency thin skinned flat plates.

1.5 The Analysis of the Vibrations of Cylindrically Curved Sandwich Plates

1.5.1 Sandwich Plate Core Equations

1.5.1.1 Stress-Strain Equations for an Anisotropic Homogeneous Medium

The convention for co-ordinates and face stress resultants is given in Fig. 2. These co-ordinates are much the same as those used by Hunter-Tod[5] and are of the cylindrical polar type. The usual θ co-ordinate is replaced by y where $y = R\theta$ and R is the cylindrical curvature radius. R is assumed to be large compared with the thickness of the panel. The co-ordinate z is used with the middle plane of the plate as its origin and with the R direction as its direction. Measurement of x is parallel to the generator of the cylinder and in the middle plane of the plate. As mentioned in the introduction, the core has had to be assumed homogeneous in order to obtain a solution. This limits the frequency and wavelength down to which it is possible to obtain an accurate solution to the vibration problem for honeycomb cores (see § 1.3.7). The stress-strain equation is:-

$$\begin{Bmatrix} \epsilon \end{Bmatrix} = \begin{bmatrix} \frac{1}{E_x} & -\frac{\nu_{xy}}{E_y} & -\frac{\nu_{xz}}{E_z} \\ -\frac{\nu_{yx}}{E_x} & \frac{1}{E_y} & -\frac{\nu_{yz}}{E_z} \\ -\frac{\nu_{zx}}{E_x} & -\frac{\nu_{zy}}{E_y} & \frac{1}{E_z} \end{bmatrix} \begin{Bmatrix} \sigma \end{Bmatrix} \qquad \ldots(1.1)$$

where

$$\left\{\epsilon\right\} = \begin{Bmatrix} \epsilon_{xx} \\ \epsilon_{yy} \\ \epsilon_{zz} \end{Bmatrix} \quad , \quad \left\{\sigma\right\} = \begin{Bmatrix} \sigma_{xx} \\ \sigma_{yy} \\ \sigma_{zz} \end{Bmatrix}$$

and the matrix of coefficients of σ must be symmetric for a linear structure due to Clerk-Maxwell's reciprocity theorem. The inversion of (1) will give:-

$$\left\{\sigma\right\} = \begin{bmatrix} A & E & F \\ E & B & H \\ F & H & C \end{bmatrix} \left\{\epsilon\right\} \qquad \ldots(1.2)$$

where the matrix of coefficients must again be symmetric. For the particular type of core considered in this Thesis (a honeycomb core) it can be assumed that $E_x = E_y = 0$, and therefore examination of equations 1.1 and 1.2 gives:- A, B, E, F, H = 0, C = E_z and the only component of 1.2 which remains is

$$\sigma_{zz} = C e_{zz} \qquad \ldots(1.3)$$

As far as shear stresses and strains are concerned it can be assumed that $G_{xy} = 0$ for the honeycomb material and we are therefore left with:-

$$\sigma_{zx} = G_{zx}\, e_{zx}$$

$$\sigma_{zy} = G_{zy}\, e_{zy} \qquad \ldots(1.4)$$

However, we will solve for the more general case of an anisotropic core (assuming there to be no coupling between shear strains and direct stresses) where the stress-strain relationships can be written:-

(i) as equation 1.2 for direct stresses, and

(ii)
$$\begin{Bmatrix} \sigma_{xy} \\ \sigma_{yz} \\ \sigma_{zx} \end{Bmatrix} = \begin{bmatrix} L & 0 & 0 \\ 0 & M & 0 \\ 0 & 0 & N \end{bmatrix} \begin{Bmatrix} e_{xy} \\ e_{yz} \\ e_{zx} \end{Bmatrix} \qquad \ldots(1.5)$$

and the special case of honeycomb cores will be brought into the solution later.

1.5.1.2 Equilibrium Relationships

The well-known equilibrium equations in cylindrical polar co-ordinates (see, for example, reference 16, p.306), when body forces are included, and conversion to our form of axes has been effected, are:-

$$\frac{\partial \sigma_{xx}}{\partial x} + \frac{\partial \sigma_{xy}}{\partial y} + \frac{\partial \sigma_{xz}}{\partial z} - \frac{1}{R}\left\{ z\frac{\partial \sigma_{xy}}{\partial y} - \sigma_{xz} \right\} + p_x = 0 \qquad \ldots(1.6)$$

$$\frac{\partial \sigma_{yx}}{\partial x} + \frac{\partial \sigma_{yy}}{\partial y} + \frac{\partial \sigma_{yz}}{\partial z} - \frac{1}{R}\left\{ z\frac{\partial \sigma_{yy}}{\partial y} - 2\sigma_{yz} \right\} + p_y = 0 \qquad \ldots(1.7)$$

$$\frac{\partial \sigma_{zx}}{\partial x} + \frac{\partial \sigma_{zy}}{\partial y} + \frac{\partial \sigma_{zz}}{\partial z} - \frac{1}{R}\left\{ z\frac{\partial \sigma_{zy}}{\partial y} - \sigma_{zz} + \sigma_{yy} \right\} + p_z = 0 \qquad \ldots(1.8)$$

where p_i is the body force per unit volume in the positive i direction.

1.5.1.3 Strain-Displacement Relationships

The equations connecting strain and displacement in cylindrical co-ordinates are also well known (see reference 16, p.305). These also have been suitably converted to the system of this work (neglecting terms in $1/R^2$), thus:-

$$\begin{aligned}
\epsilon_{xx} &= \frac{\partial u}{\partial x} \\
\epsilon_{yy} &= \frac{\partial v}{\partial y} - \frac{1}{R}\left\{z\frac{\partial v}{\partial y} - w\right\} \\
\epsilon_{zz} &= \frac{\partial w}{\partial z} \\
\epsilon_{xy} &= \frac{\partial u}{\partial y} + \frac{\partial v}{\partial x} - \frac{z}{R}\frac{\partial u}{\partial y} \\
\epsilon_{yz} &= \frac{\partial v}{\partial z} + \frac{\partial w}{\partial y} - \frac{1}{R}\left\{z\frac{\partial w}{\partial y} + v\right\} \\
\epsilon_{zx} &= \frac{\partial w}{\partial x} + \frac{\partial u}{\partial z}
\end{aligned} \qquad \ldots(1.9)$$

1.5.1.4 Overall Core Equilibrium Equations

Substituting equations 1.2, 1.5 and 1.9 in equation 1.6 we obtain:-

$$A\frac{\partial^2 u}{\partial x^2} + L\frac{\partial^2 u}{\partial y^2} + N\frac{\partial^2 u}{\partial z^2} + (E+L)\frac{\partial^2 v}{\partial x \partial y} + (F+N)\frac{\partial^2 w}{\partial x \partial z} + P_x =$$

$$\frac{1}{R}\left\{z\frac{\partial}{\partial y}\left[L\left(2\frac{\partial u}{\partial y} + \frac{\partial v}{\partial x}\right) + E\frac{\partial v}{\partial x}\right] - (E+N)\frac{\partial w}{\partial x} - N\frac{\partial u}{\partial z}\right\} \qquad \ldots(1.10)$$

and substituting equations 1.2, 1.5 and 1.9 in equation 1.7 we obtain:-

$$(L+E)\frac{\partial^2 u}{\partial x \partial y} + L\frac{\partial^2 v}{\partial x^2} + B\frac{\partial^2 v}{\partial y^2} + M\frac{\partial^2 v}{\partial z^2} + (G+M)\frac{\partial^2 w}{\partial y \partial z} + P_y =$$

$$\frac{1}{R}\left\{z\frac{\partial}{\partial y}\left[(L+E)\frac{\partial u}{\partial x} + 2B\frac{\partial v}{\partial y} + (G+M)\frac{\partial w}{\partial z}\right] - B\frac{\partial w}{\partial y} - M\left[\frac{\partial v}{\partial z} + \frac{\partial w}{\partial y}\right]\right\} \quad \ldots(1.11)$$

and substituting equations 1.2, 1.5 and 1.9 in equation 1.8 we obtain:-

$$N\frac{\partial^2 w}{\partial x^2} + M\frac{\partial^2 w}{\partial y^2} + C\frac{\partial^2 w}{\partial z^2} + (G+M)\frac{\partial^2 v}{\partial y \partial z} + (F+N)\frac{\partial^2 u}{\partial x \partial z} + P_z =$$

$$\frac{1}{R}\left\{z\frac{\partial}{\partial y}\left[(G+M)\frac{\partial v}{\partial z} + 2M\frac{\partial w}{\partial y}\right] + (E-F)\frac{\partial u}{\partial x} + (M+B)\frac{\partial v}{\partial y} - C\frac{\partial w}{\partial z}\right\} \quad \ldots(1.12)$$

1.5.2 The Equilibrium of the Face-Plates

1.5.2.1 Equilibrium Parallel to the Face Surface

The assumption of plane stress is made for the faces, i.e.

$$\sigma_{zz} = \sigma_{yz} = \sigma_{xz} = 0$$

(see reference 16, p.30). This is another assumption which will limit the frequency and wavelength to which this work will apply, but it is reasonable to make this assumption having once limited the wavelength by assuming a homogeneous core.

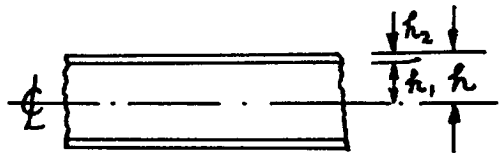

$$h = h_1 + h_2$$

For plane stresses in the faces we have

$$\sigma_{xx} = \frac{E_m}{1-\nu^2}\left(\epsilon_{xx} + \nu\epsilon_{yy}\right)$$

$$\sigma_{yy} = \frac{E_m}{1-\nu^2}\left(\nu\epsilon_{xx} + \epsilon_{yy}\right)$$

$$\sigma_{xy} = G\epsilon_{xy} = \frac{E_m}{2(1+\nu)}\epsilon_{xy}$$

...(1.13)

If quantities at the middle surfaces of the face plates (i.e. at $z = \pm\left(h_1 + \frac{h_2}{2}\right)$) are denoted by a dash and if quantities at the interface $(z = \pm h_1)$ are denoted by a subscript o then deflections in the face plates are given approximately by:

$$u = u_o \mp \left(\frac{h_2}{2} + \zeta\right)\left(\frac{\partial w}{\partial x}\right)_o$$

$$v = v_o \mp \left(\frac{h_2}{2} + \zeta\right)\left(\frac{\partial w}{\partial y}\right)_o$$

$$w = w_o$$

...(1.14)

noting that $\epsilon_{xz_o} = \left(\frac{\partial u}{\partial z}\right)_o + \left(\frac{\partial w}{\partial x}\right)_o = 0$, etc., and where ζ is a plate normal co-ordinate measured from the middle surface of the face plate (i.e. $z = z' + \zeta$ where $z' = h_1 + \frac{h_2}{2}$).

At the middle surface of the face plate $\zeta = 0$ and we have:-

$$u' = u_o \mp \frac{h_2}{2}\left(\frac{\partial w}{\partial x}\right)_o$$

$$v' = v_o \mp \frac{h_2}{2}\left(\frac{\partial w}{\partial y}\right)_o$$

$$w' = w_o$$

...(1.15)

The in-plane direct and shear stress resultants are given by:-

$$N_x = \frac{E_m h_2}{1-\nu^2}\left\{\left(\frac{\partial u}{\partial x}\right)' + \nu\left(\frac{\partial v}{\partial y}\right)' - \frac{\nu}{R}\left(\pm h_1\left(\frac{\partial v}{\partial y}\right)' - w'\right)\right\}$$

$$N_{xy} = \frac{E_m h_2}{2(1+\nu)}\left\{\left(\frac{\partial u}{\partial y}\right)' + \left(\frac{\partial v}{\partial x}\right)' \mp \frac{h_1}{R}\left(\frac{\partial u}{\partial y}\right)'\right\}$$

$$N_y = \frac{E_m h_2}{(1-\nu^2)}\left\{\nu\left(\frac{\partial u}{\partial x}\right)' + \left(\frac{\partial v}{\partial y}\right)' - \frac{1}{R}\left(\pm h_1\left(\frac{\partial v}{\partial y}\right)' - w'\right)\right\} \qquad \ldots(1.16)$$

using equations 1.13 and 1.9 and taking the middle plane value of the strains. The equilibrium of stress resultants in the x and y directions gives the equations:-

$$\frac{\partial N_x}{\partial x} + \frac{\partial N_{xy}}{\partial y} \mp \frac{h_1}{R}\frac{\partial N_{xy}}{\partial y} + f_x h_2 = \pm \sigma_{xz_o} = \pm N\left\{\left(\frac{\partial w}{\partial x}\right)_o + \left(\frac{\partial u}{\partial z}\right)_o\right\}$$

$$\frac{\partial N_{xy}}{\partial x} + \frac{\partial N_y}{\partial y} \mp \frac{h_1}{R}\frac{\partial N_y}{\partial y} + f_y h_2 = \pm \sigma_{yz_o} + \frac{Q_y}{R} = \frac{Q_y}{R} \pm M\left\{\left(\frac{\partial v}{\partial z}\right)_o + \left(\frac{\partial w}{\partial y}\right)_o\right\}$$

$$\mp \frac{M v_o}{R} - \frac{M h_1}{R}\left(\frac{\partial w}{\partial y}\right)_o \qquad \ldots(1.17)$$

where f_i is the body force per unit volume in the i direction in the face plates. Substituting equations 1.15 and 1.17 to eliminate the stress resultants, and converting the dashed terms to subscript 'o' terms using equations 1.15 we obtain the two following relationships:-

At $z = \pm h_1$

$$\frac{\partial^2 u}{\partial x^2} + \frac{1-\nu}{2}\frac{\partial^2 u}{\partial y^2} + \frac{1+\nu}{2}\frac{\partial^2 v}{\partial x \partial y} \mp h_2 \frac{\partial}{\partial x}\nabla^2 w + \frac{1-\nu^2}{E_m} f_x =$$

$$\pm K\left(\frac{\partial w}{\partial x} + \frac{\partial u}{\partial z}\right) \pm \frac{1}{R}\left\{h_1 \frac{1+\nu}{2}\frac{\partial^2 v}{\partial x \partial y} \mp \nu \frac{\partial w}{\partial x} + h_1(1-\nu)\frac{\partial^2 u}{\partial y^2}\right\} \qquad \ldots(1.18)$$

$$\frac{\partial^2 v}{\partial y^2} + \frac{1-\nu}{2}\frac{\partial^2 v}{\partial x^2} + \frac{1+\nu}{2}\frac{\partial^2 u}{\partial x \partial y} \mp \frac{h_2}{2}\frac{\partial}{\partial y}\nabla^2 w + \frac{1-\nu^2}{E_m} f_y =$$

$$\pm K^*\left(\frac{\partial w}{\partial y} + \frac{\partial v}{\partial z}\right) - \frac{K^*}{R}\left(h_1 \frac{\partial w}{\partial y} \pm v\right) \pm \frac{1}{R}\left\{h_1 \frac{1+\nu}{2}\frac{\partial^2 u}{\partial x \partial y} \mp \frac{\partial w}{\partial y}\right.$$

$$\left. + 2h_2 \frac{\partial^2 v}{\partial y^2} \pm \frac{K^*}{M} Q_y\right\} \qquad \ldots(1.19)$$

where $K = \dfrac{N(1-\nu^2)}{E_m h_2}$ and $K^* = \dfrac{M(1-\nu^2)}{E_m h_2}$

and as far as equation 1.19 is concerned

$$Q_y = -D\frac{\partial}{\partial y}\nabla^2 w$$

1.5.2.2 Equilibrium Normal to the Face Surface

For the face moment stress resultants we have, according to the code shown in Fig. 2:-

$$M_x = \pm \int_{-\frac{h_2}{2}}^{\frac{h_2}{2}} \sigma_{xx} \zeta \, d\zeta$$

$$M_y = \pm \int_{-\frac{h_2}{2}}^{\frac{h_2}{2}} \sigma_{yy} \zeta \, d\zeta \qquad \ldots(1.20)$$

$$M_{xy} = \pm \int_{-\frac{h_2}{2}}^{\frac{h_2}{2}} \sigma_{xy} \zeta \, d\zeta$$

Neglecting terms in h_2/R and $1/R^2$, the resulting equations are:-

$$M_x = -D\left[\left(\frac{\partial^2 w}{\partial x^2}\right)_o + \nu\left(\frac{\partial^2 w}{\partial y^2}\right)_o \mp \frac{\nu}{R}\left\{h_1\left(\frac{\partial^2 w}{\partial y^2}\right)_o \mp \left(\frac{\partial v}{\partial y}\right)_o\right\}\right]$$

$$M_y = -D\left[\nu\left(\frac{\partial^2 w}{\partial x^2}\right)_o + \left(\frac{\partial^2 w}{\partial y^2}\right)_o \mp \frac{1}{R}\left\{h_1\left(\frac{\partial^2 w}{\partial y^2}\right)_o \mp \left(\frac{\partial v}{\partial y}\right)_o\right\}\right]$$

$$M_{xy} = -(1-\nu)D\left[\left(\frac{\partial^2 w}{\partial x \partial y}\right)_o \mp \frac{1}{R}\left\{\frac{h_1}{2}\left(\frac{\partial^2 w}{\partial x \partial y}\right)_o \mp \frac{1}{2}\left(\frac{\partial v}{\partial x}\right)_o\right\}\right] \qquad \ldots(1.21)$$

where $D = E_m h_2^3 / 12(1-\nu^2)$. Equilibrium of the transverse loads on a skin element gives:-

$$\frac{\partial Q_x}{\partial x} + \left(1 \mp \frac{h_1}{R}\right)\frac{\partial Q_y}{\partial y} + f_z h_2 = \frac{N_y}{R} \pm \sigma_{zz_o} \qquad \ldots(1.22)$$

and by considering also the equilibrium of shears and couples on the element, we have:-

$$Q_x = \frac{\partial M_x}{\partial x} + \left(1 \mp \frac{h_1}{R}\right)\frac{\partial M_{xy}}{\partial y} + \frac{h_2}{2}\sigma_{zx_o} \qquad \ldots(1.23)$$

$$Q_y = \frac{\partial M_{xy}}{\partial x} + \left(1 \mp \frac{h_1}{R}\right)\frac{\partial M_y}{\partial y} + \frac{h_2}{2}\sigma_{zy_o} \qquad \ldots(1.24)$$

By substituting equations 1.23 and 1.24 into 1.22 to eliminate Q_x and Q_y we obtain:-

$$\frac{\partial^2 M_x}{\partial x^2} + \left(1 \mp \frac{2h_1}{R}\right)\frac{\partial^2 M_y}{\partial y^2} + 2\left(1 \mp \frac{h_1}{R}\right)\frac{\partial^2 M_{xy}}{\partial x \partial y} + \frac{h_2}{2}\left[\left(\frac{\partial \sigma_{zx}}{\partial x}\right)_o + \left(1 \mp \frac{h_1}{R}\right)\left(\frac{\partial \sigma_{zy}}{\partial y}\right)_o\right]$$

$$+ f_z h_2 = \frac{N_y}{R} \pm \sigma_{zz_o} \qquad \ldots(1.25)$$

By using equations 1.5 and 1.9 to obtain σ in terms of displacement, and by substituting equations 1.21 into 1.25 to eliminate M_x, M_y, and M_{xy} we obtain at the interface:-

$$D\nabla^4 w - \frac{h_2}{2}\left[N\left\{\frac{\partial^2 w}{\partial x^2} + \frac{\partial^2 u}{\partial x \partial z}\right\} + M\left\{\frac{\partial^2 v}{\partial z \partial y} + \frac{\partial^2 w}{\partial y^2}\right\}\right] \pm C\frac{dw}{dz} \pm \left[F\frac{\partial u}{\partial x} + G\frac{\partial v}{\partial y}\right]$$

$$- f_z h_2 = \frac{D}{R}\left[\pm 3h_1\nabla^2\frac{\partial^2 w}{\partial y^2} - \nabla^2\frac{\partial v}{\partial y}\right] \mp \frac{Mh_2}{2R}\left\{2h_1\frac{\partial^2 w}{\partial y^2} + h_1\frac{\partial^2 v}{\partial z \partial y} \pm \frac{\partial v}{\partial y}\right\}$$

$$+ \frac{G}{R}\left[h_1\frac{\partial v}{\partial y} \mp w\right] - \frac{E_m h_2}{R(1-\nu^2)}\left[\nu\frac{\partial u}{\partial x} + \frac{\partial v}{\partial y} + \frac{w}{R}\right] \qquad \ldots(1.26)$$

It will be seen that the last term is of order h_2/R^2 . This term has not been neglected because it is not multiplying a derivative and because E_m is assumed to be much greater than any of the core moduli.

Equations 1.10, 1.11, 1.12, 1.18, 1.19 and 1.26 constitute the total equilibrium equations of the composite plate when under the influence of the body force system p and f . (N.B. No external loading is included in these equations). For free motion the body forces can be expressed:-

$$p_i = -\frac{\rho_1}{g}\frac{\partial^2 u_i}{\partial t^2} \qquad (i = x, y, z)$$

$$f_i = -\left[\frac{\rho_2}{g}\frac{\partial^2 u_i}{\partial t^2} + \frac{\tau}{g h_2}\frac{\partial^2 u_i}{\partial t^2}\right]$$

ρ_1 = weight density of the core

u = displacement

where the adhesive mass is assumed to be spread uniformly over the face.

ρ_2 = weight density of the faces

τ = weight of bonding per unit area of face

If harmonic motion of frequency ω is a dynamic solution of interest

$$\frac{\partial^2 u_i}{\partial t^2} = -\omega^2 u_i$$

so

$$p_i = \rho_1 \frac{\omega^2}{g} u_i$$

$$f_i = \frac{\omega^2}{g} u_i \left[\rho_2 + \frac{\tau}{h_2}\right] = \rho f \frac{\omega^2}{g} u_i \qquad \ldots(1.27)$$

Equations 1.10, 1.11, 1.12, 1.18, 1.19, 1.26 and 1.27 now constitute the equations of harmonic motion of an elastic sandwich plate with a general anisotropic core, under the assumptions:-

(i) $\frac{h_2}{R}$ and $\frac{1}{R^2} \ll 1$

(ii) Core homogeneity

(iii) No shear deformation in the faces

1.5.3 The Differential Equations of Harmonic Vibration of Cylindrically Curved Honeycomb Cored Elastic Sandwich Plates

For honeycomb cores we have seen that we can assume that there are only three non-zero elastic moduli. In our notation these three moduli are C, M, and N. Some of the equations of motion can thus be simplified, and for honeycomb cores the six equations 1.10, 1.11, 1.12, 1.18, 1.19 and 1.26 can be rewritten:-

$$N\frac{\partial}{\partial z}\left[\frac{\partial u}{\partial z}+\frac{\partial w}{\partial x}\right] + p_x = -\frac{N}{R}\left[\frac{\partial u}{\partial z}+\frac{\partial w}{\partial x}\right] \qquad \ldots(1.28)$$

$$M\frac{\partial}{\partial z}\left[\frac{\partial v}{\partial z}+\frac{\partial w}{\partial y}\right] + p_y = \frac{M}{R}\left[z\frac{\partial^2 w}{\partial y \partial z} - \left(\frac{\partial v}{\partial z}+\frac{\partial w}{\partial y}\right)\right] \qquad \ldots(1.29)$$

$$N\frac{\partial}{\partial x}\left[\frac{\partial w}{\partial x}+\frac{\partial u}{\partial z}\right]+M\frac{\partial}{\partial y}\left[\frac{\partial w}{\partial y}+\frac{\partial v}{\partial z}\right]+C\frac{\partial^2 w}{\partial z^2}+p_z=\frac{1}{R}\left[z\frac{\partial}{\partial y}\left\{M\left[\frac{\partial v}{\partial z}+z\frac{\partial w}{\partial y}\right]\right\}+M\frac{\partial v}{\partial y}-C\frac{\partial w}{\partial z}\right] \ldots(1.30)$$

for core equilibrium in the three directions, x, y, and z. The three

boundary condition equations at the interface are:-

$$\frac{\partial^2 u}{\partial x^2} + \frac{1-\nu}{2}\frac{\partial^2 u}{\partial y^2} + \frac{1+\nu}{2}\frac{\partial^2 v}{\partial x \partial y} \mp \frac{h_2}{2}\frac{\partial}{\partial x}\nabla^2 w + \frac{1-\nu^2}{E_m} f_x =$$

$$\pm K\left(\frac{\partial w}{\partial x} + \frac{\partial u}{\partial z}\right) \pm \frac{1}{R}\left[h_1 \frac{1+\nu}{2}\frac{\partial^2 v}{\partial x \partial y} \mp \nu \frac{\partial w}{\partial x} + h_1(1-\nu)\frac{\partial^2 u}{\partial y^2}\right] \quad \ldots(1.31)$$

$$\frac{\partial^2 v}{\partial y^2} + \frac{1-\nu}{2}\frac{\partial^2 v}{\partial x^2} + \frac{1+\nu}{2}\frac{\partial^2 u}{\partial x \partial y} \mp \frac{h_2}{2}\frac{\partial}{\partial y}\nabla^2 w + \frac{1-\nu^2}{E_m} f_y =$$

$$\pm K^*\left(\frac{\partial w}{\partial y} + \frac{\partial v}{\partial z}\right) - \frac{K^*}{R}\left(h_1 \frac{\partial w}{\partial y} \pm v\right) \pm \frac{1}{R}\left[h_1 \frac{1+\nu}{2}\frac{\partial^2 u}{\partial x \partial y} \mp \frac{\partial w}{\partial y} + 2h_2 \frac{\partial^2 v}{\partial y^2} \mp \frac{K^* D}{M}\frac{\partial}{\partial y}\nabla^2 w\right] \quad \ldots(1.32)$$

$$D\nabla^4 w - \frac{h_2}{2}\left[N\frac{\partial}{\partial x}\left(\frac{\partial w}{\partial x} + \frac{\partial u}{\partial z}\right) + M\frac{\partial}{\partial y}\left(\frac{\partial v}{\partial z} + \frac{\partial w}{\partial y}\right)\right] \pm C\frac{dw}{dz} - f_z h_2 =$$

$$\frac{D}{R}\left[\pm 3h_1\nabla^2\frac{\partial^2 w}{\partial y^2} - \nabla^2\frac{\partial v}{\partial y}\right] \mp \frac{M h_2}{R}\left[2h_1\frac{\partial^2 w}{\partial y^2} + h_1\frac{\partial^2 v}{\partial y \partial z} \pm \frac{\partial v}{\partial y}\right] \quad \ldots(1.33)$$

$$- \frac{E_m h_2}{R(1-\nu^2)}\left[\nu\frac{\partial u}{\partial x} + \frac{\partial v}{\partial y} + \frac{w}{R}\right]$$

and it will be observed that equations 1.31 and 1.32 are identical to equations 1.18 and 1.19 as no simplification of these is possible.

1.6 Solutions of the Equations Listed in § 1.5.3

1.6.1 A Separable Form of Solution for Curved Panels

Let us assume a separable solution of the form:-

$$w = W(z)\sin\frac{n\pi x}{a}\sin\frac{m\pi y}{b} \quad \ldots(1.34)$$

which can only hold for simply-supported edges. The in-plate deflections u and v must then take the form:-

$$u = U(z) \cos \frac{n\pi x}{a} \sin \frac{m\pi y}{b} \qquad \ldots(1.35)$$

and

$$v = V(z) \sin \frac{n\pi x}{a} \cos \frac{m\pi y}{b} \qquad \ldots(1.36)$$

If equations 1.34, 1.35 and 1.36 are now substituted into the core equilibrium equations 1.28, 1.29 and 1.30 we obtain:-

(i) Equation (1.28)

$$\left[N\delta^2 + N\frac{\delta}{R} + \rho_1 \frac{\omega^2}{g}\right]U + N\frac{n\pi}{a}\left[\delta + \frac{1}{R}\right]W = 0 \qquad \ldots(1.37)$$

where δ is an operator denoting differentiation with respect to z;

(ii) Equation (1.29)

$$\left[M\delta^2 + M\frac{\delta}{R} + \rho_1 \frac{\omega^2}{g}\right]V + M\frac{m\pi}{b}\left[\left(1 - \frac{z}{R}\right)\delta + \frac{1}{R}\right]W = 0 \qquad \ldots(1.38)$$

(iii) Equation (1.30)

$$-N\frac{n\pi}{a}\delta U - M\frac{m\pi}{b}\left[\left(1 - \frac{z}{R}\right)\delta - \frac{1}{R}\right]V + \left[C\delta^2 + C\frac{\delta}{R} - \left\{N\left(\frac{n\pi}{a}\right)^2 + M\left(\frac{m\pi}{b}\right)^2 - 2\frac{Mz}{R}\left(\frac{m\pi}{b}\right)^2 - \rho_1\frac{\omega^2}{g}\right\}\right]W = 0 \qquad \ldots(1.39)$$

Equations 1.37, 1.38 and 1.39 are three simultaneous differential

equations in U, V, and W . The solution of these equations is complicated because the coefficients are, in some cases, variable (with z). It was thought that it might be simple to find a series type of solution to this set of equations, but this proved to be immensely cumbersome and was not completed. It was found that the six modes for the curved plate corresponding to the three symmetric and the three anti-symmetric modes for the flat plate (N.B. these modes for the curved plate are in fact neither symmetric or anti-symmetric) were coupled together, whereas for the flat plate the symmetric and anti-symmetric modes were uncoupled. The degenerate case of the flat plate can be solved by putting $1/R = 0$. A solution for curved plates is given in § 1.6.3.

1.6.2 A Solution for Flat Panels

It is now assumed that the coupling between symmetric modes with the same nodal pattern is negligible and similarly that the coupling between anti-symmetric modes with the same nodal pattern negligible. This coupling exists by virtue of x-wise and y-wise inertia forces in the core, but is only significant when the core is very heavy or the face plates are very thick. Hence we ignore the in-plate inertia terms of the core for flexural and bubbling modes. Equations 1.37 and 1.38 and 1.39 now become :-

(i) Equation (1.37)

$$\delta^2 U + \frac{n\pi}{a} \delta W = 0 \qquad \ldots(1.40)$$

(ii) Equation (1.38)

$$\delta^2 V + \frac{m\pi}{b}\,\delta W = 0 \qquad \ldots(1.41)$$

(iii) Equation (1.39)

$$-N\frac{n\pi}{a}\delta U - M\frac{m\pi}{b}\delta V + \left[C\delta^2 - \left(N\left(\frac{n\pi}{a}\right)^2 + M\left(\frac{m\pi}{b}\right)^2 - \rho_1\frac{\omega^2}{g}\right)\right]W = Q \qquad \ldots(1.42)$$

Integration of equations 1.40 and 1.41 gives:-

$$\frac{dU}{dz} = -\frac{n\pi}{a}W + U_I \qquad \ldots(1.43)$$

and

$$\frac{dV}{dz} = -\frac{m\pi}{b}W + V_I \qquad \ldots(1.44)$$

and substituting 1.43 and 1.44 in 1.42 gives:-

$$C\frac{d^2W}{dz^2} + \rho_1\frac{\omega^2}{g}W = M\frac{m\pi}{b}V_I + N\frac{n\pi}{a}U_I \qquad \ldots(1.45)$$

The solution of the differential equation 1.45 is:-

$$W = A\sin\beta z + H\cos\beta z + \frac{g}{\rho_1\omega^2}\left\{M\frac{m\pi}{b}V_I + N\frac{n\pi}{a}U_I\right\} \qquad \ldots(1.46)$$

Substituting equation 1.46 into 1.43 and 1.44 we find the

corresponding modal shapes of U and V , thus:-

$$U = -\frac{n\pi}{a}\left[-\frac{Д}{\beta}\cos\beta z + \frac{И}{\beta}\sin\beta z + \frac{zg}{\rho_1\omega^2}\left\{M\frac{m\pi}{b}Ш + N\frac{n\pi}{a}Ч\right\}\right] + Чz + Я \quad \ldots(1.47)$$

$$V = -\frac{m\pi}{b}\left[-\frac{Д}{\beta}\cos\beta z + \frac{И}{\beta}\sin\beta z + \frac{zg}{\rho_1\omega^2}\left\{M\frac{m\pi}{b}Ш + N\frac{n\pi}{a}Ч\right\}\right] + Шz + Ю \quad \ldots(1.48)$$

The solutions for U, V, and W (equations 1.46, 1.47 and 1.48) have one part corresponding to the symmetric modes, the other corresponding to the anti-symmetric modes. It can easily be shown, by substituting these equations into the boundary condition equations 1.31, 1.32 and 1.33, that the symmetric and anti-symmetric parts are not coupled in any way. They can therefore be treated separately.

1.6.2.1 A Solution for Flexural Modes of Flat Panels Ignoring Rotatory Inertia

Extracting the anti-symmetric parts of equations 1.46, 1.47 and 1.48 we have:-

$$W = И\cos\beta z + \frac{g}{\rho_1\omega^2}\left[M\frac{m\pi}{b}Ш + N\frac{n\pi}{a}Ч\right]$$

$$U = -\frac{n\pi}{a}\left[\frac{И}{\beta}\sin\beta z + \frac{zg}{\rho_1\omega^2}\left\{M\frac{m\pi}{b}Ш + N\frac{n\pi}{a}Ч\right\}\right] + Чz$$

$$V = -\frac{m\pi}{b}\left[\frac{И}{\beta}\sin\beta z + \frac{zg}{\rho_1\omega^2}\left\{M\frac{m\pi}{b}Ш + N\frac{n\pi}{a}Ч\right\}\right] + Шz \quad \ldots(1.49)$$

If these equations are substituted into the boundary condition equations 1.31, 1.32 and 1.33 with 1/R = 0, we then obtain a set of three homogeneous equations in $И$, $Ч$, and $Ш$. Thus a

determinantal frequency equation is obtained. For long wavelength flexural modes the in-plate inertia forces of the faces can be regarded as small and the f_x and f_y terms in equations 1.31 and 1.32 are thus neglected. This assumption is effectively that of ignoring rotatory inertia for ordinary sandwich plates and has been shown to hold true both by the author and by Yu[11].

The resulting frequency equation in matrix form is then:

$$\begin{bmatrix} \frac{n\pi\ell^2}{a}\left[\frac{\sin\phi}{\beta}+\frac{h_2}{2}\cos\phi\right] & M\left[\frac{mn\pi^2}{ab}\frac{g\ell^2}{\rho_1\omega^2}\left(h_1+\frac{h_2}{2}\right) - \frac{mn\pi^2}{ab}\frac{h_1}{M}\frac{1+\nu}{2}\right] & N\left[\left(\frac{n\pi}{a}\right)^2\frac{g\ell^2}{\rho_1\omega^2}\left(h_1+\frac{h_2}{2}\right) - \frac{h_1\varepsilon}{N}-\frac{K}{N}\right] \\ \frac{m\pi\ell^2}{b}\left[\frac{\sin\phi}{\beta}+\frac{h_2}{2}\cos\phi\right] & M\left[\left(\frac{m\pi}{b}\right)^2\frac{g\ell^2}{\rho_1\omega^2}\left(h_1+\frac{h_2}{2}\right) - \frac{K^*}{M}-\frac{h_1\varepsilon^*}{M}\right] & N\left[\frac{mn\pi^2}{ab}\frac{g\ell^2}{\rho_1\omega^2}\left(h_1+\frac{h_2}{2}\right) - \frac{mn\pi^2}{ab}\frac{h_1}{N}\frac{1+\nu}{2}\right] \\ \left(D\ell^4-h_2\rho_f\frac{\omega^2}{g}\right)\cos\phi - C\beta\sin\phi & M\left[\left(D\ell^4-h_2\rho_f\frac{\omega^2}{g}\right)\frac{g}{\rho_1\omega^2}\frac{m\pi}{b} + \frac{h_2}{2}\frac{m\pi}{b}\right] & N\left[\left(D\ell^4-h_2\rho_f\frac{\omega^2}{g}\right)\frac{g}{\rho_1\omega^2}\frac{n\pi}{a} + \frac{h_2}{2}\frac{n\pi}{a}\right] \end{bmatrix} \begin{Bmatrix} H \\ W \\ Y \end{Bmatrix} = 0 \quad \ldots(1.50)$$

where $\beta^2 = \frac{\omega^2}{g}\rho_1$, $\phi = \beta h_1$, $\ell^2 = \left(\frac{n\pi}{a}\right)^2 + \left(\frac{m\pi}{b}\right)^2$,

$\varepsilon = \left(\frac{n\pi}{a}\right)^2 + \frac{1-\nu}{2}\left(\frac{m\pi}{b}\right)^2$, and $\varepsilon^* = \left(\frac{m\pi}{b}\right)^2 + \frac{1-\nu}{2}\left(\frac{n\pi}{a}\right)^2$

The frequency equation is obtained by putting the determinant of the matrix equal to zero. This equation is then easily non-dimensionalised by substituting the following non-dimensional

quantities:-

$$\mu = \frac{h_2}{h_1} \qquad A_n = \frac{a}{nh_1} \qquad A_m = \frac{b}{mh_1}$$

$$\lambda = \frac{E}{C} = \frac{\rho_2}{\rho_1} \qquad \bar{\varepsilon} = h_1^2 \varepsilon \qquad \bar{\varepsilon}^* = h_1^2 \varepsilon^*$$

$$\gamma = \frac{N}{C} \qquad \bar{\psi} = h_1^2 \ell^2$$

$$\frac{3\gamma}{2} = \frac{M}{C}$$

and by suitable rearrangement to obtain zeros the determinantal frequency equation becomes:-

$$\begin{vmatrix} 0 & \left[A_m^2\left(\bar{\varepsilon}^* + \frac{3\gamma}{2\mu\lambda}(1-\nu^2)\right) - \pi^2\frac{1+\nu}{2}\right] & \left[\frac{5}{4}\pi^2(1+\nu) - \frac{3}{2}A_n^2\bar{\varepsilon} - A_m^2\bar{\varepsilon}^* - \frac{3\gamma}{2\mu\lambda}(1-\nu^2)(A_n^2+A_m^2)\right] \\ \bar{\psi}\pi\left[\frac{\sin\phi}{\phi} + \frac{\mu}{2}\cos\phi\right] & A_m^2\left[\left(1+\frac{\mu}{2}\right)\frac{3\gamma\bar{\psi}\pi^2}{2A_m^2\phi^2} - \bar{\varepsilon}^* - \frac{3\gamma}{2\mu\lambda}(1-\nu^2)\right] & \left[A_m^2\left(\bar{\varepsilon}^* + \frac{3\gamma}{2\mu\lambda}(1-\nu^2)\right) - \frac{3\pi^2}{2}\frac{1+\nu}{2}\right] \\ \lambda\mu\cos\phi\left(\frac{\mu^2\bar{\psi}^2}{12(1-\nu^2)} - \phi^2\right) - \phi\sin\phi & \frac{3\pi\gamma}{2}\left[\frac{\mu}{2} - \mu\lambda + \frac{\lambda\mu^3\bar{\psi}^2}{12(1-\nu^2)\phi^2}\right] & 0 \end{vmatrix} \qquad \ldots(1.51)$$

It will be observed that ρ_f/ρ_1 has been replaced by λ in some places and that in this way the weight of the bonding has been omitted. This has been done so that non-dimensional graphs of frequency can be plotted against the variables A_n, A_m and μ (γ and λ are regarded as constants for one type of honeycomb). The results of computations using equation 1.51 are shown in Fig. 3.

All of the graphs at the end of this chapter were computed using quantities associated with British CIBA (ARL) 'Aeroweb' honeycomb type 142. This aluminium foil honeycomb, with a cell size of 0.25 inches,

is commonly used by the British Aircraft Industry. Other design graphs, like those given in this report, however, can easily be constructed for other materials by solving the equations given herein. Values of constants for 'Aeroweb' 142 are as follows:-

$$M = 31{,}900 \text{ lb/in}^2$$

$$N = 21{,}300 \text{ lb/in}^2$$

$$C = 238{,}640 \text{ lb/in}^2$$

$$\rho_1 = 4 \text{ lb/ft}^3$$

and the constants used were:-

$$E_m = 10^7 \text{ lb/in}^2 \text{ (Aluminium)}$$

$$c = 1123 \text{ ft/sec (air)}$$

$$g = 32.2 \text{ ft/sec}^2$$

$$\rho_2 = 167.5 \text{ lb/ft}^3$$

$$\tau = 0.09228 \text{ lb/ft}^2$$

$$\nu = 0.34 \text{ (Aluminium)}$$

The range of values of parameters for which these computations were carried out is as follows:-

(i) Non-dimensional wavelength

$$\text{From } A_{n,m} = 16 \text{ to } A_{n,m} = 96$$

(ii) Core-face-plate thickness ratio

$$\text{From } \mu = 0.05 \text{ to } \mu = 0.20$$

For a particular honeycomb panel the apparent natural frequency, ω_o , is computed from the value of ϕ thus:-

$$\omega_o = \frac{\phi}{h_1}\sqrt{\frac{Cg}{\rho_1}} \qquad \ldots(1.52)$$

and this must then be corrected for the mass of the interface adhesive using the equation

$$\left(\frac{\omega}{\omega_o}\right)^2 = \frac{\rho_1 + \mu\rho_2}{\rho_1 + \mu\rho_2 + \frac{12\tau}{h_1}} \qquad \ldots(1.53)$$

where h_1 is measured in inches and τ is in lb/ft^2.

This equation has been derived assuming that w does not vary with z in the core (flexural modes only).

This method of correction does not give exact answers, but the maximum error for the range of values of the variables used in the computations is small (not greater than 4 per cent). Equations 1.52 and 1.53 are plotted in Figs. 4 and 5 for use in calculating natural frequencies of actual sandwich panels in conjunction with graphs similar to Fig. 3 (N.B. Fig. 3 applies only to sandwiches with cores of CIBA honeycomb type 142 and aluminium faces).

1.6.2.2 A Solution for Bubbling Modes of Flat Panels

Again, the in-plane inertia of the core is neglected as it will be small. The symmetric mode of principal interest is the bubbling mode because its frequency is lower than the frequencies of the corresponding longitudinal modes (to which it is only very lightly coupled - § 1.6.2).

Extracting the symmetric parts of equations 1.46, 1.47 and 1.48 we find for symmetric modes that:

$$W = \mathcal{A} \sin \beta z$$

$$U = \frac{n\pi}{a} \frac{\mathcal{A}}{\beta} \cos \beta z + \mathcal{R}$$

$$V = \frac{m\pi}{b} \frac{\mathcal{A}}{\beta} \cos \beta z + \mathcal{W}$$

...(1.54)

If this set of equations is now substituted into the interface boundary condition equations 1.31, 1.32 and 1.33 with $1/R = 0$ (as before in § 1.6.2.1) a set of homogeneous equations in $\mathcal{A}$, $\mathcal{R}$, and $\mathcal{W}$ is found, thus:-

$$\begin{bmatrix} \ell^2 \frac{n\pi}{a}\left[\frac{\cos\beta h_1}{\beta} - \frac{h_2}{2}\sin\beta h_1\right] & \varepsilon & \frac{1+\nu}{2}\frac{mn\pi^2}{ab} \\ \ell^2 \frac{m\pi}{b}\left[\frac{\cos\beta h_1}{\beta} - \frac{h_2}{2}\sin\beta h_1\right] & \frac{1+\nu}{2}\frac{mn\pi^2}{ab} & \varepsilon^* \\ \left[D\ell^4 - h_2\rho_f\frac{\omega^2}{g}\right]\sin\beta h_1 + C\beta\cos\beta h_1 & 0 & 0 \end{bmatrix} \begin{Bmatrix} \mathcal{A} \\ \mathcal{R} \\ \mathcal{W} \end{Bmatrix} = 0$$

...(1.55)

The only permissible solution to this equation is:-

$$\tan\beta h_1 = - \frac{C\beta}{\left[D\ell^4 - h_2\rho_f\frac{\omega^2}{g}\right]}$$

...(1.56)

or, by using the non-dimensional form of § 1.6.2.1:-

$$\tan\phi = \frac{\phi}{\mu\lambda\phi^2 - \dfrac{\lambda\mu^3\bar{\psi}^2}{12(1-\nu^2)}} \qquad \ldots(1.57)$$

It has been found that the second term in the denominator of the right hand side of equation 1.57 is much smaller (10^{-4} x at least) than the first term, for ordinary sandwich plates, and it can therefore be neglected. Equation 1.57 then becomes:-

$$\mu\lambda\phi\tan\phi - 1 = 0 \qquad \ldots(1.58)$$

Thus the bubbling mode frequency is virtually independent of wavelength. This would be expected because the contribution of the flexural strain energy of the face plates to the total strain energy is clearly very small.

Bubbling mode frequency parameter is shown plotted against μ in Fig. 6.

Here again for non-dimensional plotting λ has been used in place of ρ_f / ρ_1 . However, for the bubbling mode, w varies considerably with z and the mass ratio of equation 1.53 will not apply. The generalised mass in this mode will depend on an integration of mass times displacement squared throughout the depth of the plate. If we assume the face and bonding to move as point masses, and if we assume a linear deformation of the core (this latter should be sufficiently accurate, as the core is usually much lighter than the

faces) then the frequency correction equation corresponding to equation 1.53 becomes:-

$$\left(\frac{\omega}{\omega_0}\right)^2 = \frac{\rho_1 + 3\rho_2\mu(1+\mu)}{\rho_1 + 3\rho_2\mu(1+\mu) + 36\tau/h_1} \qquad \ldots(1.59)$$

for bubbling modes. This is plotted in Fig. 7.

1.6.2.3 Flat Panel Thickness Shear and Longitudinal Modes

These vibration modes are of less interest than the flexural and bubbling modes because they are usually of a higher natural frequency and because they would not be directly excited by normal pressures. However, in certain cases, it may be desirable to calculate their natural frequencies and this can be done by including the in-plate inertias in the equilibrium and boundary condition equations. The frequency equations can be found as before but the solution (i.e. finding the roots of the determinantal equation) is rather more tedious.

1.6.3 A Solution for Cylindrically Curved Panels

In § 1.6.1 a separable form of solution was assumed for a cylindrically curved panel and equations 1.37, 1.38 and 1.39 were derived for the z-wise variation of the three orthogonal deflections in the core. Inertia terms in the plane of the plate are now ignored for flexural and bubbling vibrations and these core equilibrium

equations become:

$$\left[\delta^2 + \underline{\underline{\frac{\hat{r}}{h_1}\delta}}\right]U + \frac{n\pi}{a}\left[\delta + \underline{\underline{\frac{\hat{r}}{h_1}}}\right]W = 0 \qquad \ldots(1.67)$$

$$\left[\delta^2 + \underline{\underline{\frac{\hat{r}}{h_1}\delta}}\right]V + \frac{m\pi}{b}\left[\left(1 - \frac{z}{h_1}\hat{r}\right)\delta + \underline{\underline{\frac{\hat{r}}{h_1}}}\right]W = 0 \qquad \ldots(1.68)$$

$$C\delta^2 W = N\frac{n\pi}{a}\delta U + M\frac{m\pi}{b}\left[\left(1 - \frac{z}{h_1}\hat{r}\right)\delta - \frac{\hat{r}}{h_1}\right]V$$
$$+ \left[-C\hat{r}\frac{\delta}{h_1} + \left\{N\left(\frac{n\pi}{a}\right)^2 + M\left(\frac{m\pi}{b}\right)^2 - \rho_1\frac{\bar{\omega}_n^2}{g}\right\} - 2M\frac{z}{h_1}\hat{r}\left(\frac{m\pi}{b}\right)^2\right]W \qquad \ldots(1.69)$$

Now an exact solution of these core equilibrium equations is not feasible and an alternative approach must be sought. If the terms in the core equations with r as a factor are neglected the general solution can be found for the core, exactly similar to the flat plate core deflection solution given in equations 1.47, 1.48 and 1.49. Applying the curved boundary conditions of equations 1.31, 1.32 and 1.33 to this core solution (i.e. retaining the 1/R terms here) we can obtain a set of frequencies and modes shapes for this hypothetical condition which will be denoted by a zero subscript. An attempt was made to perturb this solution for deflection of the core in order to obtain a more accurate solution for the complete curved problem. In fact we will argue that the frequency obtained using the flat plate core deflection is sufficiently accurate for this particular core configuration. The hypothetical core deflection solution is perturbed

in order to fit it to the full core equilibrium equations 1.67, 1.68 and 1.69 above, thus:

$$U_n = U_{n_0} + \hat{r}\, U_{n_0}^*$$

$$V_n = V_{n_0} + \hat{r}\, V_{n_0}^*$$

$$W_n = W_{n_0} + \hat{r}\, W_{n_0}^*$$

...(1.70)

and a perturbation of frequency must also be allowed:

$$\bar{\omega}_n = \omega_{n_0} + \hat{r}\, \omega_{n_0}^* \qquad \text{...(1.71)}$$

In this way, only a first-order perturbation is allowed, but this will be sufficient for sufficiently small r. If equations 1.70 are now substituted into equations 1.67, 1.68 and 1.69, the terms with different powers of r can be separately equated to zero because the equations are valid for all r. The equations of order one are:

$$\delta^2 U_{n_0} + \frac{n\pi}{a}\,\delta W_{n_0} = 0$$

$$\delta^2 V_{n_0} + \frac{m\pi}{b}\,\delta W_{n_0} = 0$$

$$-N\frac{n\pi}{a}\delta U_{n_0} - M\frac{m\pi}{b}\delta V_{n_0} + \left[C\delta^2 - \left\{N\left(\frac{n\pi}{a}\right)^2 + M\left(\frac{m\pi}{b}\right)^2 - \rho_1 \frac{\omega_{n_0}^2}{g}\right\}\right] W_{n_0} = 0$$

...(1.72)

These equations correspond exactly to equations 1.40, 1.41 and 1.42. The solution of equations 1.72 is exactly similar to the flat

plate solution obtained earlier, equations 1.46, 1.47 and 1.48, but the constants will be slightly different (they will be denoted $\psi, \omega, \lambda, \eta, \rho, \kappa$) because curvature terms will be retained in the boundary conditions (equations 1.31, 1.32 and 1.33).

Now the equations of order $\hat{r}$ derived from the substitution of the perturbed deflection are as follows:

$$\delta^2 U_{n_0}^* + \frac{n\pi}{a}\delta W_{n_0}^* = -\left[\delta U_{n_0} + \frac{n\pi}{a} W_{n_0}\right]$$

$$\delta^2 V_{n_0}^* + \frac{m\pi}{b}\delta W_{n_0}^* = -\left[\delta V_{n_0} + \frac{m\pi}{b}(1-z\delta) W_{n_0}\right]$$

$$-N\frac{n\pi}{a}\delta U_{n_0}^* - M\frac{m\pi}{b}\delta V_{n_0}^* + \left[C\delta^2 - \left\{N\left(\frac{n\pi}{a}\right)^2 + M\left(\frac{m\pi}{b}\right)^2 - \rho_1\frac{\omega_{n_0}^2}{g}\right\}\right] W_{n_0}^* =$$

$$-M\frac{m\pi}{b}(1+z\delta)V_{n_0} - \left[C\delta + 2Mz\left(\frac{m\pi}{b}\right)^2\right] W_{n_0} \qquad \ldots(1.73)$$

This set of equations gives the differential relationships for the perturbation deflections $U_{n_0}^*$, etc., and because these functions must also satisfy the identical boundary conditions to the solution of equations 1.72 we can expand them as an infinite series of the natural modes of equations 1.72 but omitting the mode with which we are concerned i.e.

$$U_{r_0}^* = \sum_{\substack{n=1 \\ n\neq r}}^{\infty} a_n U_{n_0}$$

$$V_{r_0}^* = \sum_{\substack{n=1 \\ n\neq r}}^{\infty} a_n V_{n_0}$$

$$W_{r_0}^* = \sum_{\substack{n=1 \\ n\neq r}}^{\infty} a_n W_{r_0} \qquad \ldots(1.74)$$

Note that a_n is the same for all series as the combination U, V, W makes up the natural mode. Substitution of equation 1.74 into equations 1.73 gives:

(a) For the first two equations, some trivial equation because inertia terms have been dropped.

(b) For the third equation:

$$\frac{\rho_1}{g}\sum_{\substack{n=1\\ n\neq r}}^{\infty} a_n\left(\omega_{r_o}^2-\omega_{n_o}^2\right)W_{n_o} = -M\frac{m\pi}{b}\left(1+z\delta\right)V_{r_o}-\left[C\delta+\frac{\rho_1}{g}2\omega_{r_o}\omega_{r_o}^{*}+2Mz\left(\frac{m\pi}{b}\right)^2\right]W_{r_o} \quad \ldots(1.75)$$

If equation 1.75 is differentiated with respect to z, multiplied by δW_{r_o}, and integrated over the z-domain, we get:

$$\begin{aligned}\frac{\rho_1}{g}\sum_{\substack{n=1\\ n\neq r}}^{\infty}\left\{a_n\left(\omega_{r_o}^2-\omega_{n_o}^2\right)\int_{-h_1}^{h_1}\delta W_{n_o}\delta W_{r_o}\,dz\right\} &= -M\frac{m\pi}{b}\int_{-h_1}^{h_1}\left(2\delta+z\delta^2\right)V_{r_o}\,\delta W_{r_o}\,dz\\ &\quad-\int_{-h_1}^{h_1}\left(C\delta^2+2M\left(\frac{m\pi}{b}\right)^2+2Mz\left(\frac{m\pi}{b}\right)^2\delta\right)W_{r_o}\,\delta W_{r_o}\,dz\\ &\quad-\frac{\rho_1}{g}2\omega_{r_o}\omega_{r_o}^{*}\int_{-h_1}^{h_1}\delta W_{r_o}\,\delta W_{r_o}\,dz \qquad \ldots(1.76)\end{aligned}$$

Now the first two terms on the right hand side of equation 1.76 can be neglected. If the combination U_{r_o}, V_{r_o}, W_{r_o} was either a purely symmetrical or a purely anti-symmetrical mode these two terms would be identically zero because the integrands would be odd functions of z (the z-domain being from $z = -h_1$ to $z = h_1$). Now this would be true for flat plate core deflection solutions when bounded by flat face-plates (the problem in § 1.6.2). However, for curved face-plates bounding a flat plate core deflection, small cross-coupling

terms exist between the symmetrical and anti-symmetrical core modes. The modes previously called 'symmetrical' now have a very small anti-symmetric component and vice-versa. Thus, these two integrals have non-zero, but small values derived from the cross-coupling between the now wrongly called symmetric and anti-symmetric modes. These terms, being small, will be neglected. The equation 1.76 then reduces to:

$$\frac{\omega_{r_o}^*}{\omega_{r_o}} = \sum_{\substack{n=1 \\ n\neq r}}^{\infty} \frac{a_n}{2}\left(\frac{\omega_{n_o}^2}{\omega_{r_o}^2} - 1\right) \quad \frac{\int_{-h_1}^{h_1} \delta W_{r_o}\, \delta W_{n_o}\, dz}{\int_{-h_1}^{h_1} \delta W_{r_o}\, \delta W_{r_o}\, dz} \qquad \ldots(1.77)$$

If the flat plate core deflection solution is to be a sufficiently accurate solution for this problem then it must be shown that $\omega_{r_o}^*/\omega_{r_o}$ is a small quantity ($\ll$ 1). If this can be proved then we can say that $\overline{\omega_r}$ is sufficiently represented by ω_{r_o}, the error term being of second order of small magnitude, and only a flat plate core deflection solution is needed to find this frequency. In order to show that $\omega_{r_o}^*/\omega_{r_o}$ is small we must:

(a) Find some value for a_n, using an orthogonality condition.

(b) Show that the product of the large term $\left(\frac{\omega_{n_o}^2}{\omega_{r_o}^2} - 1\right)$ a_n, and the ratio of integrals is small.

(c) Show that the series converges, and that it converges on to a small value.

These tasks are complicated and have not, as yet, been completed. However, this hypothetical solution can be shown intuitively to be a

good approximation. The application of the face plate boundary conditions to a core solution of deflection for honeycomb sandwiches is, in essence, a matching of the surface impedances of the face plates to the core. Now following from the explanation in the introduction, the surface impedances of a curved plate to flexural type deflection are considerably different from those of a flat plate because in-plane direct strain occurs. On the other hand, the surface impedance of a cylindrical honeycomb core of normal proportions is likely to be little different from that of a flat core since direct in-plane strain effects are negligible (A and B are very small) and curvature shear effects (terms underlined in equations 1.67 and 1.68) are also likely to be negligible. Therefore, the use of a flat core deflection solution (and hence of a flat core surface impedance) should not give rise to large errors in the natural frequencies of curved sandwich plates. The effect of curvature on the assembled plate is restricted to the face plates, therefore, which will be stiffer when curved. Thus, the matching of impedances which occurs when the full face-plate boundary conditions are applied to the flat plate core deflection solution will ensure that the major effects of curvature are included in this analysis. ω_{n_o} will therefore give a good approximation to the true natural frequency.

The solution for ω_{n_o} is easily found by substituting a flat plate type core solution for deflection (see equations 1.46, 1.47 and 1.48) into the curved plate boundary condition equations, viz. equations 1.31, 1.32 and 1.33.

Six homogeneous equations result thus:

$$\left[A\right]\left\{Ч'\right\} = 0 \qquad \ldots(1.78)$$

where $\{Ч'\}$ is the column vector $\{Ч', Ш', Д', И', Я', Ю'\}$

The characteristic determinant of equation 1.78 is equated to zero to give natural frequencies. A simplified and non-dimensionalised form of this determinant is shown in Table 1. The characteristic equation has been solved numerically for flexural and bubbling frequencies using a digital computer. The numerical method used to obtain the solution of the characteristic equation was a successive application of the rule of false position. Results are shown in Tables 2 and 3 and specimen graphs show typical variation of frequency with the various parameters involved. The frequencies were evaluated for the set of constants and the range of wavelength given in § 1.6.2.1. The range of values of $\hat{r}$ for which frequencies were calculated is from $\hat{r}$ = zero to $\hat{r}$ = 0.020. This range is likely to cover the curvatures of fuselage, wing and control surface panels. A correction to be applied to frequencies to take account of the bonding mass is, to the same degree of approximation used in the solution, the same as that given in § 1.6.2.1 and 1.6.2.2 for flexural and bubbling modes of flat panels.

1.7 Conclusions

This analysis has assumed that a state of plane stress exists in the face plates of the sandwich and an exact deformation solution has been found for the core under this assumption. On the other hand, Yu, in his recent work, has made the assumption of planar deformation in the core but has included shear effects in the face plates. Yu's analysis therefore applies to vibrations of sandwich plates with all thicknesses of face plates but is frequency limited because of the breakdown of the planar deformation assumption at high frequency. Thus, his work applies perfectly adequately to the low-order flexural vibrations of most sandwich plates. This paper is necessarily limited in application to sandwiches with thinner face plates, but will treat high frequency modes (bubbling modes for example) with accuracy. As this work is being carried out with aircraft sandwich structures specifically in mind, the assumption that face plates are thin is reasonable. The analysis of this paper applies down to wavelengths of approximately four inches (for a core depth of 0.5 inches and a cell size of 0.25 inches). The cell size is the critical parameter for the lower limit of wavelength because the assumption of a homogeneous core becomes doubtful when the plate half-wavelength is less than about 16 times the cell size. This length, however, should be adequate enough for the analysis of first-order modes of typical aircraft sandwich panels.

The vibration solution for sandwich plates has been found by solving the core differential equations under the boundary conditions imposed on them by the face plates. The determinantal frequency

equations for the flexural and bubbling modes (predominantly z-wise motions) have been obtained by neglecting the in-plane-of-plate inertia of the core and faces. This assumption, which is, in effect, the neglect of rotatory inertia, has been found to be sufficiently accurate for all of the configurations of sandwich plate under consideration (Yu also draws the same conclusion in reference 11). These equations are in non-dimensional form for ease of display, and, because the bonding weight has been included in the analysis, a correction has been applied to the frequencies obtained, as this parameter could not be included in non-dimensional work. This correction is not exact, but it does not give rise to errors in excess of 4% over the ranges of variables considered. The error is due, of course, to the assumed form of displacement used in the calculation of the generalised mass. For flat plates, flexural mode frequencies, in their non-dimensional form, are shown in Fig. 1 for various values of μ , the ratio of skin to core thickness. Bubbling mode frequencies are shown in Fig. 6. Neither the cross-sectional mode shapes for the flexural modes nor those for the bubbling modes have been computed. For flat plates, these ratios can easily be found however by substituting the appropriate frequency back into either equation 1.50 or equation 1.55. Figs. 3 and 6 for frequencies of flexural and bubbling modes of flat plates were computed for CIBA(A.R.L.) 'Aeroweb' Honeycomb type number 3142, which is a honeycomb commonly used by the British Aircraft Industry.

Fig. 3 shows that the variation of frequency with wavelength takes the usual form. It was found that the bubbling mode frequencies were

virtually independent of wavelength (see Fig. 6), for the range of wavelengths considered. This is due to the relatively small amount of strain energy stored by flexure of the face plates. Computations carried out by the author, but not described here, have shown that Rotatory Inertia of the cross-sections can be safely regarded as negligible for the range of values described in § 1.6.2.1 but that shear deformation effects in the core must be included for an accurate analysis of the flexural and bubbling vibrations of sandwich plates. This confirms the identical conclusion reached by Yu in reference 11.

The frequencies of flexural and bubbling modes have also been found for cylindrically curved sandwich plates. They are shown in their non-dimensional formin Tables 2 and 3. The anomalous variation of frequency with circumferential wavelength shown in Fig. 9 was not unexpected. This effect, viz. a decrease in frequency with decrease in circumferential wavelength for some plate configurations, is associated with the relative proportions of strain energy stored by flexure and in-plane stretching, and was first found and explained by Arnold and Warburton[19]. It should be noted, however, that this effect is only sufficiently significant to show this decrease in frequency with a decrease in wavelength at higher curvatures. An inspection of Table 2 will confirm this statement. (i.e. Fig. 9 is not a typical variation of frequency with circumferential wavelength). Figs. 10, 11 and 12 show the typical variations of flexural frequency with axial wavelength, skin-core thickness ratio, and curvature respectively.

Fig. 13 shows the variation of bubbling mode frequency with skin-core thickness ratio for the curved plates. For the ranges of

parameters chosen it was found that the variation of bubbling mode frequency with both wavelengths and curvature was only very slight. The maximum variation of this frequency with wavelength was less than 0.1%, and with curvature less than 0.2%. This is due, in exactly the same way as it was for flat plates, to the high proportion of strain energy stored in direct stretching of the core, compared with the strain energy stored in flexure and stretching of the faces.

A correction must be applied to the computed natural frequencies of curved plates to take account of the bonding mass. Now the curved plate core mode shape has been assumed, on reasonable grounds, to be of the same form as the flat plate core mode shape, to the first order of magnitude. Therefore the correction equations 1.53 and 1.59 for flat panels (and also Figs. 5 and 7) will apply to the flexural and bubbling mode frequencies of the curved panel.

The ranges of parameters chosen for the computations of natural frequencies of curved plates were the same as those chosen for the flat panel. These ranges were considered to be representative of aircraft structural elements. The values of curvature used in the computations covered the range which included low curvature wing panels and the higher curvature fuselage panels.

The modal shapes have not been computed for the curved plate core because of the complexity of the terms involved. However, these mode shapes can be found by substituting the frequency back into the equation 1.78 in the usual way.

The problem has not yet been solved of showing analytically that

the flat-plate core deflections applied to the curved boundary conditions do give satisfactory values for curved plate frequencies. The difficulties involved in showing that the perturbation of frequency will only be of second order of small magnitude compared with the first order perturbation of deflection have been described in the text. However, it has been possible to explain why this simplification can be made, on physical grounds. It appears to give reasonable results which conform to established patterns.

CHAPTER TWO

The Acoustic Excitation of Flat Rectangular Sandwich Plates

Summary

The possibility of the excitation of sandwich panels by the acoustic coincidence effect is first discussed. A Fourier-type analysis is then carried out to find the bond normal stress in a honeycomb sandwich panel excited by general random noise pressures. This general solution is restricted successively to solutions for random plane waves at a fixed incidence and then for random normal plane waves. A Fourier analysis is also carried out, for normal plane wave excitation only, for the bond bending stress. This stress is found to be of the same order of magnitude as the bond normal stress.

It is found that large bond stresses occur when sandwich panels are excited by the acoustical coincidence effect. These stresses can be of sufficient magnitude to precipitate fatigue failures in the bond of a honeycomb sandwich panel.

2.1 Introduction

The problem of the excitation of sandwich panels by random noise pressures has been analysed in this chapter in order to explain the fatigue failures which have been occurring in practice in the bonding of aircraft sandwich panels. These failures, as explained in the Introduction to the Thesis, have consisted of a debonding of the faces of the sandwich from the core, usually at the panel centre. This failure position indicates that direct stresses in the bond (i.e. the

stress normal to the panel and the panel bending stress) are responsible for failure and that the effect of core shear stresses is not significant in this respect. Therefore, the analysis of this chapter is confined to an analysis of the direct stresses in the bond of the sandwich panel. A preliminary simple analysis of the direct stresses in the bond of a freely vibrating honeycomb beam (given in Appendix A.2.1) shows that these two stresses are of the same order of magnitude. A full analysis has been carried out in § 2.2.2 for the normal direct stress in the bond of a sandwich panel excited by random noise pressures. Application of the results of this section is a very complicated procedure. For this reason restrictions have been placed on the generality of the noise field and on the plate in §'s 2.2.3 and 2.2.4 so that the salient features of the analysis become more readily apparent, even though these restrictions move the analysis away from the practical case. In § 2.2.3 the panel has been assumed to be simply supported and the noise pressure field has been restricted to random plane waves at a fixed incidence. § 2.2.4 is a further restriction of § 2.2.3 whereby the normal plane waves are assumed to be of normal incidence to the plate. A full analysis has not been carried out for the bending stress in the bond. However, a simplified-analysis has been carried out for this stress for a plate being excited by a random plane wave noise field at normal incidence. The results of this analysis (§ 2.2.5) are compared with the normal stresses in the bond found for a similar sandwich plate under similar conditions in § 2.2.4.

The two stresses are again found to be of the same order of

magnitude for a simply-supported sandwich plate under these excitation conditions and indicate an order of magnitude similarity under all conditions likely to be met with in practice.

Because of the low damping of the flexural modes of vibration of sandwich panels it is certain that the most dangerous state, as far as failures are concerned, is when some form of resonant excitation is taking place. For this reason, the possibility of the excitation of sandwich panels by the acoustical coincidence effect is discussed in § 2.2.1. This effect is a "double" resonance. It occurs most severely when harmonic plane pressure waves of a frequency the same as the plate mode natural frequency are incident upon the plate at such an angle that the intercepted sound wavelength on the plate is the same as the modal wavelength. A less severe coincidence effect arises for the more practical case of a real random sound field. This condition occurs when the wavelength of a particular vibration mode of the plate is equal to the "wavelength" of the spatial correlation of pressure when the pressure has been filtered by a narrow-band filter centred at the mode natural frequency. The correlation function is described in § 2.2.2.1 where the meaning of the term "wavelength" of the correlation function is made apparent. Special reference is made in this section (§ 2.2.1) to the results of chapter one for flat sandwich panels.

Section 2.2.2 predicts the r.m.s. bond normal stress σ_z in a honeycomb sandwich plate for a general acoustic field using the powerful Fourier method of analysis of random variables. Subsequent sections evaluate this expression for simpler noise fields. The

analysis is an extension of the single mode analysis by Mead[20] to include the effect of response in an infinite set of modes. The method used to determine the bond normal stress is essentially the same as a method used by Williams[21] in connection with loads in a structure subjected to transient loading. The stress is regarded as a sum of (i) the stress due to the local instantaneous pressure, if this pressure has been applied slowly, plus (ii) the stress due to the inertia loading from the face acting on the core through the bond. (i) may be called the 'static' loading and, (ii) the 'dynamic' or 'inertia' loading. Williams proved for his problem that this method converged on to an accurate result using fewer modes than would be required using a method involving a sum of strain effects in each mode. No proof is given here that this method will converge more quickly for this problem but a proof should be obtainable which is essentially the same as Williams' proof. In § 2.2.5 where an analysis is made for bending stress in the sandwich bond for comparison with the results of § 2.2.4 this rapidly convergent method is not used. Here the stress at a point is derived from a sum of strain effects in each mode. Although this is less accurate than the Williams approach for a given number of modes it has the advantage of simplicity, and, as only an order of magnitude comparison is required it has been regarded as sufficiently accurate for this purpose. It is pointed out in § 2.2.2.1 that use can be made of the results of chapter one to calculate the generalised coefficients of each mode of motion of a sandwich plate, if the plate is simply-supported.

Acoustic forces on the plate, both reactive and resistive, generated by the motion of the plate itself, have not been taken explicitly into account in the estimate of bond stress (although an indication of how this can be done is given). These forces, have, however, been implicitly included in the generalised mass and the generalised damping coefficient which feature in the generalised receptance. This receptance appears in the expression for the stress (N.B. Receptance is the reciprocal of impedance). It has been assumed, in doing this, that the acoustic damping is viscous so that it can be added directly to the structural damping (which, incidentally, has also been assumed to be viscous). This assumption will not affect the results if damping is small. A note on these self-generated forces is included as an appendix (A.2.3).

Extensive spectral analysis ($\frac{1}{3}$-octave bandwidth) has been carried out on the noise from a Rolls Royce Avon[22]. From the noise spectra given in that work, which are specified in dB, linear spectra have been computed. From these values, values of the noise spectrum parameter ϕ, defined in § 2.2.4, have been calculated for a severe case (close to the jet) and are shown in Fig. 14. The spectral qualities of the noise, however, do not completely describe it, because it is necessary to know something of the spatial variation of pressure at any instant. It has proved impossible to treat the effects of any real spatial pressure distributions in this chapter. Only the simpler distributions of plane waves have been treated numerically. This treatment however points out the most significant terms in the stress analysis.

2.2 Mathematical Analyses of the Problem

2.2.1 The Possibility of Excitation of Flat Finite Sandwich Panels by the Acoustical Coincidence Effect

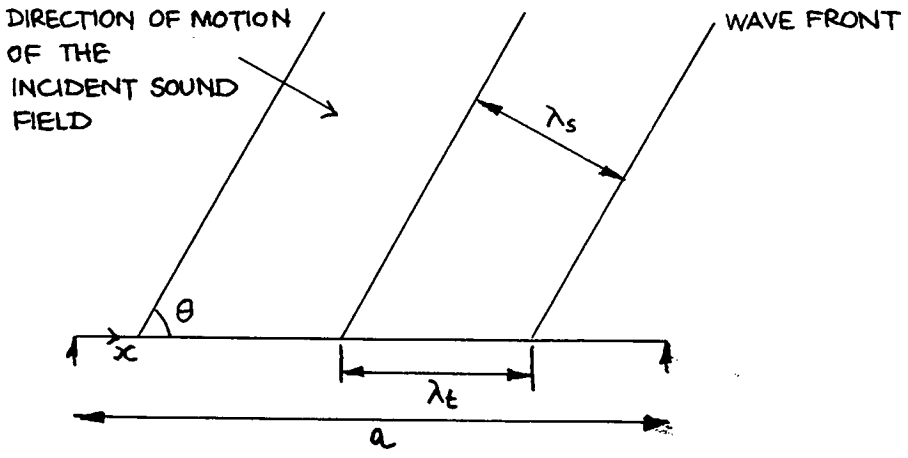

If harmonic plane waves of frequency ω impinge on a one-dimensional flat plate at a fixed angle θ to the plate (see the diagram) then there is a unique type of excitation possible, known as the coincidence effect. The coincidence effect occurs when the intercepted wavelength of the sound on the plat (called the trace wavelength and shown in the diagram by λ_t) is the same as the plate modal wavelength (λ_{mr}) and when the frequency of the sound pressure waves is the same as the natural frequency of the plate mode (ω_r). If we have a simply-supported plate vibrating in the mode $w = w_0 \sin \frac{r\pi x}{a}$, then $\lambda_{mr} = \frac{2a}{r}$. When the effect occurs with higher order modes the generalised force exciting the mode is very much larger than that occurring when waves of normal incidence impinge on the plate. If there is no structural damping the panel then becomes virtually 'transparent' to the acoustic pressure field (i.e. the panel surface is vibrating at the particle velocity

of the incident acoustic field and the pressure field passes through the plate as though it were not there). If the plate is excited by a general random noise field, large amplitudes of vibration can be excited due to the coincidence effect under the conditions described in the Introduction to this chapter.

Considering now coincidence excitation of a one-dimensional plate by harmonic plane waves, as in the diagram, the two conditions for coincidence can be written:

(i) $$\lambda_{m_r} = \lambda_t \qquad \ldots(2.1)$$

and (ii) $$\omega = \omega_r \qquad \ldots(2.2)$$

From the geometry of the diagram it can be seen that

$$\lambda_s = \lambda_t \sin\theta \qquad \ldots(2.3)$$

It is evident that the coincidence effect cannot possibly occur in the r^{th} mode if $\lambda_s < \lambda_{m_r}$. Now the wavelength of the sound field λ_s is given by the equation:

$$\lambda_s = \frac{2\pi c}{\omega} \qquad \ldots(2.4)$$

where c is the speed of sound in air. A combination of equations 2.1, 2.2, 2.3, and 2.4 shows that the required incidence of the harmonic plane wave field for the coincidence effect is specified by the equation:

$$\sin\theta = \frac{2\pi c}{\omega_r \lambda_{m_r}} \qquad \ldots(2.5)$$

If we now apply this result to the coincidence excitation of the 'two-dimensional' plate of chapter one and use the non-dimensional notation of that chapter for natural frequency and modal wavelength equation 2.5 becomes:

$$\sin\theta_{m,n} = \frac{\pi c}{A_{m,n}\phi}\sqrt{\frac{\rho_1}{c_g}} \qquad \ldots(2.6)$$

Calculations have been carried out taking a particular honeycomb sandwich configuration (as in § 1.6.2.1). In consequence a specific (constant) value of $\sqrt{\frac{\rho_1}{c_g}}$ has been used, together with a value for c of 1123 ft. per sec. Equation 2.6 then reduces to:

$$\sin\theta_{m,n} = \frac{0.2125}{A_{m,n}\,\phi} \qquad \ldots(2.7)$$

Curves representing this equation can be superimposed on the frequency vs. wavelength graphs derived in chapter one (Fig. 3) by plotting lines of constant sound field incidence angle θ . This superposition is shown in Fig. 8. Owing to the way in which Fig. 3 has been plotted, there are two sets of constant θ lines, one set for coincidence in the x-direction and the other for coincidence in the y-direction. As mentioned above, a necessary condition for the coincidence effect to occur is that $\lambda_s < \lambda_{m,}$ or alternatively that the right hand side of equation 2.7 must be less than unity. There are small regions of Fig. 8 (edged by shaded lines) for which this condition is not fulfilled and in these regions no coincidence effect can occur. Interpretation of Fig. 8 is as following: At the point at which one of the θ_m (or θ_n) lines crosses a natural

frequency line, the coihcidence effect is possible for the plate mode defined by this point. The harmonic plane waves must be incident upon the plate at the prescribed angle (θ_m or θ_n) and must be of the same frequency as the plate natural frequency given by the value of at the point.

No coincidence effect is considered in detailed for bubbling modes as the frequencies of these modes are comparatively high. To illustrate this we will consider two examples:

(i) For a plate 24" x 24", skin thickness 0.036", core depth 0.5", ϕ = 0.448 (bubbling mode, frequency = 56,900 c/s) A_n = 96 and thus from equation (2.7), $\theta_n = 0.283^\circ$

(ii) For a plate 24" x ∞ , skin thickness 0.024", core depth 6". (corresponding approximately to a control surface constructed from a honeycomb wedge) ϕ = 1.89 (frequency = 12,600 c/s) A_n = 8 and from equation (2.7), $\theta_n = 1.278^\circ$

From these examples it can be seen that (a) the frequency of bubbling modes of normal sandwich plates is well outside the expected excitation range (0 - 20 Kc/s), and (b) that the bubbling modes of all sandwich plates are only excited by the acoustical coincidence effect when the sound field wave fronts are nearly parallel to the plate surface.

In fact, normal aircraft sandwich panels have thinner face plates than those quoted above, and therefore their frequencies will be even higher.

2.2.2 An Analysis of the Bond Normal Stress (σ_z) for a Sandwich Panel Excited by a General Acoustic Pressure Field

The motion of a sandwich panel being excited by random noise pressures can be analysed by regarding this motion as an infinite sum of the natural modes of the plate. This method is always valid, because the natural modes form a 'complete set', but it is sometimes not convenient. If there is damping coupling between the theoretical undamped natural modes, in the practical case, then subsequent analysis becomes open to doubt because the uncoupled equations of motion are then not strictly true. If damping is fairly high in each mode or if natural frequencies are close then a very large number of modes takes significant part in the motion because of the overlap of adjacent resonant peaks and this makes a sum of natural modes analysis unduly lengthy. Other methods of approach in these cases have been investigated. In this chapter, however, we are dealing with the flexural motion of sandwich plates which is known empirically to be quite lightly damped. Therefore for the likely acoustic fields to be met with significant motion only occurs in a few modes and for this reason a sum of natural modes analysis has been used here.

There are two possible ways of expressing the value of the bond stress. The first, and simpler method is to evaluate this stress in terms of the direct strain of the mode. For the bond normal stress this is impossible to evaluate without assuming some variation of the normal deflection through the core. The second method is to evaluate the stress as a sum of two superimposable parts:

(i) The 'static' loading

and (ii) The inertia or 'dynamic' loading

as described in the introduction. This second method is preferable to the first because of its more rapid convergence, but for the bond normal stress we must use it anyway, because of the lack of definition of core normal strain in each flexural mode. Using this method the bond stress is expressed as the sum of the external pressure acting on the panel and the inertia loading on the bond due to motion of the adjacent face.

We now proceed to use a Fourier analysis to obtain a mean square value of stress. This is the usual method employed to analyse random variables, and to obtain the mean square value it involves the use of three steps.

The first step is to take the Fourier Transform of the stress, thus:-

$$\mathfrak{F}_\sigma(\omega) = \frac{1}{2\pi}\int_{-\infty}^{\infty} e^{-i\omega t}\,\sigma(t)\,dt \qquad \ldots(2.8)$$

The second step is to evaluate the 'Power Spectrum' of the stress. This quantity, so called because of its original relevance to random electrical power, indicates how much of the mean square value of the random signal exists in a narrow frequency band centred on the particular frequency. This Power Spectrum of Stress is given by the equation:

$$W_\sigma(\omega) = \lim_{T\to\infty} \frac{\pi}{T}\,\mathfrak{F}_\sigma(\omega)\,\mathfrak{F}_\sigma^*(\omega) \qquad \ldots(2.9)$$

This quantity is always positive because of the squared

term involved in its derivation

The third and last step is to evaluate the mean square stress using the Power Spectrum. Bearing in mind the explanation of Power Spectrum given above, it can be shown that:

$$\overline{\sigma^2(t)} = \int_{-\infty}^{\infty} W_\sigma(\omega)\, d\omega \qquad \ldots(2.10)$$

It can be seen from this equation that the Power Spectrum $W_p(\omega)$ is an index of the contribution to the mean square stress of the narrow-band filtered stress, the narrow band being centred at the frequency ω . The Fourier Transform is effectively this filter. Two codes of Fourier Transform notation are in common use and these are shown and compared in Appendix A.2.1.

2.2.2.1 Derivation of the Power Spectrum of Bond Normal Stress

If we now consider a rectangular sandwich panel vibrating under acoustic excitation, the normal displacement is given by an infinite sum of the displacements in the undamped natural modes:

$$w(t,s') = \sum_{r=1}^{\infty} q_r(t) f_r(s') \qquad \ldots(2.11)$$

where $f_r(s')$ is the normalised modal shape, a function of S' where S' denotes the position on the plate (x, y). q_r is the generalised displacement. If the pressure acting on one side of the panel is $p(t,s')$ then the generalised force $F_r(t)$ corresponding

to the r^{th} mode is given by the equation

$$F_r(t) = \int_S p(t,s') f_r(s') dS' \qquad \ldots(2.12)$$

The Fourier Transform of $F_r(t)$ is denoted by $\mathfrak{F}_{F_r}(\omega)$ and the Fourier Transform of the r^{th} generalised displacement is found from the modal equation of motion to be:

$$\mathfrak{F}_{q_r}(\omega) = \frac{\mathfrak{F}_{F_r}(\omega)}{Z_r(\omega)} \qquad \ldots(2.13)$$

This equation assumes that the natural modes are not coupled. $Z_r(\omega)$ is the complex generalised impedance of the r^{th} mode and is given by:

$$Z_r(\omega) = -M_r(\omega^2 - \omega_r^2) + i\omega B_r \qquad \ldots(2.14)$$

M_r is the generalised mass of the sandwich plate in the r^{th} mode, B_r is the generalised viscous damping coefficient in the r^{th} mode, and ω_r is the r^{th} natural frequency. For flexural modes of ordinary sandwich panels the generalised mass is given quite accurately by the equation

$$M_r = \beta \int_S m f_r^2(s') dS' \qquad \ldots\ldots(2.15)$$

where $\beta = \frac{2m + m_1}{m}$

m is the mass per unit area of one face plate and m_1 is the mass per unit area of the core. The accuracy of this equation is only

impaired significantly when the core centre moves a significant amount more than the faces in the normal direction. This could occur in the unlikely case of the core being thick, heavy, and flexible. A small contribution to the generalised mass also exists from the reactive component of the acoustic forces generated by the motion of the plate itself. This component is discussed in Appendix A.2.3. The damping of the flexural vibrations of sandwich panels is assumed to be viscous. This assumption holds true for the low damping involved. The sources of damping are structural and acoustic. Structural damping derives mostly from the joints at the edges of the panel. Very little hysteretic damping occurs in the sandwich components and in the bond. It is fortunate that acoustic damping is quite small for a sandwich panel of the usual dimensions, because this damping would significantly couple the various modes of vibration, thus invalidating this analysis. If the damping ratio can be estimated either theoretically or empirically for a sandwich plate flexural mode (the latter is more likely) then B_r can be found from the equation:

$$B_r = 2M_r \delta_r \omega_r \qquad \ldots(2.16)$$

The transform ('Fourier' understood) of the r^{th} generalised acceleration is $-\omega^2 \Im q_r(\omega)$ and hence the transform of the inertia force per unit area acting on the face-plate is given by the expression

$$-m\omega^2 \sum_{r=1}^{\infty} f_r(s') \frac{\Im F_r(\omega)}{Z_r(\omega)} \qquad \ldots(2.17)$$

We will make thin plate assumptions for the faces of the sandwich so that the normal shear stresses in the faces are zero. Then, the total force per unit area transmitted to the core through the bond is the sum of the external pressure and the inertia force acting on the face plate. If the core is homogeneous (which will be assumed for the time being) we can write:

$$\mathfrak{F}_{\sigma_z}(\omega) = \mathfrak{F}_p(\omega,s') + m\omega^2 \sum_{r=1}^{\infty} f_r(s') \frac{\mathfrak{F}_{F_r}(\omega)}{Z_r(\omega)} \qquad \ldots(2.18)$$

This equation does not include a term due to the damping pressure which may be acting. This term has been assumed to be small. It could be included, so that equation 2.18 would read:

$$\mathfrak{F}_{\sigma_z}(\omega,s') = \mathfrak{F}_p(\omega,s') + \sum_{r=1}^{\infty} (m\omega^2 f_r(s') - i\psi_r) \frac{\mathfrak{F}_{F_r}(\omega)}{Z_r(\omega)} \qquad \ldots(2.19)$$

The subsequent analysis would become very complicated if this term were significant enough to be included. Consequently, equation 2.18 is used in the following analysis.

The first of the three stages involved in defining the mean square stress is therefore complete. The next stage, in which the Power Spectrum of the stress is derived starts with the relationship for the Power Spectrum:

$$W_{\sigma_z}(\omega,s') = \lim_{T\to\infty} \frac{\pi}{T} \mathfrak{F}_{\sigma_z}(\omega) \mathfrak{F}^*_{\sigma_z}(\omega) \qquad \ldots(2.20)$$

We can now substitute equation 2.18 into equation 2.20 to give for the Power Spectrum of Stress:

$$W_{\sigma_z}(\omega,s') = W_p(\omega,s') + \lim_{T\to\infty}\frac{\pi m\omega^2}{T}\sum_{r=1}^{\infty} f_r(s')\left[\mathfrak{I}_p(\omega,s')\frac{\mathfrak{I}^*_{F_r}(\omega)}{Z_r^*(\omega)} + \mathfrak{I}_p^*(\omega,s')\frac{\mathfrak{I}_{F_r}(\omega)}{Z_r(\omega)}\right]$$

$$+ \lim_{T\to\infty}\frac{\pi m^2\omega^4}{T}\sum_{r=1}^{\infty}\sum_{\Delta=1}^{\infty} f_r(s')\frac{\mathfrak{I}_{F_r}(\omega)}{Z_r(\omega)}\frac{\mathfrak{I}^*_{F_\Delta}(\omega)}{Z^*_\Delta(\omega)} f_\Delta(s') \qquad \ldots(2.21)$$

The first term in this equation is the Power Spectrum of the local pressure; the last term is the Power Spectrum of the sum of inertia forces in the modes. This last term can be regarded as consisting of two parts. The first part is a sum of all those terms for which $r=\Delta$ This part is a sum of the power spectra of the inertia forces in each mode. There is, however, some correlation between any two different modes because they are both being excited by the same pressure field. For this reason there is also a cross term given by the second part. Although this cross term is usually small we will retain it for the time being. The second term in equation 2.21 represents the correlation between the local pressure and the local inertia force. The factor in the square brackets is a sum of two terms which are complex conjugates so that twice the real part of one of the terms is equal to the sum of the two terms. If we choose the second of the two terms it can be shown that:

$$\frac{1}{Z_r(\omega)}\lim_{T\to\infty}\frac{\pi}{T}\mathfrak{I}_p^*(\omega,s')\mathfrak{I}_{F_r}(\omega) = \frac{\overline{p^2(t)}}{Z_r(\omega)}\left(\chi_{c_r} - i\chi_{s_r}\right) \qquad \ldots(2.22)$$

where $$X_{c_r} - i X_{s_r} = \int_S f_r(s) \frac{1}{2\pi} \int_{-\infty}^{\infty} e^{-i\omega\tau} \overline{\psi}^{x}(s,s',\tau)\, d\tau\, ds \qquad \ldots(2.23)$$

This assumes that the random pressure field is homogeneous (i.e. that the mean square pressure is the same everywhere). $\overline{\psi}^{x}(s,s',\tau)$ is the normalised cross-correlation function. The correlation function is defined by the integral

$$\psi_{12} = \lim_{T\to\infty} \frac{1}{8T} \int_{-T}^{T} p_1 p_2\, dt \qquad \ldots(2.24)$$

and can be normalised by dividing by the mean square pressure at either of the positions 1 and 2. Provided that the pressure field is homogeneous the normalised correlation coefficient cannot exceed unity. If p_1 and p_2 are measured at the same position and a time delay is introduced between them then the auto-correlation function is obtained. This is an even function of time delay. A useful relationship concerning the auto-correlation function is that;

$$W_p(\omega) = \frac{1}{2\pi} \int_{-\infty}^{\infty} e^{i\omega\tau} \psi(\tau)\, d\tau \qquad \ldots(2.25)$$

i.e., the Power Spectrum of a random quantity is the Fourier Transform of its auto-correlation function.

If the two points at which pressure is measured are separated spatially and correlation measurements are made with various time delays then the function obtained is the cross-correlation function. If we have some sort of convected flow, as for example in a boundary

layer, then the cross-correlation function can look rather like a shifted auto-correlation function, the shift time being given by the spatial separation divided by the convection velocity. The normalised cross-correlation function might then be as shown in the sketch below

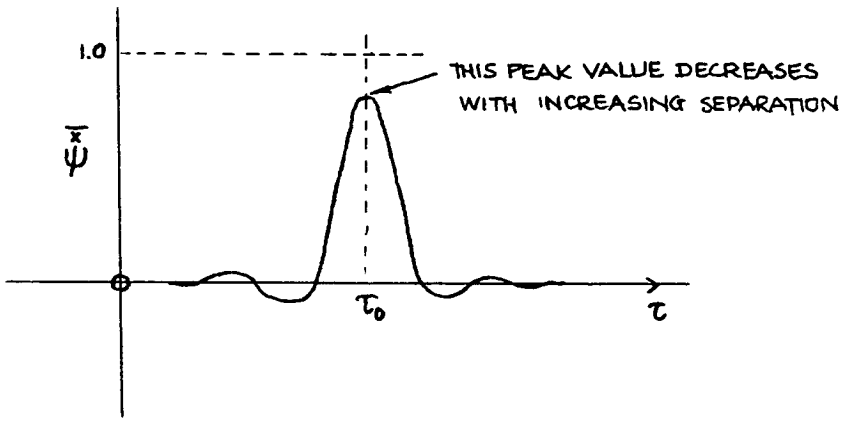

If the rate of decay of this is rapid with respect to τ , certain approximations and deductions can be made.

This cross-correlation function can be replaced approximately by a double step function, as shown below, of the appropriate width $\Delta\tau_0$ at τ_0 (τ_0 represents the time taken for convection from point S to point S' to occur). The innerr integral of equation 2.23 then has real and imaginary parts χ_c and χ_s . χ_c is represented by the integral of the product of the two functions shown below:

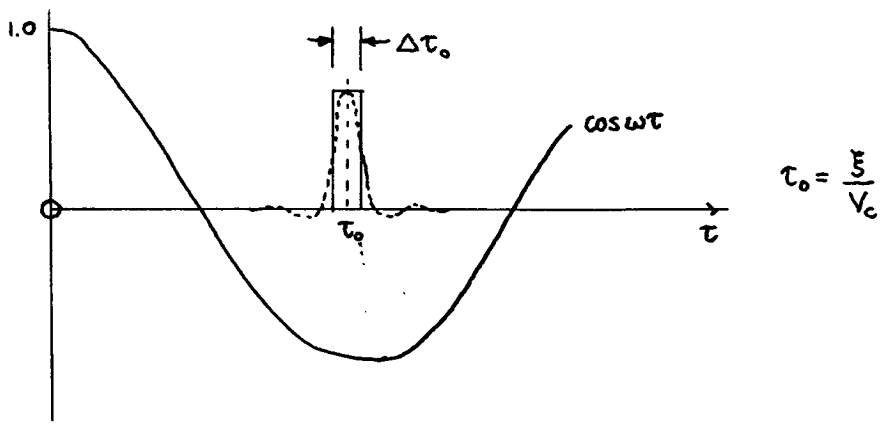

χ_c therefore has the form of $\cos \frac{\omega \xi}{V_c}$ and χ_s the form of $\sin \frac{\omega \xi}{V_c}$ where ξ is the separation of the points S and S' and V_c is the convection velocity from S to S'. χ_c and χ_s are functions of the spatial separation ξ and the particular frequency ω under consideration. It can be seen that χ_c and χ_s will have a wavelength given by $\frac{2\pi V_c}{\omega}$ for the frequency ω. For real convected flows these waves are decaying cosine and sine waves because of imperfections in the convection of turbulence and because of turbulence decay. If $\Delta\tau_o$ is larger than the cosine or sine half period (which becomes true at high frequency) then the integral will diminish considerably. The evaluation of χ_{cr} and χ_{sr} now depends critically on the relative magnitudes of the plate modal wavelength and the wavelength of χ_c and χ_s for the particular frequency under consideration.

If the noise field consisted of random plane waves at fixed incidence travelling along the plane, then the functions χ_c and χ_s would tend to oscillate indefinitely. For a one-dimensional plate, the

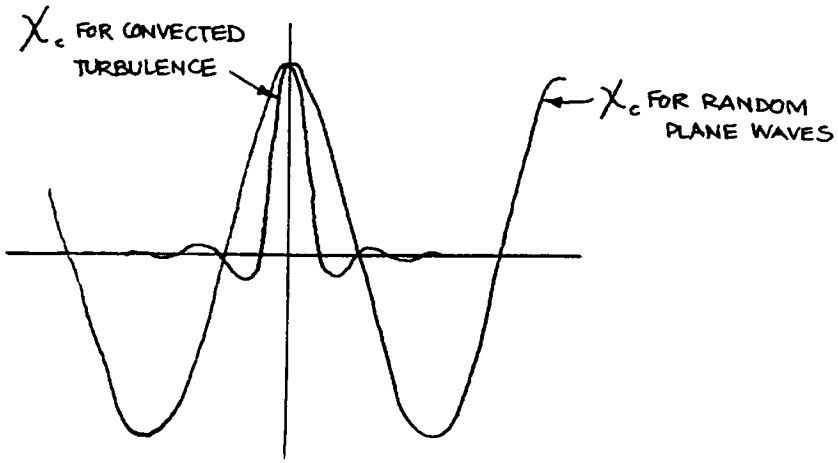

wavelength of the χ_c for convected flow is defined as four times the distance from the origin to the first zero crossing.

The wavelength of χ_c and χ_s is of the utmost importance in deciding the value of this coupling between local pressure and local inertia force. If the wavelength is equal to the modal wavelength of $f_r(s')$ then it can be seen that a maximum value of χ_{cr} occurs. This condition corresponds to the acoustical coincidence effect. Usually cross-correlation functions are not so regular as in the simple cases mentioned.

Using equations 2.22 and 2123 and splitting the last term of equation 2.21 into its two parts, the Power Spectrum of bond normal stress can now be described by the equation:

$$W_{\sigma_z}(\omega,s') = W_p(\omega,s') - 2m\omega^2\,\overline{p^2(t)}\sum_{r=1}^{\infty} f_r(s')\frac{M_r}{|Z_r(\omega)|^2}\left\{\chi_{cr}(\omega^2-\omega_r^2) + 2\delta_r\omega\omega_r\chi_{sr}\right\}$$

$$+m^2\omega^4\sum_{r=1}^{\infty} f_r^2(s')\frac{W_{Fr}(\omega)}{|Z_r(\omega)|^2} + m^2\omega^4\sum_{\substack{r=1\\ r\neq\Delta}}^{\infty}\sum_{\Delta=1}^{\infty}\frac{f_r(s')f_\Delta(s')}{Z_r(\omega)\,Z_\Delta^*(\omega)}\lim_{T\to\infty}\frac{\pi}{T}\,\mathfrak{F}_{F_r}(\omega)\,\mathfrak{F}_{F_\Delta}^*(\omega)$$

...(2.26)

In a very similar way to the derivation of equation 2.22, part of the last term in equation 2.26 can be written as follows:

$$\lim_{T\to\infty} \frac{\pi}{T}\, \mathcal{J}_{Fr}(\omega)\, \mathcal{J}_{F\Delta}^{*}(\omega) = \overline{p^2(t)}\left(Y_{cr\Delta} + i\, Y_{sr\Delta}\right) \qquad \ldots(2.27)$$

where in this case:

$$Y_{cr\Delta} + i\, Y_{sr\Delta} = \iint_{S_1 S_2} f_r(s_1) f_\Delta(s_2) \frac{1}{2\pi} \int_{-\infty}^{\infty} e^{i\omega\tau}\, \overline{\psi}^{x}(s_1 s_2 \tau)\, d\tau\, ds_1\, ds_2 \qquad \ldots(2.28)$$

The similarities between equations 2.23 and 2.28 are readily apparent and the comments which have been made concerning convected flow, when the cross-correlation coefficient is similar to a shifted auto-correlation function, apply here too. The spatial integral is rather more complicated in the case of equation 2.28 although the same general remarks apply as before. Y_c and Y_s are functions only of the frequency ω, whereas X_c and X_s are functions of the frequency and of one plate position. Y_{cw} also has a maximum value when the wavelength of χ_c and χ_s is the same as the modal wavelength. When the last term of equation 2.26 is paired with a similar term in which r and Δ have been interchanged we again have a sum of complex conjugates so that only the real part of this term need be considered. More will be said of the functions $Y_{cr\Delta}$ at a later stage. The power spectrum of the bond normal stress can therefore finally be written thus:

$$W_{\sigma_z}(\omega,s') = W_p(\omega,s') - 2m\omega^2\,\overline{p^2(t)}\sum_{r=1}^{\infty} f_r(s')\,\frac{M_r}{|Z_r(\omega)|^2}\left\{X_{cr}(\omega^2-\omega_r^2) + 2\delta_r\omega\omega_r X_{sr}\right\}$$

$$+m^2\omega^4\sum_{r=1}^{\infty} f_r^2(s')\,\frac{W_{F_r}(\omega)}{|Z_r(\omega)|^2} + R\,m^2\omega^4\sum_{r=1}^{\infty}\sum_{\substack{\Delta=1\\ r\neq\Delta}}^{\infty}\frac{f_r(s')f_\Delta(s')}{Z_r(\omega)\,Z_\Delta^*(\omega)}\,\overline{p^2(t)}\left[Y_{cr\Delta}+iY_{sr\Delta}\right]$$

...(2.29)

2.2.2.2 Derivation of the Mean Square Value of Bond Normal Stress

We now come to the final stage in the analysis of the bond normal stress, which is to find the mean square value of this stress using the equation:

$$\overline{\sigma_z^2(t)} = \int_{-\infty}^{\infty} W_{\sigma_z}(\omega)\,d\omega \qquad \ldots(2.30)$$

Thus the terms of equation 2.29 will be integrated over frequency to find this mean square stress. If we deal with the integration of the four terms of 2.29 one at a time we have:

(i) $$\int_{-\infty}^{\infty} W_p(\omega,s')\,d\omega = \overline{p^2(t)}$$ for the homogeneous field assumed previously

...(2.31)

This is the direct mean square pressure from the external field which acts through the face on to the bond.

(ii) It is well known that the mean square value of the sum of two random variables is the sum of the mean square values, provided that the two variables are not statistically correlated. In our case the two variables are the external pressure and the inertia force imposed by the face plate. These two variables are correlated because the total effect of the pressure is to cause the inertia term. Integration of the first term has produced the mean square pressure - integration of the third and fourth terms will produce the mean square inertia stress: The second term represents the correction due to correlation between the local pressure and the inertia stress. If the area over which the local pressure is correlated significantly, in a narrow frequency band centred on the mode natural frequency, is small compared with the modal wavelength then this term will be sufficiently small to neglect.

If we can assume that X_{c_r} is reasonably constant throughout the frequency range and that ωX_{s_r} does not vary greatly in the region of the r^{th} resonance (and the truth of these assumptions will have to be decided in a practical case after measurement of the cross-correlation functions has been made) then the second term of equation 2.29 integrates thus:

$$-\int_{-\infty}^{\infty} 2m\omega^2 \overline{p^2(t)} \sum_{r=1}^{\infty} f_r(s') \frac{M_r}{|Z_r(\omega)|^2} \left\{ X_{c_r}(\omega^2 - \omega_r^2) + 2\delta_r \omega \omega_r X_{s_r} \right\} d\omega$$

$$= 2\overline{p^2(t)} \sum_{r=1}^{\infty} \left[\frac{m}{M_r} f_r(s') \int_{-\infty}^{\infty} X_{c_r}(\omega) d\omega + 2 X_{c_r}(\omega_r) \pi \omega_r \delta_r \frac{m}{M_r} f_r(s') \right.$$

$$\left. - X_{s_r}(\omega_r) \pi \omega_r \frac{m}{M_r} f_r(s') \right] \qquad \ldots(2.32)$$

The X_c part of this integration is carried out in the following manner. The frequency dependent part of the integral is

$$\int_{-\infty}^{\infty} X_{cr} \frac{\omega^2(\omega^2-\omega_r^2)}{|Z_r(\omega)|^2} d\omega$$

and this can be evaluated as the integral of the product of the two functions X_{cr} and

$$\frac{\omega^2(\omega^2-\omega_r^2)}{|Z_r(\omega)|^2}$$

as seen in the diagram, considering only positive frequencies because both functions are even functions of ω.

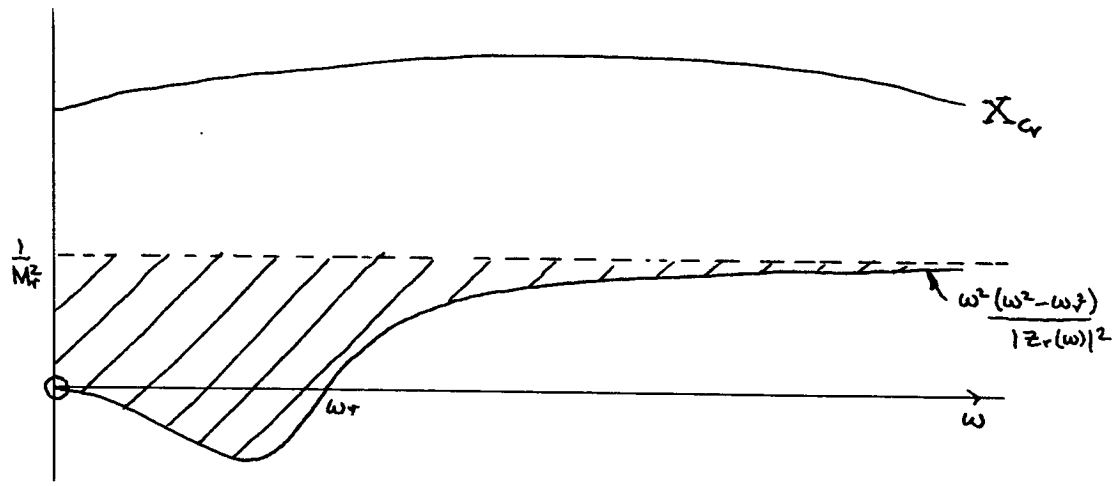

The first part of the integral is the integral of the product of the constant $\frac{1}{M_r^2}$, to which

$$\frac{\omega^2(\omega^2-\omega_r^2)}{|Z_r(\omega)|^2}$$

is asymptotic, and X_{cr}, and produces the first term in the square brackets of equation 2.32. The second part of the integral is the integral of the product of the shaded portion and X_{cr} and produces the second term in the square brackets of equation 2.32. For the

function

$$\frac{\omega^2(\omega^2-\omega_r^2)}{|Z_r(\omega)|^2}$$

there is not, unfortunately a peak at ω_r as there is for the function

$$\frac{1}{|Z_r(\omega)|^2}$$

If there was a peak at ω_r we would only require that X_{cr} remained constant in the region of ω_r. In order to evaluate this integral, it is necessary to assume that X_{cr} is sensibly constant over the frequency range $0<\omega<\omega_r$. The shape of the function X_{cr} as it varies with frequency depends upon the plate position for which it is being evaluated, and on the function χ_{cr}. χ_{cr}, in turn, depends on the characteristics of the noise field. Consideration of some typical variations of χ_{cr} has indicated that X_{cr} may take a variety of forms. The assumption that X_{cr} is constant over the frequency range $0<\omega<\omega_r$ is therefore, not likely to be valid. Fortunately, it is unlikely that even this whole term (L.H.S. of equation 2.32), which derives from the correlation between local pressure and local inertia force, will make a significant contribution to the mean square stress. For the purpose of evaluating this X_c term, the integral:

$$\int_{-\infty}^{\infty} \frac{A\omega^2+B}{|Z_r(\omega)|^2}\,d\omega = \frac{\pi}{2M_r^2\delta_r\omega_r^3}\left(A\omega_r^2+B\right) \qquad \ldots(2.33)$$

(which has been obtained by contour integration) has been used. The X_s part of the integration has been evaluated by assuming ωX_s to be sensibly constant in the region of the r^{th} resonance and then by using a similar method to the second part of the X_c integration involving use of equation 2.33.

(iii) The mean square inertia stress has been divided into direct terms, given by the third term of equation 2.29, and the cross terms given by the fourth term. Here we are dealing with the third term which is likely to be the most important term in the whole expression for stress. Under resonant conditions the inertia loading is inversely proportional to the damping ratio and is much larger than the static stresses. From equation 2.27 we can deduce that the Power Spectrum of the generalised force is given generally by the equation:

$$W_{Fr}(\omega) = \overline{p^2(t)}\, Y_{crr} \qquad \ldots(2.34)$$

Substituting this equation in the third term of equation 2.29 we find that the contribution to mean square stress of this direct inertia term is given by:

$$\int_{-\infty}^{\infty} m^2\omega^4 \sum_{r=1}^{\infty} \frac{f_r^2(s')W_{Fr}(\omega)}{|Z_r(\omega)|^2}\, d\omega = \int_{-\infty}^{\infty} m^2\omega^4 \sum_{r=1}^{\infty} \frac{f_r^2(s')\,\overline{p^2(t)}}{|Z_r(\omega)|^2}\, Y_{crr}\, d\omega \qquad \ldots(2.35)$$

As argued before for X_{cr}, Y_{crr} has a maximum value when the wavelength of χ_{cr} is equal to the modal wavelength. The function Y_{crr} which describes the wavelength filtering capabilities of the

plate (and not the frequency filtering capabilities) is directly proportional to the function which Powell[25] calls the 'joint acceptance' (j_{rr}) and is related to this function by the equation:

$$Y_{C_{rr}} = \frac{W_p(\omega)}{\overline{p^2(t)}} S^2 j_{rr}^2 \qquad \ldots(2.36)$$

where S is the area of the plate.

If the maximum value of the joint acceptance occurs at the natural frequency of the mode concerned, then the coincidence effect occurs causing large amplitudes of motion.

(iv) The integration of the last term in the equation 2.29 can be carried out if it is assumed that $Y_{C_{rs}}$ and $Y_{S_{rs}}$ are smooth functions in the region of the r^{th} and s^{th} natural frequencies and that these natural frequencies are well separated. In order to perform this integration the integral

$$\int_{-\infty}^{\infty} \frac{(A\omega^6 + B\omega^4 + C\omega^2 + D)}{|Z_r(\omega)|^2 |Z_s(\omega)|^2} d\omega = \frac{\pi}{2M_r^2 M_s^2 (\omega_r^2 - \omega_s^2)} \left\{ \frac{(A\omega_r^6 + B\omega_r^4 + C\omega_r^2 + D)}{\delta_r \omega_r^3} + \frac{(A\omega_s^6 + B\omega_s^4 + C\omega_s^2 + D)}{\delta_s \omega_s^3} \right\} \qquad \ldots(2.37)$$

has been evaluated by contour integration and used. Equation 2.37 has been derived by assuming the damping ratios to be small. The integral of this last term then becomes:

$$R\int_{-\infty}^{\infty} m^2\omega^4\left[\sum_{r=1}^{\infty}\sum_{\substack{s=1\\ r\neq s}}^{\infty}\frac{f_r(s')\,f_s(s')}{Z_r(\omega)\,Z_s^*(\omega)}\,\overline{p^2(t)}\left[Y_{c_{rs}}+i\,Y_{s_{rs}}\right]\right]d\omega$$

$$=\overline{p^2(t)}\,m^2\sum_{\substack{r=1\\ r\neq s}}^{\infty}\sum_{s=1}^{\infty}\frac{\mathcal{F}_r(s')\,f_s(s')}{M_r\,M_s}\left[\int_{-\infty}^{\infty}Y_{c_{rs}}d\omega+\pi\left(\omega_r\,Y_{s_{rs}}(\omega_r)+\omega_s\,Y_{s_{rs}}(\omega_s)\right)\right]$$

...(2.38)

The assumptions made in the derivation of this equation, as outlined above, are open to some doubt, but because the term as a whole is small these assumptions will not affect the mean square stress unduly. $Y_{c_{rs}}$ corresponds to Powell's cross joint acceptance and is connected to it by the equation

$$Y_{c_{rs}}=\frac{W_p(\omega)}{\overline{p^2(t)}}\,S^2\,j_{rs}^2 \qquad \text{...(2.39)}$$

as in equation 2.36.

We can now collect together the various terms which constitute the mean square stress in the plate normal direction in the sandwich bond:-

(i) the mean square pressure (equation 2.31)

(ii) The 'correction' term due to correlation between local pressure and local inertia force (equation 2.32)

(iii) the 'direct' inertia force terms (equation 2.35)

and

(iv) the cross-coupled inertia force terms due to inter-modal inertia correlation (equation 2.38)

The total expression becomes:

$$\overline{\sigma^2(t,s')} = \overline{p^2(t)} + 2\overline{p^2(t)} \sum_{r=1}^{\infty} \left[-\frac{m}{M_r} f_r(s') \int_{-\infty}^{\infty} X_{c_r}(\omega)\, d\omega + 2X_{c_r}(\omega_r)\pi\omega_r\delta_r \frac{m}{M_r} f_r(s') \right.$$

$$\left. - X_{s_r}(\omega_r)\pi\omega_r \frac{m}{M_r} f_r(s') \right] + \overline{p^2(t)} \int_{-\infty}^{\infty} m^2\omega^4 \sum_{r=1}^{\infty} \frac{f_r(s')\, Y_{c_{rr}}}{|Z_r(\omega)|^2}\, d\omega$$

$$+ \overline{p^2(t)}\, m^2 \sum_{\substack{r=1 \\ r\neq\Delta}}^{\infty} \sum_{\Delta=1}^{\infty} \frac{f_r(s')\, f_\Delta(s')}{M_r M_\Delta} \left[\int_{-\infty}^{\infty} Y_{c_{r\Delta}}\, d\omega + \pi\left\{\omega_r Y_{s_{r\Delta}}(\omega_r) + \omega_\Delta Y_{s_{r\Delta}}(\omega_\Delta)\right\} \right]$$

...(2.40)

The term which is likely to be the largest when the plate is being excited at a resonance is the direct inertia term as explained previously. It is quite possible that the major part of this response could be in a mode other than the fundamental if suitable conditions prevail. This stress has been obtained for a homogeneous core. If the forces on the bond are being reacted by a honeycomb core, then it can be expected that the local stress, where the core meets the bond, will be higher by a factor equal to the area-ratio* of the honeycomb. In fact some alleviation of this maximum stress takes place because of

*The area-ratio λ is the ratio of the total exposed cross-sectional area to the cross-sectional area of the honeycomb when the core is cut in a plane parallel to one of the faces.

the fillet of bonding which forms at the joint.

2.2.3 A Restriction of the General Acoustic Field to Random Plane Waves of a Fixed Incidence

This restriction of the general acoustic field is not a very practical restriction as far as aircraft are concerned because the plane wave condition only exists in the far field of jet noise. However, treatment of real acoustic fields is somewhat complicated and relies on empirical data, so that in this section it is convenient to demonstrate the significant features of the expression for stress by choosing a sound field which can be described mathematically.

Let the random plane waves travel in the direction shown below. The wavefronts are inclined at an angle θ to the plate.

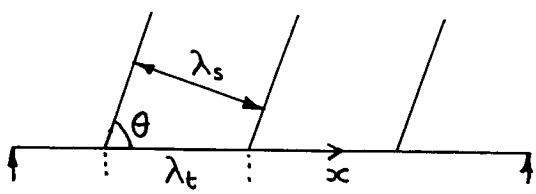

The cross-correlation function between the pressures at two points on the plate S and S' is a "shifted" auto-correlation, and we can write:

$$\overline{\psi}^{x}(s,s';\tau) = \overline{\psi}\left(\tau - \frac{\xi \sin\theta}{c}\right)$$

where ξ is the x-wise separation of the points S and S' and c is the speed of sound in the medium. Substituting this into

equation 2.23 we have:

$$X_{C_r} + iX_{S_r} = \frac{W_p(\omega)}{\overline{p^2(t)}} \int_S f_r(s')\, e^{i\omega\xi \frac{\sin\theta}{c}}\, dS \qquad \ldots(2.41)$$

Similarly for $Y_{C_{r\Delta}}$ and $Y_{S_{r\Delta}}$ we have from equation 2.28 that:

$$Y_{C_{r\Delta}} + Y_{S_{r\Delta}} = \frac{W_p(\omega)}{\overline{p^2(t)}} \iint_{S\,S'} f_r(s)\, f_\Delta(s')\, e^{i\omega\xi \frac{\sin\theta}{c}}\, dS \qquad \ldots(2.42)$$

For a given mode r, X_{C_r} and X_{S_r} are functions not only of the frequency ω but also of the position S' on the plate. For a pair of given modes, r and s, $Y_{C_{r\Delta}}$ and $Y_{S_{r\Delta}}$ are functions of the frequency only. $Y_{C_{r\Delta}}$ and $Y_{S_{r\Delta}}$ can be described as functions only of the trace wavelength of each frequency component of the sound field because the trace wavelength is inversely proportional to the frequency. In the previous section it has been stated that $Y_{C_{rr}}$ is directly proportional to the joint acceptance squared. $Y_{C_{rr}}$ can be plotted as a function of the ratio of modal wavelength λ_m to the trace wavelength λ_t. It has a maximum value when $\lambda_m/\lambda_t = 1$ For sinusoidal deflection modes of a one dimensional plate, $Y_{C_{rr}}$ has the form shown below:

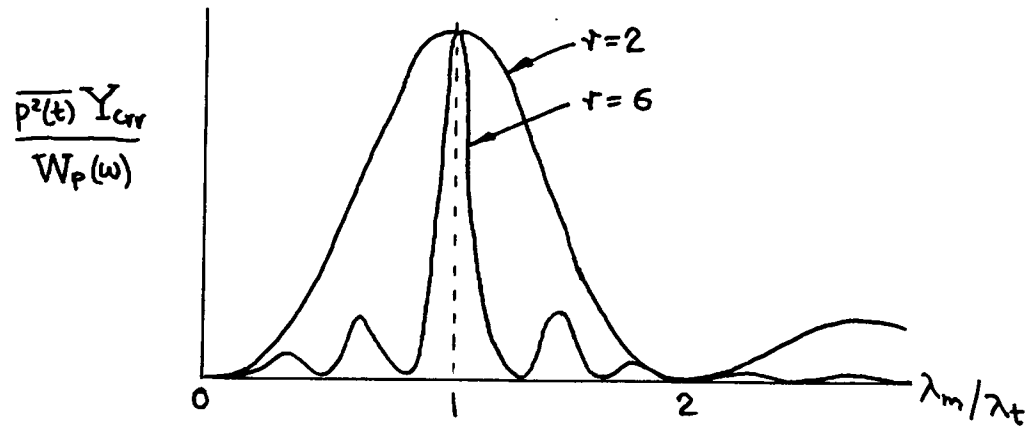

It can easily be shown, by using equation 2.41 and then reversing the order of integration, that:

$$\int_{-\infty}^{\infty} X_{c_y}(\omega)\, d\omega = \int_S f_r(s)\, \bar{\psi}\left(\xi \frac{\sin\theta}{c}\right) ds \qquad \ldots(2.43)$$

In a similar manner, using equation 2.42:

$$\int_{-\infty}^{\infty} Y_{c_{y\Delta}}(\omega)\, d\omega = \iint_{S'S} f_r(s')\, f_\Delta(s)\, \bar{\psi}\left(\xi \frac{\sin\theta}{c}\right) ds\, ds' \qquad \ldots(2.44)$$

If we incorporate the results of equations 2.41, 2.42, 2.43 and 2.44, which have been derived for the random plane wave pressure field, into the general equation for mean square stress (equation 2.40) we derive an expression for the mean square stress (in the bond and normal to the plate) for this pressure field:

$$\overline{\sigma_z^2(t,s')} = \overline{p^2(t)}\left[1 - 2\sum_{r=1}^{\infty}\left\{\frac{m}{M_r} f_r(s')\int_s f_r(s)\,\bar{\psi}\left(\xi\frac{\sin\theta}{c}\right)ds - 2\pi\omega_r\delta_r\frac{m}{M_r}f_r(s')\frac{W_p(\omega_r)}{\overline{p^2(t)}}\cdot\right.\right.$$

$$\cdot\int_s f_r(s)\cos\left(\omega_r\xi\frac{\sin\theta}{c}\right)ds + \pi\omega_r\frac{m}{M_r}f_r(s')\frac{W_p(\omega_r)}{\overline{p^2(t)}}\int_s f_r(s)\sin\left(\omega_r\xi\frac{\sin\theta}{c}\right)ds\Bigg\} +$$

$$\frac{m^2}{\overline{p^2(t)}}\sum_{r=1}^{\infty} f_r^2(s')\iint_{s_1 s} f_r(s_1)f_r(s)\int_{-\infty}^{\infty}\frac{\omega^4 W_p(\omega)}{|Z_r(\omega)|^2}\cos\left(\omega\xi\frac{\sin\theta}{c}\right)d\omega\,ds\,ds_1 +$$

$$\sum_{\substack{r=1\\ r\neq\Delta}}^{\infty}\sum_{\Delta=1}^{\infty}\frac{m^2 f_r(s')f_\Delta(s')}{M_r M_\Delta}\left[\iint_{s_1 s} f_r(s_1)f_\Delta(s)\bar{\psi}\left(\xi\frac{\sin\theta}{c}\right)ds\,ds_1 + \pi\left(\omega_r\frac{W_p(\omega_r)}{\overline{p^2(t)}}\cdot\right.\right.$$

$$\left.\left.\cdot\iint_{s_1 s} f_r(s_1)f_\Delta(s)\sin\left(\omega_r\xi\frac{\sin\theta}{c}\right)ds\,ds_1 + \frac{\omega_\Delta W_p(\omega_\Delta)}{\overline{p^2(t)}}\iint_{s_1 s} f_r(s_1)f_\Delta(s)\sin\left(\omega_\Delta\xi\frac{\sin\theta}{c}\right)ds\,ds_1\right)\right] \qquad \ldots(2.45)$$

Under the severest excitation conditions, when some form of resonant excitation is taking place, the term containing the sum of inertia stresses in each mode will be the largest contributor to the mean square stress.

The term in equation 2.45 which is due to the correlation between the local pressure and the local inertia force (inside curly brackets) contains three integrals. This term is a small component of the mean square stress when the panel is being excited at a

resonance. The maximum values of the first and second integrals occur at plate anti-nodes but they are small at plate nodes. The maximum value of the third integral occurs at plate nodes whereas it is small at plate anti-nodes. However, the term containing the third integral is multiplied by $f_r(s')$ so that it will be a small term for all plate positions. The largest values of these terms occur when the plate is being excited by the coincidence effect.

The integrals involved in the cross-correlation term between inertia effects in different modes (the double sum in equation 2.45) are similar to those mentioned in the paragraph above. We now introduce the following symbols:

$$\int_S f_r(s)\, e^{i\omega_r \xi \frac{\sin\theta}{c}}\, ds = I_{c_{rr}} + i\, I_{s_{rr}}$$

$$\text{and} \quad \iint_{S_1 S} f_r(s_1) f_\delta(s)\, e^{i\omega_r \xi \frac{\sin\theta}{c}}\, ds\, ds_1 = I_{c_{r\delta r}} + i\, I_{s_{r\delta r}}$$

$$\text{and} \quad \int_S f_r(s)\, \bar{\psi}\left(\xi \frac{\sin\theta}{c}\right) ds = I_{\psi_r}$$

$$\text{and} \quad \iint_{S_1 S} f_r(s_1) f_\delta(s)\, \bar{\psi}\left(\xi \frac{\sin\theta}{c}\right) ds\, ds_1 = I_{\psi_{r\delta}} \qquad \ldots(2.46)$$

The term in equation 2.45 containing the sum of inertia stresses in each mode, which is the most important term in the expression for mean square stress, contains the following integral:

$$\iint_{S_1 S} f_r(s_1) f_r(s) \int_{-\infty}^{\infty} \frac{\omega^4 W_p(\omega)}{|Z_r(\omega)|^2} \cos\left(\omega \xi \frac{\sin\theta}{c}\right) d\omega \, ds \, ds_1 =$$

$$\frac{\overline{p^2(t)}}{M_r^2} \iint_{S_1 S} f_r(s_1) f_r(s) \bar{\psi}\left(\xi \frac{\sin\theta}{c}\right) ds ds_1 + \frac{W_p(\omega_r)}{M_r^2} \pi \frac{\omega_r}{\delta_r} (1 - 4\delta_r^2) \frac{8a^2b^2}{m^2n^2\pi^4} L_r$$

...(2.47)

This equation has been derived in Appendix A2.4 by assuming the simply-supported mode of deflection:

$$f_r(s) = \sin\frac{n\pi x}{a} \sin\frac{m\pi y}{b} \qquad \ldots(2.48)$$

It only holds true when m is an odd integer; if m is an even number the whole term is zero. We call L_r the 'Joint Magnification Factor'. L_r has been formed in such a way that it is equal to unity or zero (depending on the mode) when the plane waves are at normal incidence. It is clear that for a mode with low damping (and for sandwich plates the mode damping ratios are small) the term containing L_r is the larger component of this inertia stress. A typical variation of L_r (L_5) is shown in Figure 15. It is seen that it reaches a maximum value when the modal wavelength is equal to the plate trace wavelength. This maximum value of L_r is larger for smaller

damping. In the sub-section 2.2.3.1, which follows shortly, an explanation is given of why this is so.

Substituting equations 2.47 and 2.46 into equation 2.45 we have an equation for mean square bond stress in the normal direction for a simplyesupported sandwich plate being excited by random plane waves:

$$\overline{\sigma_z^2(t,s')} = \overline{p^2(t)}\left[1 - 2\sum_{r=1}^{\infty}\frac{m}{M_r}f_r(s')\left\{I_{\psi_r} - 2\pi\omega_r\delta_r\frac{W_p(\omega_r)}{\overline{p^2(t)}}I_{c_{rr}} + \pi\omega_r\frac{W_p(\omega_r)}{\overline{p^2(t)}}I_{s_{rr}}\right\}\right.$$

$$+\frac{m^2}{\overline{p^2(t)}}\sum_{r=1}^{\infty}f_r^2(s')\left[\frac{\overline{p^2(t)}}{M_r^2}I_{\psi_{rr}} + \frac{W_p(\omega_r)}{M_r^2}\frac{\pi\omega_r}{\delta_r}(1-4\delta_r^2)\frac{8a^2b^2}{m^2n^2\pi^4}L_r\right]$$

$$\left.+\sum_{\substack{r=1\\r\neq s}}^{\infty}\sum_{s=1}^{\infty}m^2\frac{f_r(s')f_s(s')}{M_r M_s}\left[I_{\psi_{rs}} + \pi\left\{\omega_r\frac{W_p(\omega_r)}{\overline{p^2(t)}}I_{s_{rsr}} + \omega_s\frac{W_p(\omega_s)}{\overline{p^2(t)}}I_{s_{rss}}\right\}\right]\right] \quad \ldots(2.49)$$

We now introduce the non-dimensional parameter ϕ , thus:

$$\phi_r = \frac{\pi\omega_r W_p(\omega_r)}{2\overline{p^2(t)}} \quad \ldots(2.50)$$

ϕ_r is a function solely of the pressure field and the modal natural frequency. If we have a Power Spectrum of pressure as shown below then $\omega_r W_p(\omega_r)$ is represented by the shaded area while $\overline{p^2(t)}$ is represented bythe total area under the spectrum. When the spectrum is

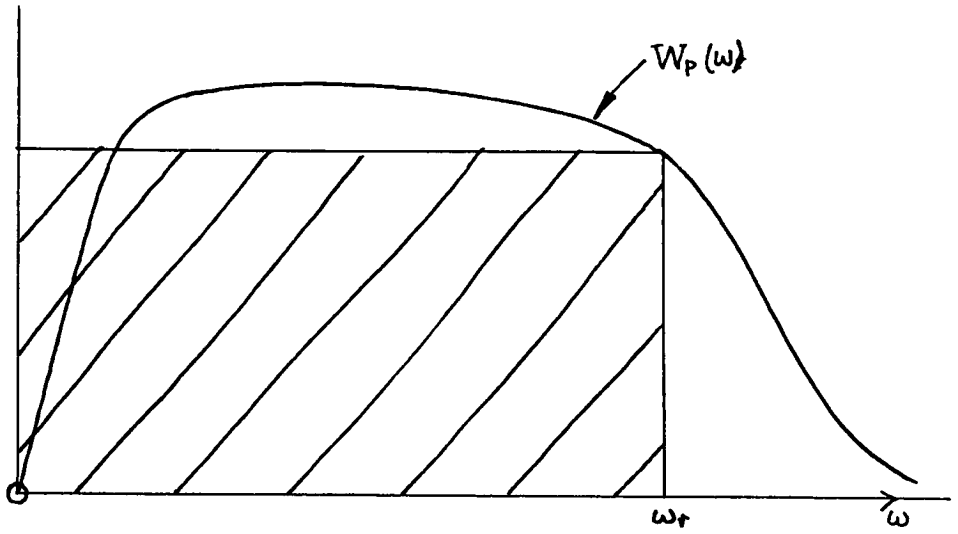

of this form, ϕ_r is of the order of unity. Large values of ϕ_r can clearly occur when the spectrum has one peak which occurs at ω_r. A typical variation of $\phi(\omega)$ is shown in Figure 14. Equation 2.49 now becomes:

$$\overline{\sigma_z^2(t,s')} = \overline{p^2(t)}\left[1 - 2\sum_{r=1}^{\infty}\frac{m}{M_r}f_r(s')\left[I_{\psi_r} - 4\delta_r\phi_r I_{c_{rr}} + 2\phi_r I_{s_{rr}}\right]\right.$$
$$+\sum_{r=1}^{\infty}\frac{m^2 f_r^2(s')}{M_r^2}\left[I_{\psi_{rr}} + \frac{16}{\delta_r}(1-4\delta_r^2)\phi_r\frac{a^2b^2}{m^2n^2\pi^4}L_r\right]$$
$$\left.+\sum_{\substack{r=1\\ r\neq A}}^{\infty}\sum_{A=1}^{\infty}m^2\frac{f_r(s')f_A(s')}{M_r M_A}\left[I_{\psi_{rA}} + 2\left\{\phi_r I_{s_{rAr}} + \phi_A I_{s_{rAA}}\right\}\right]\right] \quad \ldots(2.51)$$

From this equation we can see that the important direct inertia term is inversely proportional to the damping ratio and is multiplied by a function L_r which can become large if the acoustical coincidence effect occurs. To reduce this stress, therefore, damping of the

flexural vibrations of the panel would be the most effective step. Care should also be taken, in designing the panel, to avoid, as far as is possible, the likelihood of excitation by the acoustical coincidence effect.

2.2.3.1 A Comment on the 'Joint Magnification Factor', L_r

We have seen in § 2.2.3 that there is a term in the expression for mean square bond stress which derives from a sum of mean square inertia stresses in each mode of vibration. This term is large under severe response conditions. It has been evaluated in Appendix A.2.4 and is given by the following equation:

$$\int_{-\infty}^{\infty} \frac{\omega^4 W_{F_r}(\omega)}{|Z_r(\omega)|^2}\, d\omega = \int_{S_1}\int_{S_2} \frac{\overline{p^2(t)}}{M_r^2} f_r(s_1) f_r(s_2)\, \bar{\psi}\left(\xi \frac{\sin\theta}{c}\right) ds_1\, ds_2$$

$$+ \frac{W_p(\omega_r)}{M_r^2} \frac{\pi \omega_r}{\delta_r} (1 - 4\delta_r^2) \frac{8a^2b^2}{m^2n^2\pi^4} L_r \qquad \ldots(2.52)$$

This equation has been derived for a simply-supported plate. Calling to mind equations 2.34 and 2.36, viz.

$$W_{F_r}(\omega) = W_p(\omega) S^2 j_{rr}^2$$

we can see that the left hand side of equation 2.52 is the integral of the product of the three functions j_{rr}^2, $\omega^4 / |Z_r(\omega)|^2$, and $W_p(\omega)$. Here, we are supposing that the spatial integral has been carried out first. In the appendix it is convenient to perform first the

integration with respect to frequency. Now the function $\omega^4/|Z_r(\omega)|^2$ has the form shown below:

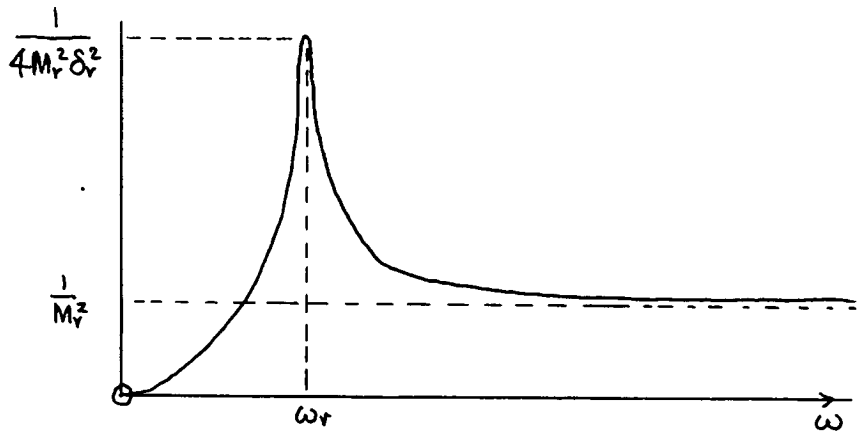

It can be split into two parts, viz. a constant $1/M_r^2$, and another function which has a peak at $\omega = \omega_r$. The left hand side of equation 2.52 may therefore be split into two parts. The first part, involving the integration of the product of the constant $1/M_r^2$, j_{rr}^2 and $W_p(\omega)$ yields the first term in equation 2.52 above; the second part yields the second term in equation 2.52. The function L_r in this term is called the 'Joint Magnification Factor'. For a mode with m and n odd it represents the factor by which the response in that mode to plane waves of normal incidence must be multiplied to give the response to plane waves of general incidence. It therefore has unit value for normally incident waves and for modes with m and n odd. If either m or n is even, L_r is zero for normally incident fields. L_r depends on both the plate dynamic characteristics and the external pressure field and can be expressed as a function of the modal damping ratio and of λ_m/λ_{tr}.

Here, λ_{tr} is the trace wavelength on the plate of the component of the sound field of frequency ω_r. In Figure 15 it can be seen that the maximum value of L_r occurs when $\lambda_m/\lambda_{tr}=1$. This maximum value increases as the damping decreases. The main purpose of this section is to explain why this variation occurs.

If we assume that $W_p(\omega)$ is reasonably constant in the region of the rth natural frequency then the second part of the integral 2.52, with L_r as a factor, is derived from the integration of the product of the two functions shown below:

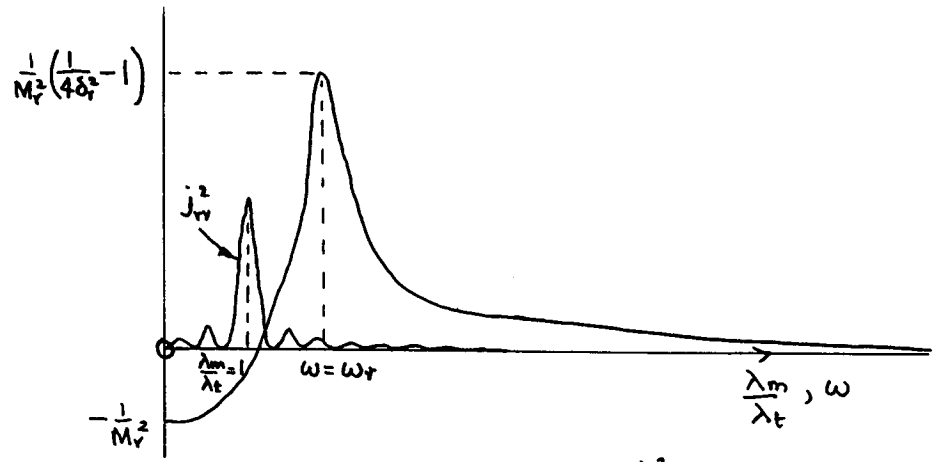

A sketch of typical values of j_{rr}^2 has been seen before.

If the peak value of j_{rr}^2 occurs at the natural frequency of the mode, ω_r, then the maximum value of this second term occurs and corresponds to acoustical coincidence effect excitation. For high order modes the peak of j_{rr}^2 becomes very narrow and can be replaced by a narrow double step function of the same height. The maximum value of this second term then derives from the integral of

the product of the two functions shown below:

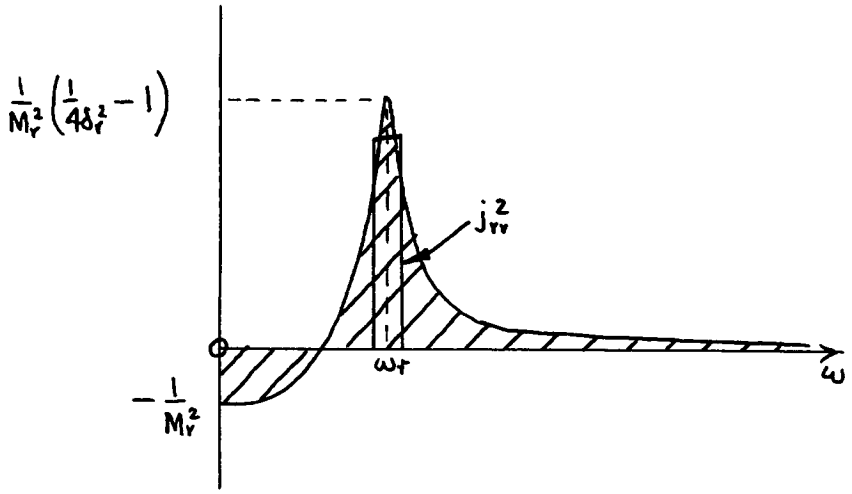

This maximum value is therefore proportional to $(1/4\delta_r^2 - 1)$. For normally incident plane waves j_{rr}^2 is a flat function, so that the value of this second term here is proportional to the area under the curve shown shaded in the sketch above. This area is proportional to $(1-4\delta_r^2)/\delta_r$. L_r has been obtained by dividing the general value of this term by the value obtained for normally incident plane waves. Therefore, the maximum value of L_r (at $\lambda_m/\lambda_{tv} = 1$) is proportional to $(1/4\delta_r^2-1) \div (1-4\delta_r^2)/\delta_r$. Thus the maximum value of L_r is proportional to $1/\delta_r$, provided that the form of j_{rr}^2 is such that its peak is contained within the resonant peak.

It will be noted (from Figure 15) that the variation of the maximum value of L_s with damping is not as strong as $1/\delta_r$ for the values of δ_r considered. This is because the width of the peak of j_{rr}^2 is in fact rather greater than the resonant peak width. In this case the maximum value of L_r corresponds to some intermediate condition between the very shapp j_{rr}^2 (for which $L_{r_{max.}} \propto 1/\delta_r$), and the flat j_{rr}^2 for which $L_{r_{max}} = 1$.

2.2.4 A Restriction of the General Acoustic Field to Normal Incidence Random Plane Waves

For normal plane waves the incidence angle θ is zero so that $\xi \frac{\sin\theta}{c} = 0$. Therefore $\sin\left(\omega_r \xi \frac{\sin\theta}{c}\right) = 0$ and $\cos\left(\omega_r \xi \frac{\sin\theta}{c}\right) = 1$. The pressure is now perfectly correlated over the plate so that $\bar{\psi}\left(\xi \frac{\sin\theta}{c}\right) = 1$ everywhere. Under these conditions we see that the following simplifications are possible:

$$I_{C_{rr}} = \int_S f_r(s)\,ds = I_r \text{ (say)}$$

$$I_{S_{rr}} = 0$$

$$I_{S_{r\Delta r}} = I_{S_{r\Delta\Delta}} = 0$$

$$I_{\psi_r} = I_r$$

$$I_{\psi_{r\Delta}} = I_r I_\Delta$$

$$I_{\psi_{rr}} = I_r^2$$

...(2.53)

and equation 2.51 for mean square stress can be rewritten:

$$\overline{\sigma^2(t,s')} = \overline{p^2(t)}\left[1 - 2\sum_{r=1}^{\infty}\frac{m}{M_r} f_r(s')\, I_r\left(1 - 4\delta_r\phi_r\right)\right.$$
$$+ \sum_{r=1}^{\infty}\left(\frac{m}{M_r} f_r(s')\right)^2\left(1 + \frac{(1-4\delta_r^2)}{\delta_r}\phi_r\right)$$
$$\left. + \sum_{r=1}^{\infty}\sum_{\substack{\Delta=1 \\ r\neq\Delta}}^{\infty}\frac{m^2 f_r(s') f_\Delta(s')}{M_r M_\Delta} I_r I_\Delta\right]$$

...(2.54)

bearing in mind that for the assumed mode of equation 2.48:

$$I_r^2 = \frac{16\,a^2b^2}{m^2n^2\pi^4} L_r = \frac{a^2b^2}{m^2n^2\pi^4}\left(1-\cos n\pi\right)^2\left(1-\cos m\pi\right)^2 \qquad \ldots(2.55)$$

If, therefore, either m or n is an even integer the integral I_r is zero and the generalised force is zero. No motion in this mode then takes place. We will assume therefore that for mode r, m and n are now restricted to odd integers. If we now replace the non-dimensional function $\frac{m}{M_r} f_r(s') I_r$ by C_r we can rewrite equation 2.54 thus:

$$\overline{\sigma_z^2(t,s')} = \overline{p^2(t)}\left[\left\{1-\sum_{r=1}^{\infty} C_r\right\}^2 + \sum_{r=1}^{\infty} \phi_r C_r^2\left(\frac{1}{\delta_r} - 4 + \frac{8\delta_r}{C_r}\right)\right] \qquad \ldots(2.56)$$

It has been shown in the appendix A.2.1 that the two direct stresses in the bond of a honeycomb beam vibrating freely in a single mode are of the same order of magnitude. A similar comparison will now be made for the direct stresses at the centre of a sandwich plate vibrating in a set of modes excited by normal incidence plane waves. The value of mean square normal stress is calculated here, the mean square bending stress being calculated in the next section.

Sample Calculation: A calculation using equation 2.56 above is made for the mean square normal bond stress at the centre of a honeycomb sandwich plate. The plate chosen is identical to the plate used in the experiments described in chapter three. Empirical values of natural

frequencies and damping ratios are taken from chapter three. Motion of the plate will be restricted to the two natural modes:

$$f_1(s) = \sin\frac{\pi x}{a} \sin\frac{\pi y}{b}$$

and $$f_2(s) = \sin\frac{3\pi x}{a} \sin\frac{\pi y}{b}$$

The panel characteristics are as follows:

a = 42.5 ins

b = 24 ins

h_2 = 0.0124 ins

h_1 = 0.425 ins

λ = 72.27

β = 2.95

The two modes chosen only allow a single half wave in the y-direction.

A table of quantities relative to the problem is given below. Values of ϕ_r are taken from Figure 14 for the Rolls-Royce Avon. These values of ϕ_r are not at all representative of a normal incidence plane wave sound field but they will serve for this comparison of the two stresses

MODE	ω_r c/s	δ_r	$\phi_r(\omega_r)$	$C_r\ (16/\beta\pi^2)$
1	204	0.015	0.04	+0.550
2	579	0.005	0.27	-0.183

To find the direct normal stress in the honeycomb core we apply a

factor λ to the normal stress to take account of the local stress magnification at the cell wall-bond joint. Equation 2.56 can thus be written for the plate we have chosen:

$$\overline{\sigma^2(t)} = \lambda^2 \overline{p^2(t)} \left[\left\{ 1 - \sum_{r=1}^{2} C_r \right\}^2 + \sum_{r=1}^{2} \phi_r C_r^2 \left(\frac{1}{\delta_r} - 4 + \frac{8\delta_r}{C_r} \right) \right] \qquad \ldots(2.57)$$

$$\overline{\sigma_z^2(t)} = \lambda^2 \overline{p^2(t)} \left[\left\{ 1 - 0.367 \right\}^2 + 2.614 - 0.085 + 0.005 \right]$$

$$\overline{\sigma_z^2(t)} = \lambda^2 \overline{p^2(t)} \left[0.401 + 2.534 \right]$$

$$\overline{\sigma_z(t)} = \lambda \, \overline{p(t)} \, 1.713$$

$$\overline{\sigma_z(t)} = 124 \, \overline{p(t)}$$

It can be seen from this calculation that the mean square stress is given by:

$$\overline{\sigma_z^2(t)} \simeq \lambda^2 \overline{p^2(t)} \sum_{r=1}^{\infty} \phi_r \frac{C_r^2}{\delta_r} \qquad \ldots(2.58)$$

within an order of magnitude. As is to be expected, the inertia term is predominant for a plate with flexural modes having low damping.

Subjection of a panel such as that above to a noise level of 170 dB would therefore only produce an r.m.s. stress level of the order of 100 lb/in^2. This would be unlikely to produce fatigue failures. However, for a plate undergoing coincidence effect excitation or excitation of a similar sort this stress could rise appreciably because $\sqrt{L_r}$, which is approximately the scaling factor to be used, can, for example, be as high as 2.36 for the third mode. Coincidence

[redacted] effect excitation affects panel fatigue characteristics adversely in two ways as the mode number rises, provided that vibrations occur at a higher frequency, as they usually do: The first is that the value of the term containing L_f rises approximately in proportion to the natural frequency (see Appendix A.2.4). The second is that the number of cycles occurring in a given time is increased, thereby reducing the time to failure.

2.2.5 An Analysis of the Mean Square Bending Stress in the Bond of a Simply Supported Sandwich Panel when under Excitation by Normal Acoustic Plane Waves

In Appendix A.2.1 it is shown that the bending and normal direct stresses in the bond of a freely vibrating honeycomb beam are of the same order of magnitude. The analysis of this section shows that this conclusion is also true for the stresses in the bond of a simply-supported honeycomb plate which is being excited by normal incidence random plane waves. As only an order of magnitude comparison is to be made, the more accurate method due to Williams, mentioned in the introduction to this chapter, is not used. Instead the stress is derived from the strain in each mode and not as a sum of the static and dynamic loadings. The advantage of using this strain method lies in its simplicity. The analysis is carried out for the bending stress in the x-direction and assumes a series of modes in the x-direction only, as has been assumed in the sample calculation of § 2.2.4. This is a reasonable assumption for the sandwich panel already considered.

Consider a simply-supported rectangular sandwich panel of

dimensions a by b undergoing excitation by random acoustic plane waves at normal incidence. The transverse response of the panel in flexural modes is given by equation 2.11. Suppose that we can restrict $f_r(S')$ to a single set of modes, thus:

$$f_r(x,y) = \sin \frac{n\pi x}{a} \sin \frac{\pi y}{b} \qquad \ldots(2.59)$$

so that only one half-wave is allowed in the y-direction. The bond strain in the x-direction is given by:

$$e_x = h_1 \sum_{r=1}^{\infty} q_r(t) a_r \frac{\partial^2 f_r(S')}{\partial x^2} \qquad \ldots(2.60)$$

a_r is a factor less than unity and takes account of the alleviation of e_x due to core shear distortion. It can be shown that if we assume a linear core distortion (see § 1.3.2) then a_r is given by the equation:

$$a_r = 1 - \frac{\mu\lambda\bar{\psi}_r}{(1-\nu^2)\gamma} \qquad \ldots(2.61)$$

Note that here, $\bar{\psi}_r$ is the non-dimensional wavelength parameter given in chapter one and is not a correlation coefficient.

Now provided that the bond obeys the usual type of stress-strain relationships used for homogeneous materials, the bond bending stress in the x-direction is given by the equation:

$$\sigma_x = \frac{E_b}{1-\nu^2}(e_x + \nu e_y) \qquad \ldots(2.62)$$

where E_b is the Youngs Modulus of the bonding material. Substitution of equation 2.60 and a similar one for ϵ_y into equation 2.62 gives:

$$\sigma_x = \frac{E_b h_1}{1-\nu^2} \sum_{r=1}^{\infty} q_r(t)\, a_r \left\{ \frac{\partial^2 f_r(s')}{\partial x^2} + \nu \frac{\partial^2 f_r(s')}{\partial y^2} \right\} \qquad \ldots(2.63)$$

The Fourier Transform of this stress is given by the equation:

$$\mathcal{F}_{\sigma_x}(\omega, s') = -\frac{E_b h_1}{1-\nu^2} \sum_{r=1}^{\infty} a_r \left[\left(\frac{n\pi}{a}\right)^2 + \nu \left(\frac{\pi}{b}\right)^2 \right] f_r(s') \frac{\mathcal{F}_{F_r}(\omega)}{Z_r(\omega)} \qquad \ldots(2.64)$$

bearing in mind equation 2.13.

Using equation 2.64, the Power Spectrum of the x-wise bending stress is given by the equation:

$$W_{\sigma_x}(\omega, s') = \left\{ \frac{E_b h_1}{1-\nu^2} \right\}^2 \sum_{r=1}^{\infty} \sum_{\Delta=1}^{\infty} a_r a_\Delta f_r(s') f_\Delta(s') \frac{\left[\left(\frac{n\pi}{a}\right)^2 + \nu \left(\frac{\pi}{b}\right)^2 \right] \left[\left(\frac{n'\pi}{a}\right)^2 + \nu \left(\frac{\pi}{b}\right)^2 \right]}{Z_r(\omega)\, Z_\Delta^*(\omega)} \lim_{T \to \infty} \frac{\pi}{T} \mathcal{F}_{F_r}(\omega) \mathcal{F}_{F_\Delta}^*(\omega) \qquad \ldots(2.65)$$

For the purpose of this analysis we will assume that we can neglect the cross terms in this equation. Equation 2.65 then reduces to:

$$W_{\sigma_x}(\omega, s') = \left\{ \frac{E_b h_1}{1-\nu^2} \right\}^2 \sum_{r=1}^{\infty} a_r^2 f_r^2(s') \left[\left(\frac{n\pi}{a}\right)^2 + \nu \left(\frac{\pi}{b}\right)^2 \right] \frac{W_{F_r}(\omega)}{|Z_r(\omega)|^2} \qquad \ldots(2.66)$$

For normal incidence random plane waves the Power Spectrum of the Generalised Force is given by:

$$W_{F_r}(\omega) = W_p(\omega)\, I_r^2$$

and substitution of this into equation 2.66 gives:

$$W_{\sigma_x}(\omega,s') = \left\{\frac{E_b h_1}{1-\nu^2}\right\}^2 \sum_{r=1}^{\infty} a_r^2 f_r^2(s') \left[\left(\frac{n\pi}{a}\right)^2 + \nu\left(\frac{\pi}{b}\right)^2\right]^2 \frac{W_p(\omega)\, I_r^2}{|Z_r(\omega)|^2} \qquad \ldots(2.67)$$

The mean square stress is given by the integral of the Power Spectrum of stress as in equation 2.10 giving:

$$\overline{\sigma_x^2(s')} = \left\{\frac{E_b h_1}{1-\nu^2}\right\}^2 \sum_{r=1}^{\infty} a_r^2 f_r^2(s') \left[\left(\frac{n\pi}{a}\right)^2 + \nu\left(\frac{\pi}{b}\right)^2\right]^2 I_r^2 \int_{-\infty}^{\infty} \frac{W_p(\omega)}{|Z_r(\omega)|^2}\, d\omega \qquad \ldots(2.68)$$

Making the usual assumptions regarding $W_p(\omega)$ and using equation 2.33 this becomes

$$\overline{\sigma_x^2(s')} = \left\{\frac{E_b h_1}{1-\nu^2}\right\}^2 \sum_{r=1}^{\infty} a_r^2 f_r^2(s') \left[\left(\frac{n\pi}{a}\right)^2 + \nu\left(\frac{\pi}{b}\right)^2\right]^2 I_r^2 W_p(\omega_r) \frac{\pi}{2M_r^2 \delta_r \omega_r^3} \qquad \ldots(2.69)$$

For the purpose of comparing the magnitude of this stress with the normal stress of equation 2.58 it is convenient to introduce the non-dimensional notation used before in this chapter, viz:

$$\phi_r = \frac{\pi}{2}\, \omega_r \frac{W_p(\omega_r)}{\overline{p^2(t)}}$$

and

$$C_r = \frac{m}{M_r} f_r(s')\, I_r$$

the expression for mean square stress then becomes:

$$\overline{\sigma_x^2(s')} = \overline{p^2(t)} \left\{\frac{E_b h_1}{1-\nu^2}\right\}^2 \sum_{r=1}^{\infty} \left[\left(\frac{n\pi}{a}\right)^2 + \nu\left(\frac{\pi}{b}\right)^2\right]^2 \frac{a_r^2 C_r^2 \phi_r}{m^2 \delta_r \omega_r^4} \qquad \ldots(2.70)$$

The differential equation of motion of a sandwich plate in which there is no shear deformation is

$$D\nabla^4 w - m\frac{\partial^2 w}{\partial t^2} = q \qquad \ldots(2.71)$$

where the symbols have their usual meanings. If the plate is rectangular, simply-supported, has a rigid core, and vibrates freely in the mode $\sin\frac{n\pi x}{a} \cdot \sin\frac{\pi y}{b}$ the natural frequency (ω_r) is found to be given by

$$\beta m\omega_r^2 = 2E_m\frac{h_2 h_1^2}{1-\nu^2}\left[\left(\frac{n\pi}{a}\right)^2+\left(\frac{\pi}{b}\right)^2\right]^2 \qquad \ldots(2.72)$$

β has been defined after equation 2.15. Core shear effects have been neglected in the derivation of this equation yet included in the derivation of equation 2.60. This is because the effect of core shear on the natural frequency is expected to be less than the effect on the bond stress.

It will be noted that the symbol ν has been used for the Poissons ratio of both bond and face materials. We have therefore assumed that these two ratios are equal. Using equation 2.72, equation 2.70 becomes:

$$\overline{\sigma_x^2(t)} = \overline{p^2(t)}\,\frac{\beta^2\alpha^2}{4\mu^2}\sum_{r=1}^{\infty}\left\{\frac{\left(\frac{n\pi}{a}\right)^2+\nu\left(\frac{\pi}{b}\right)^2}{\left[\left(\frac{n\pi}{a}\right)^2+\left(\frac{\pi}{b}\right)^2\right]^2}\right\}^2\frac{a_r^2 C_r^2\phi_r}{h_1^4\delta_r} \qquad \ldots(2.73)$$

where $\alpha = E_b/E_m$

or alternatively:

$$\overline{\sigma_x^2(s')} = \overline{p^2(t)}\,\frac{\beta^2\alpha^2 A_m^4 \nu^2}{4\mu^2\pi^4}\sum_{r=1}^{\infty}\left\{\frac{\left[1+\frac{n^2}{\nu}\left(\frac{b}{a}\right)^2\right]}{\left[1+n^2\left(\frac{b}{a}\right)^2\right]^2}\right\}^2 a_r^2 C_r^2 \frac{\phi_r}{\delta_r} \qquad \ldots(2.74)$$

If we now put:

$$\frac{\left[1+\frac{n^2}{\nu}\left(\frac{b}{a}\right)^2\right]}{\left[1+n^2\left(\frac{b}{a}\right)^2\right]^2} = \gamma_r \qquad \ldots(2.75)$$

equation 2.74 becomes:

$$\overline{\sigma_x^2(s')} = \overline{p^2(t)}\,\frac{\beta^2\alpha^2 A_m^4 \nu^2}{4\mu^2\pi^4}\sum_{r=1}^{\infty}\gamma_r^2 a_r^2 C_r^2 \frac{\phi_r}{\delta_r} \qquad \ldots(2.76)$$

If $\gamma_r^2 a_r^2$ is approximately unity we can see, by comparing equation 2.76 and equation 2.58, that

$$\frac{\overline{\sigma_x}}{\overline{\sigma_z}} \simeq \frac{\beta\alpha\nu A_m^2}{2\mu\lambda\pi^2} \qquad \ldots(2.77)$$

For the lower order modes this assumption holds reasonably true but for higher modes $\gamma_r^2 a_r^2$ drops below unity quite rapidly. For an ordinary honeycomb sandwich panel the factor given in equation 2.77 is shown, below, to be of the order of unity. Therefore, the conclusion reached in the Appendix A.2.1 concerning stresses in the bond of honeycomb beams holds true for honeycomb plates which are being excited by normal incidence random plane waves. The factor given in

equation 2.77 is similar to that obtained in the Appendix A.2.1 for sandwich beams.

Sample Calculation: A sample calculation is now carried out for $\overline{\sigma_x}$ using equation 2.76 above, to find the magnitude of this stress. The calculation is carried out for a panel identical to that chosen for the sample calculation of § 2.2.4 and under the same excitation condition. Again, motion is restricted to the two modes cited in § 2.2.4. For this panel we have the following information which is additional to that given in § 2.2.4:

$$\alpha = 0.1$$

$$\nu = 0.3$$

$$A_m = 56$$

$$\mu = 0.03$$

For mode 1 we find:

$$a_1^2 = 0.796$$

$$\gamma_1^2 = 1.409$$

and $$a_1^2\gamma_1^2 = 1.121$$

For mode 2 we find

$$a_2^2 = 0.523$$

$$\gamma_2^2 = 0.500$$

and $$a_2^2\gamma_2^2 = 0.262$$

The factor of equation 2.77 is given by:

$$\frac{\beta \alpha \nu A_m^2}{2\mu\lambda\pi^2} = 6.48$$

Using equation 2.76:

$$\overline{\sigma_x^2(t)} = \overline{p^2(t)}\,\lambda^2\, 6.48^2 \sum_{r=1}^{2} a_r^2 \gamma_r^2 \frac{C_r^2 \phi_r}{\delta_r}$$

$$= \overline{p^2(t)}\,\lambda^2\, 6.48^2\, 1.378$$

The values for C_r , ϕ_r and δ_r given in § 2.2.4 have been used here. The r.m.s. bending stress is therefore given by:

$$\overline{\sigma_x(t)} = 7.60\,\lambda\,\overline{p(t)}$$

$$= 550\ \overline{p(t)}$$

This stress can also be magnified considerably when coincidence effect excitation takes place and stresses may then be of sufficient magnitude to cause fatigue failures (see the results of Chapter 4).

2.3 General Remarks

It is evident that the normal stress and the bending stress in the bond of a honeycomb sandwich panel are of the same order of magnitude when the panel is being excited in flexural modes. For the worked example given in this chapter the bending stress was the larger stress of the two by a factor of 4.4. This plate was simply-supported at its edges and was excited by random plane waves at normal incidence. Motion was restricted to two modes. The maximum bending stress in the

bond was 550 times the incident r.m.s. pressure. Had the motion been restricted to bubbling modes alone then the bending stress would have been very much less than the normal stress in the bond. The likelihood of the acoustic excitation of bubbling modes is quite remote, however, because of their high natural frequencies, as explained in Chapter one. The factor $\frac{\beta\alpha\nu A_m^2}{2\mu\lambda\pi^2}$ derived in § 2.2.5, as an approximate expression for the ratio of the bending stress $\overline{\sigma_x}$ to the normal stress $\overline{\sigma_z}$ can quickly be calculated for any panel. For the worked example this factor was 6.58 compared with the actual stress ratio of 4.4. If this ratio is very large or very small then $\overline{\sigma_x}$ or $\overline{\sigma_z}$ will be the predominant stress, respectively. If the bending stress is larger than the normal stress in the bond, fatigue failures of the debonding type are not necessarily precluded in favour of fatigue failures due to the bending stress. The reason for this is that when cracks start to form, normal to the bending stress, some of the bending load which the bond had been taking is shed into the faces. Also, these cracks will not penetrate as far as the face because of the close adhesion of the bond to the face. Cracks forming normal to the bond normal stress can propagate quickly, however, as there is no other medium to which the load can be shed. The initiation of cracks normal to the bending stress can cause stress concentrations which will accelerate the debonding type of failure, especially if cracks are formed where the honeycomb joins the bond.

If we consider an aircraft sandwich panel being excited by jet noise then the likelihood that the bending stress is of the same

order of magnitude as the normal stress in the bond, depends on the characteristics of the noise field. If the overall correlation length of the pressure field is extremely short then negligible motion will take place because generalised forces are very small. For this pressure field the normal stress will be the larger stress in the bond and will be due to the incident pressure only. The bending stress will be zero. On the other hand, if the wavelength of the filtered space correlation of the pressure field, at the natural frequency of one of the modes, is the same as the modal wavelength then large motion occurs in this mode due to the coincidence effect. Here, the bending and normal stresses will be of the same order of magnitude and the most significant parts of both stresses will be due to inertia effects. The real noise field for (say) a rudder panel is closer to the latter case, e.g. a typical rudder panel might be four feet long and might have a fundamental natural frequency of about 100 c/s. The half-wavelength of the filtered lateral space-correlation of noise pressure at 100c/s is larger than four feet for a typical jet engine. It is therefore likely that these two stresses will be of the same order of magnitude for aircraft sandwich panels.

In the analysis of this chapter no restriction has been specifically applied to limit the plate velocity to the acoustic particle velocity. This restriction would have been applied if the acoustic reactive and resistive forces had been included in the analysis. However, if the damping ratios used in any application of this chapter are greater than the actual acoustic damping ratio

for the panel concerned, then it is impossible for the normal velocity of the panel surface to exceed the particle velocity. The acoustic damping of a panel is usually much smaller than the structural damping so that a reasonable estimate of the total damping will not permit the normal velocity of the panel surface to exceed the acoustic particle velocity.

The factor L_r can become large for higher order modes because its peak value is proportional to r^2. However, the factor by which L_r is multiplied to give that part of the inertia stress, is proportional to $\omega_r \cdot r^2$. Thus, as the mode number rises, the peak value of this term is proportional to the natural frequency of the mode. With regard to fatigue therefore, coincidence effect excitation becomes more dangerous as the mode number rises (assuming that the natural frequency rises) because of the rise in bond stress and also because the number of cycles occurring in a given time is increased. The magnitude of stresses calculated for plane wave excitation of sandwich panels is quite small, viz. about 500 lb/in^2 for the severe condition of 170 dB (re 0.0002 $dynes/cm^2$). It has been pointed out, however, that when the panel is under the influence of a noise field with suitable spatial pressure correlation (e.g. inclined plane waves at the coincidence angle) magnification of these stresses can take place. Some simple calculations have been carried out by the author to investigate this magnification. The sandwich panel - normally incident noise field configuration of the sample calculations has been changed by rotating the panel so that the noise field is incident upon the plate at the correct angles for the coincidence effect excitation of the second and third modes of the panels (viz. those modes with two and three half-waves in the x-direction). Under this excitation the predominant term in the expression for stress (equation 2.51) is the

direct inertia term of the mode concerned. This term has been evaluated for the coincidence excitation of these two modes. For the coincidence excitation of the second mode the maximum bond normal stress is 75 lb/in^2 and for a similar excitation of the third mode the maximum bond normal stress is 173 lb/in^2. These figures compare with the 125 lb/in^2 maximum bond normal stress when the panel is being excited by normally incident plane waves. The stresses of 75 lb/in^2 and 173 lb/in^2 will in fact be a little larger due to contributions from other modes. If the incident angle for coincidence is similar for several modes (as in the case examined) then this further magnification can be large. These figures, are, for obvious reasons, highly dependent on the damping of the mode concerned and the power spectrum of pressure at the modal frequency. These effects can be reduced by careful design combined with a knowledge of likely noise fields and especially by the use of damping.

One of the factors which makes any application of the work of this chapter approximate only is the difference between the ideal single simply-supported panel of this chapter and the real panel, which is joined to a structure of a similar stiffness to itself at its edges, and has associated acoustic cavities which modify its impedance. Another factor is the difference between the ideal noise field considered here and real noise fields. The predicted values of bond stresses for aircraft sandwich panels can therefore only be within an order of magnitude of the actual values.

A P P E N D I C E S

Appendix A.2.1 A Magnitude Comparison of the Normal Direct Stress and the Bending Stress in the Bond of a Sandwich Beam Vibrating Freely in a Single Flexural Mode

This short and simplified analysis is carried out to show that these two stresses are of the same order of magnitude in the bond of a honeycomb sandwich beam. Consider the simply-supported beam shown below:

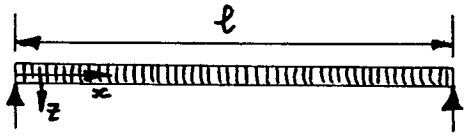

The characteristics of the sandwich are given by the following symbols:

μ = the mass per unit length

μ_2 = the mass of one face per unit length

$2h_1$ = the core depth

h_2 = the face thickness

λ = the area-ratio of the honeycomb

If the mode of natural vibration of the beam, without damping, is given by:

$$w = w_0 \sin\frac{\pi x}{\ell} \cos\omega t \qquad \ldots(2.78)$$

then the maximum bending strain in the bond is

$$\epsilon_x = \omega_0 h_1 \left(\frac{\pi}{\ell}\right)^2 \qquad \ldots(2.79)$$

at the beam centre. This is approximate only because the alleviation of this strain due to shear distortion of the core has been neglected. So the maximum bending stress is given by

$$\sigma_x = E_b \epsilon_x = E_b h_1 \left(\frac{\pi}{\ell}\right)^2 \omega_0$$

The maximum stress in the z-direction in the bond (normal stress) is due to inertia loading from the vibrating face and for a homogeneous core this maximum stress, which will again occur at the beam centre, is given by the equation:

$$\sigma_z = \mu_2 \omega_0 \omega^2 \qquad \ldots(2.80)$$

However the direct stress in a honeycomb core will be magnified by a factor approximately equal to the area ratio, so that the maximum stress is given by:

$$\sigma_z = \lambda \mu_2 \omega_0 \omega^2 = \lambda \omega_0 \frac{\mu_2}{\mu} \mu \omega^2 \qquad \ldots(2.81)$$

Now the equation of motion of the mode of vibration of the beam gives rise to the frequency equation, thus:

$$E_m I \left(\frac{\pi}{\ell}\right)^4 - \mu \omega^2 = 0 \qquad \ldots(2.82)$$

where I is the second moment of area of the beam cross-section and E_m is the Young's Modulus of the faces. This equation does

not take into account core shear distortion effects unless a modified value of I is used. If we now substitute for $\mu\omega^2$ in equation 2.81 using equation 2.82 the bond normal stress becomes:

$$\sigma_z = \lambda\omega_o \frac{\mu_2}{\mu} E_m I \left(\frac{\pi}{\ell}\right)^4 \qquad \ldots(2.83)$$

and if $I = 2h_1^2 h_2$, the results of equations 2.83 and 2.79 can be compared by writing

$$\frac{\sigma_x}{\sigma_z} = \frac{\mu}{\mu_2} \frac{E_b}{E_m} \frac{\ell^2}{\lambda\pi^2 h_1 h_2} \qquad \ldots(2.84)$$

This non-dimensional expression is of the order of one for ordinary sandwich configurations and therefore shows that the two stresses are of the same order of magnitude in the bond of a honeycomb sandwich beam vibrating in a single flexural mode.

Appendix A.2.2 Two Codes of Fourier Transform Notation used in the Analysis of Random Processes

The two codes listed below are those primarily used by mathematicians (a) in which the transform and inverse transform are of a similar form, and those used more often by engineers (b). Either code can be used but a mixture of the two is inadmissible. Code (b) has been used throughout this chapter and chapter 3.

Title	Code (a)	Code (b)
Fourier Transform	$\mathfrak{F}(\omega) = \frac{1}{\sqrt{2\pi}} \int_{-\infty}^{\infty} e^{-i\omega t} F(t)\, dt$	$\mathfrak{F}(\omega) = \frac{1}{2\pi} \int_{-\infty}^{\infty} e^{-i\omega t} F(t)\, dt$
Inverse Fourier Transform	$F(\tau) = \frac{1}{\sqrt{2\pi}} \int_{-\infty}^{\infty} e^{i\omega\tau} \mathfrak{F}(\omega)\, d\omega$	$F(\tau) = \int_{-\infty}^{\infty} e^{i\omega\tau} \mathfrak{F}(\omega)\, d\omega$
Power Spectrum	$W_F(\omega) = \lim_{t_o \to \infty} \frac{\mathfrak{F}(\omega)\, \mathfrak{F}^*(\omega)}{t_o}$	$W_F(\omega) = \lim_{t_o \to \infty} \frac{\pi}{t_o} \mathfrak{F}(\omega)\, \mathfrak{F}^*(\omega)$
Autocorrelation Function	$\psi(\tau) = \lim_{T \to \infty} \frac{1}{2T} \int_{-T}^{T} F(t) F(t+\tau)\, dt$	$\psi(\tau) = \lim_{T \to \infty} \frac{1}{8T} \int_{-T}^{T} F(t) F(t+\tau)\, dt$
	$W_F(\omega) = \frac{1}{\pi} \int_{-\infty}^{\infty} e^{-i\omega\tau} \psi(\tau)\, d\tau$	$W_F(\omega) = \frac{1}{2\pi} \int_{-\infty}^{\infty} e^{-i\omega\tau} \psi(\tau)\, d\tau$
Mean Square Force	$\overline{F^2(t)} = 2 \int_{-\infty}^{\infty} W_F(\omega)\, d\omega$	$\overline{F^2(t)} = \int_{-\infty}^{\infty} W_F(\omega)\, d\omega$

Appendix A.2.3 A Note on Acoustic Radiation and Reaction Forces (Damping and Virtual Mass)

In the text of chapter two no account has been taken explicitly of acoustic radiation and reaction forces other than an implied inclusion of the acoustic damping (assumed to be viscous) in the modal damping ratio δ_r . These forces are in fact small for a plate without an enclosed cavity behind so that neglect of them is justifiable. However, some account is given of them here for completeness.

The acoustic pressure dp on an element of area dS_1 , due to harmonic motion of another element, a distance h from it, of area dS_2 is given, by:

$$dp = -i\left(\frac{\rho f u_2}{h} dS_2\right) e^{ik(h-ct)} \qquad \ldots.(2.85)$$

(see Morse; Theory of Sound or other standard textbooks.) where f is the frequency of harmonic vibration of the plate in c/s, u_2 is the velocity amplitude of dS_2 and k is the wave-number ($= 2\pi f/c$). The velocity at dS_1 is $u_1 e^{-ikct}$, therefore the amplitudes of the two pressure components at dS_1 are $\frac{\rho f u_2}{h} \sin kh \cdot dS_2$ in phase with velocity and $\frac{\rho f u_2}{h} \cos kh \cdot dS_2$ lagging behind velocity by 90^0.

The first component is the damping force and has been dealt with by Mead[22] and by Mangiarotty[23]. The second force is the pressure exerted in phase with acceleration and can therefore be

regarded as a virtual mass.

The total virtual mass pressure acting at the point due to all elemental pistons is:

$$-i\int_S \frac{\rho f u_2}{h}\cos kh\, dS_2 = i\dot{q}\frac{\rho\omega}{2\pi}\int_S \frac{\cos kh}{h} f(s_2)\, dS_2 \qquad \ldots(2.86)$$

now $-i\omega\dot{q} = \ddot{q}$

and thus the generalised force on the plate in the same mode is of amplitude

$$\ddot{q}\,\frac{\rho}{2\pi}\int_{S'} f(s_1)\int_S \frac{\cos kh}{h} f(s_2)\, dS_2\, dS_1 \qquad \ldots(2.87)$$

This is a generalised (virtual)inertia force, and the coefficient of $\ddot{q}$ may be called the generalised virtual mass of the air surrounding the plate, corresponding to the mode $f(s)$

$$\text{i.e.}\quad M_v = \frac{\rho}{2\pi}\int_{S'} f(s')\int_S \frac{\cos kh}{h} f(s)\, ds\, ds' \qquad \ldots(2.88)$$

The 'uniform pressure' approach which Mead applied to acoustic damping forces (this theory assumes kh small so that $\sin kh = kh$ and $\cos kh = 1$) cannot be applied accurately to the virtual mass of air surrounding sandwich plates although it provides an upper bound to the virtual mass for the fundamental mode of vibration of the plate. This upper bound has been computed for the inner integral of 2.88 by a matrix method and results indicate that virtual masses are of the order of one tenth of the plate masses for the plate of chapter three.

Appendix A.2.4 Evaluation of the Integral of Equation 2.35 for Random Plane Waves at a Fixed Incidence

This integral is the contribution to the mean square normal stress in the bond of the sum of inertia effects in the modes. It can be rearranged thus:

$$\int_{-\infty}^{\infty} m^2\omega^4 \sum_{r=1}^{\infty} \frac{f_r^2(s')\, W_{F_r}(\omega)}{|Z_r(\omega)|^2}\, d\omega = \sum_{r=1}^{\infty} m^2 f_r^2(s') \int_{-\infty}^{\infty} \frac{\omega^4\, W_{F_r}(\omega)}{|Z_r(\omega)|^2}\, d\omega \qquad \ldots(2.89)$$

It was originally thought that this integral could be evaluated by assuming $W_{F_r}(\omega)$ to be constant in the region of the rth resonance. However, although the pressure spectrum, $W_p(\omega)$, might be constant near ω_r, the generalised force spectrum, $W_{F_r}(\omega)$ can be highly variable near ω_r. A more accurate analysis follows, taking account of this variation for inclined plane waves. We can expect this integral to be large when the coincidence effect occurs.

Extracting the integral of the right hand side of equation 2.89 we have:

$$\int_{-\infty}^{\infty} \frac{\omega^4\, W_{F_r}(\omega)}{|Z_r(\omega)|^2}\, d\omega = \iint_{S_1 S_2} f_r(s_1) f_r(s_2) \int_{-\infty}^{\infty} \frac{\omega^4\, W_p(\omega)}{|Z_r(\omega)|^2} \cos\left(\omega \xi \frac{\sin\theta}{c}\right) d\omega\, ds_1\, ds_2 \qquad \ldots(2.90)$$

where $\xi = (x_1 - x_2)$ for random plane waves travelling parallel to the x-axis and incident upon the plate at an angle θ. The inner

integral is given by:

$$\int_{-\infty}^{\infty} \frac{W_p(\omega)}{M_r^2} \cos\left(\omega \xi \frac{\sin\theta}{c}\right)\left\{1 + \frac{2(1-2\delta_r^2)\omega^2\omega_r^2 - \omega_r^4}{\omega^4 - 2(1-2\delta_r^2)\omega^2\omega_r^2 + \omega_r^4}\right\} d\omega =$$

$$\frac{1}{M_r^2}\left\{\overline{p^2(t)}\,\bar{\psi}\left(\xi\frac{\sin\theta}{c}\right) + W_p(\omega_r)\int_{-\infty}^{\infty}\left\{\frac{2(1-2\delta_r^2)\omega^2\omega_r^2 - \omega_r^4}{\omega^4 - 2(1-2\delta_r^2)\omega^2\omega_r^2 + \omega_r^4}\right\}\cos\left(\omega\xi\frac{\sin\theta}{c}\right)d\omega\right\}$$

...(2.91)

The integral in the second term on the right hand side of equation 2.91 is found by contour integration to be:

$$\frac{\pi\omega_r e^{-|\xi\sin\theta/c|\omega_r\delta_r}}{2\delta_r\sqrt{1-\delta_r^2}} \; R\, e^{i\omega|\xi\sin\theta/c|\sqrt{1-\delta_r^2}}\left(\sqrt{1-\delta_r^2}(1-4\delta_r^2) + i\delta_r(3-4\delta_r^2)\right)$$

...(2.92)

The right hand side of equation 2.90 becomes:

$$\frac{\overline{p^2(t)}}{M_r^2}\iint_{S_1 S_2} f_r(s_1) f_r(s_2)\,\bar{\psi}\left(\xi\frac{\sin\theta}{c}\right) ds_1 ds_2 + \frac{W_p(\omega_r)\,\pi\omega_r}{2M_r^2\delta_r\sqrt{1-\delta_r^2}}\, R\left\{(1-4\delta_r^2)\sqrt{1-\delta_r^2} + i\delta_r(3-4\delta_r^2)\right\}$$
$$\iint_{S_1 S_2} f_r(s_1) f_r(s_2)\, e^{\omega_r|\xi\sin\theta/c|\left(-\delta_r + i\sqrt{1-\delta_r^2}\right)} ds_1 ds_2$$

...(2.93)

Now the double integral in the second term of equation 2.93 (for convenience called I) can be evaluated further for a simply-supported plate mode. Put

$$a^* = \omega_r\left(-\delta_r + i\sqrt{1-\delta_r^2}\right)\frac{\sin\theta}{c}$$

and $$f_r(s') = \sin\frac{n\pi x}{a}\sin\frac{m\pi y}{b}$$

then:

$$I = \frac{a^2b^2}{m^2n^2\pi^4} \cdot \frac{(1-\cos m\pi)^2}{\left[1+\left(\frac{aa^*}{n\pi}\right)^2\right]} \left[\frac{2\left(1-e^{aa^*}.\cos n\pi\right)}{\left[1+\left(\frac{aa^*}{n\pi}\right)^2\right]} - aa^* \right] \quad \ldots(2.94)$$

Now $\frac{a\omega_r}{n\pi}\frac{\sin\theta}{c} = \lambda_m / \lambda_{t_r}$ so that we can write

$$\frac{aa^*}{n\pi} = \frac{\lambda_m}{\lambda_{t_r}}\left(-\delta_r + i\sqrt{1-\delta_r^2}\right) \quad \ldots(2.95)$$

Consequently, provided that m is odd, we can write

$$I = \frac{8a^2b^2}{m^2n^2\pi^4}\left\{\frac{\left[1-\cos n\pi . e^{-n\pi\alpha\left(\delta_r - i\sqrt{1-\delta_r^2}\right)}\right]}{\left[1-2\alpha^2(1-2\delta_r^2)+\alpha^4\right]^2}\left[1-2\alpha^2(1-2\delta_r^2)\right.\right.$$

$$\left.+\alpha^4(1-8\delta_r^2+8\delta_r^4)+4i\delta_r\alpha^2\sqrt{1-\delta_r^2}\left(1-\alpha^2(1-2\delta_r^2)\right)\right]$$

$$\left.-\frac{n\pi\alpha}{2}\frac{\left[-\delta_r+i\sqrt{1-\delta_r^2}+\alpha^2\left(-\delta_r-i\sqrt{1-\delta_r^2}\right)\right]}{\left[1-2\alpha^2(1-2\delta_r^2)+\alpha^4\right]}\right\} \quad \ldots(2.96)$$

in which $\alpha = \lambda_m / \lambda_{t_r}$. If m is even, I = 0.

Equation 2.96 can be written:

$$I = \frac{8a^2b^2}{m^2n^2\pi^4} A \quad \ldots(2.97)$$

A is the term inside curly brackets in equation 2.96 . The second part of expression 2.93 is given by:

$$\frac{W_P(\omega_r)}{2M_r^2\delta_r\sqrt{1-\delta_r^2}} \cdot \frac{8a^2b^2}{m^2n^2\pi^4} \mathrm{R}\left[(1-4\delta_r^2)\sqrt{1-\delta_r^2}+i\delta_r(3-4\delta_r^2)\right] A \quad \ldots(2.98)$$

This can be normalised by dividing its general value by that which would be obtained for plane waves at normal incidence ($\alpha = 0$) when n is odd. This quotient is, of course, L_r . For normal plane waves, $A = (1 - \cos n\pi)$ and when n is odd expression becomes:

$$\frac{W_p(\omega_r)}{M_r^2} \quad \frac{\pi\omega_r}{\delta_r} \quad (1-4\delta_r^2) \quad \frac{8a^2b^2}{m^2n^2\pi^4} \qquad \ldots(2.99)$$

(If n is even, the expression 2.98 is zero). The total integral (expression 2.98) can now be written:

$$\int_{-\infty}^{\infty} \frac{\omega^4 W_{Fr}(\omega)}{|Z_r(\omega)|^2}\, d\omega = \frac{\overline{p^2(t)}}{M_r^2} \iint_{S_1 S_2} f_r(s_1) f_r(s_2)\, \bar{\psi}\left(\xi \frac{\sin\theta}{c}\right) ds_1\, ds_2$$

$$+ \frac{W_p(\omega_r)}{M_r^2} \quad \frac{\pi\omega_r}{\delta_r} \quad (1-4\delta_r^2) \quad \frac{8a^2b^2}{m^2n^2\pi^4} \quad L_r \qquad \ldots(2.100)$$

and we find that L_r is given by the equation:

$$L_r = \frac{1}{2(1-4\delta_r^2)\sqrt{1-\delta_r^2}\left[1-2\alpha^2(1-2\delta_r^2)+\alpha^4\right]} \left\{ \frac{1}{\left[1+2\alpha^2(1-2\delta_r^2)+\alpha^4\right]} \left[\left(1 - e^{-n\pi\alpha\delta_r} \cdot \cos n\pi \cdot \cos n\pi\alpha\sqrt{1-\delta_r^2}\right) \cdot \right.\right.$$

$$\left. \cdot \sqrt{1-\delta_r^2}\left((1-4\delta_r^2) - 2\alpha^2 + \alpha^4\right) + \delta_r e^{-n\pi\alpha\delta_r} \cdot \cos n\pi \cdot \sin n\pi\alpha\sqrt{1-\delta_r^2} \cdot \left((3-4\delta_r^2) - 2\alpha^2 - \alpha^4\right) \right]$$

$$\left. + n\pi\alpha\delta_r\sqrt{1-\delta_r^2} \cdot \left[2(1-2\delta_r^2) - \alpha^2\right] \right\} \qquad \ldots(2.101)$$

L_r (called the 'Joint Magnification Factor') provides the maximum magnification of the response quantities when α is near one (in addition to the dynamic magnification arising from the $(1-4\delta_r^2)/\delta_r$

"resonance" term). This is a direct result of the acoustical coincidence effect. In designing a panel it is therefore necessary to avoid the coincidence effect as far as is possible.

The maximum values of L_r can be roughly gauged by putting $\alpha = 1$ in equation 2.101 above (the lower the damping ratio, the nearer will this approximation be). Assuming that the damping is small, equation 2.101becomes

$$L_{r_{\alpha=1}} = \frac{n\pi}{8}\left\{\frac{n\pi}{2} - \delta_r\left(\frac{n^2\pi^2}{16} - \frac{1}{2}\right)\right\} \qquad \ldots(2.102)$$

The maximum value of L_r evidently becomes larger as δ_r becomes smaller, and we also see that or very small damping:

$$L_{r_{\alpha=1}} = \frac{n^2\pi^2}{16} \qquad \ldots(2.103)$$

If we have coincidence effect excitation in the rth mode and the damping is small the second term on the right hand side of equation 2.100 becomes (using equation 2.103):

$$\frac{W_p(\omega_r)}{2M_r^2}\ \frac{\pi\omega_r}{\delta_r}\ \frac{a^2b^2}{m^2n^2\pi^4} \qquad \ldots(2.104)$$

We see that this contribution to the mean square stress is inversely proportional to the damping ratio, proportional to the modal natural frequency, and proportional to the panel length squared. To keep this quantity to a minimum, therefore, panels should be short between stiffeners, and maximum damping should be introduced. A typical variation of L_r with α and δ_r is shown in Figure 15.

Appendix A.2.5 The Integrals $I_{C_{rr}}$, $I_{S_{rr}}$, $I_{C_{r\Delta r}}$, and $I_{S_{r\Delta r}}$

These integrals are evaluated in this section for a double sine mode of deflection and for plane wave excitation (at general fixed incidence to the plate). For normally incident plane waves they reduce to very simply forms (see equation 2.53). The results of this section are not used in the body of this Thesis, and are included here only for completeness. Equation 2.46 gives

$$I_{C_{rr}} + i\, I_{S_{rr}} = \int_S f_r(s)\, e^{i\omega_r \xi \frac{\sin\theta}{c}}\, ds$$

Now if $f_r(s) = \sin\frac{n\pi x}{a} \sin\frac{m\pi y}{b}$ this equation becomes:

$$I_{C_{rr}} + i\, I_{S_{rr}} = \int_S \sin\frac{m\pi y}{b}\, dy \cdot \int_S \sin\frac{n\pi x}{a} \cdot e^{i\omega_r (x-x') \frac{\sin\theta}{c}}\, dx$$

$$= \frac{2ab}{mn\pi^2} \frac{e^{-i\omega_r \frac{\sin\theta}{c} \cdot x'}}{\left[1 - \left(\frac{a\omega_r \sin\theta}{n\pi c}\right)^2\right]} \left[1 - \cos n\pi \cdot e^{i\omega_r \sin\theta \cdot \frac{a}{c}}\right] \quad \ldots(2.105)$$

for m odd only. This expression is a function of the mode (m, n, ω_r) and of the sound field inclination.

Similarly:

$$I_{C_{r\Delta r}} + i\, I_{S_{r\Delta r}} = \frac{4a^2b^2}{m_r m_\Delta n_r n_\Delta \pi^4} \cdot \frac{\left[1 - e^{-i\omega_r \sin\theta \cdot \frac{a}{c}}\right]\left[1 - \cos n_r\pi \cdot e^{i\omega_r \sin\theta \cdot \frac{a}{c}}\right]}{\left[1 - \left(\frac{a\omega_r \sin\theta}{n_r \pi c}\right)^2\right]\left[1 - \left(\frac{a\omega_r \sin\theta}{n_\Delta \pi c}\right)^2\right]} \quad \ldots(2.106)$$

for m_Δ and m_r odd only.

The integrals I_{ψ_r} and $I_{\psi_{rA}}$ cannot be integrated analytically for this type of acoustic excitation.

CHAPTER THREE

Some Experiments with a Honeycomb Sandwich Panel

Summary

Experimental verification of the theories of chapters one and two has been provided by harmonic and random plane wave excitation, at grazing incidence, of a simply-supported sandwich panel measuring 42.5 in. by 24 in. The excitation facility was the University of Southampton Siren Tunnel.

Measurements have been made of panel surface strains at three stations. These values are compared with values predicted by a theory similar in content to that of chapter two. Discrepancies between the theory and experiment are almost certainly attributable to the effect of the cavity between the panel and the siren wall, the experimental values of stress being higher than expected.

3.1 Introduction

The experiments with a sandwich panel described in this chapter have two major objectives. These are:

(i) To verify the theory given in Appendix A.3.1 for the strain in the face of a simply-supported sandwich panel when it is excited by random plane waves at grazing incidence, and

(ii) To verify the theory of chapter one, which predicts the natural frequencies of the principal modes of vibration of the panel.

Unfortunately it is a very difficult, if not impossible, task for

obvious reasons to measure the direct strain in the bond of a vibrating sandwich panel. Therefore a theory has been derived in an Appendix for the strain in the face plate of a sandwich panel which is similar in derivation to that of chapter two. Direct verification of this theory is a relatively simple matter because panel surface strain can be measured easily. A verification of this theory will indicate that the Fourier Analysis treats this sort of problem with reasonable accuracy.

The experimental programme can be split into two parts: The first series of experiments consists of harmonic excitation of the panel in order to find the natural frequencies of the panel and to derive the damping ratio in each mode. The second objective given above can thus be fulfilled. The second series of experiments consists of random excitation of the panel. Two measurements are made in these random experiments. The first is the value of r.m.s. strain at three plate stations. The second is the power spectrum of the pressure acting at the plate centre. From this second quantity, and the dynamic parameters of the plate modes found from the harmonic tests, theoretical values of the r.m.s. strains are computed using the theory of Appendix A.3.1. These values are then compared with the measured strains to fulfil the first objective given above.

3.2 The Experimental Equipment

3.2.1 The Sandwich Panel

The design of the sandwich panel was based on three requirements. First, the panel size was limited by the test facility which was to be

used to excite it, and therefore panel dimensions of 42.5 inches by 24 inches were chosen. Second, to fulfil part of the purpose of the experiment, the panel had to be simply-supported or as nearly simply-supported as possible. The development of suitable supports is described in the next section. Third and last, it was desirable that the panel should be representative of sandwiches in current use for aircraft. To this end sandwich dimensions were chosen which are identical to those used in VC-10 rudder and elevator panels. The specification of the sandwich is:

(i) Core: Aeroweb Type 141, core depth, 0.85 in.

(ii) Faces: Alclad 0.0124 in. thick (30 S.W.G.)

(iii) Bond: Redux type 775R

The first four theoretical natural modes of vibration of this panel lay in the frequency range 0 to 1 Kc/s (the frequency limits of the excitation range of the random tests). These four modes had only one half-wave in the y-direction, so simplifying the calculations based on the theory of the Appendix A.3.1. To the surface of the panel three strain gauges were attached. The first was attached at $x/a = 0.5$, the second at $x/a = 0.25$, and the third at $x/a = 0.125$ (see Figure 17). These are known as Strain Gauge 1, Strain Gauge 2 and Strain Gauge 3, respectively.

3.2.2 The Panel Simple-Supports: Their Development

(i) Development of the Simple Supports

In some experiments carried out previously at Southampton University, using a sandwich panel in an acoustic resonance tube[26],

a method of simple support using a steel shim was evolved. To the edge of the sandwich panel a strip was attached sealing off the core. To this strip a singbe shim of steel was attached. The other side of the shim was attached to the surrounding structure (see the sketch below).

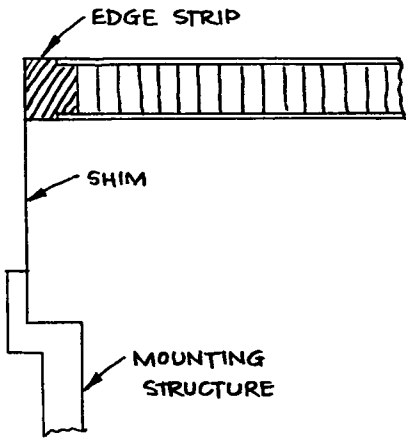

This method of support offered negligible resistance to rotation, but unfortunately fatigue failures of the support shim occurred rapidly. These failures were attributed to buckling of the shim on the compression half of each cycle. Accordingly, for the experiment described in this chapter, a method of simple support was designed, as a development of that shown above, whereby the panel was supported on <u>both</u> sides by shim steel (see Figure 17).

Preliminary experiments to evaluate this double sided support were carried out with a vibrating sandwich beam, of length 36 inches. The properties investigated here were:

(i) The rotational stiffness of the support and its acceptability as a simple support. This was investigated by comparing the natural frequencies of the beam with different thicknesses of supporting shim

and,

(ii) The life of the shim under intense loading. This was investigated by endurance tests at high vibration amplitudes.

The results of the first test are shown in the table below:

Shim Thickness (in.)	0.005	0.002	0.000(Theory)
Natural Frequency c/s	42.38	42.28	42.26

The endurance test was carried out with the beam supported on 0.002 in. steel shims and excited to a peak-to-peak amplitude of 0.6 inches at its fundamental resonant frequency (42.28 c/s). The shims had not broken after ten hours when the test was terminated.

(ii) The Test Panel Support Shims

The results of the experiments with beams seemed to be quite satisfactory. This new support system was therefore used for the panel. The 0.002 in. thick steel shims used for the test were attached to the panel in the manner indicated in Figure 17. A thin coating of Aquaplas, a commercial damping compound, was applied to the shims as an extra precaution against fatigue failures of the supports. The supporting structure to which the shims were attached was itself adjustable against a frame (see Figure 17) so that fitting of the panel to the frame was a simple though laborious task. Figure 16 shows the panel mounted in this frame.

3.2.3 The Siren Tunnel

The facility which provided the acoustic excitation of the panel

in these tests was the University of Southampton siren tunnel. This facility was designed to propagate accustic plane waves down a tunnel of rectangular cross-section. The siren element is an electromagnetically driven air modulator, the air speed in the tunnel being about 2 feet/sec. The tunnel produces quite good plane waves except when the frequency of the sound is near one of the cavity resonant frequencies of the tunnel. As far as theoretical calculations are concerned however the tunnel was assumed to propagate plane waves.

For this experiment use was made of a heavy steel trolley running on rails which moved up against the tunnel wall. The specimen in its frame was mounted on this trolley and wheeled up against the tunnel working section. The panel thus became part of the tunnel wall. Consequently, it was being excited by plane waves at grazing incidence.

3.2.4 The Siren Driving Equipment

A conventional electrical system was used to drive the siren element under both harmonic and random operating conditions. For harmonic tests a 0 to 1 Kc/s oscillator was connected to the siren element via a 100-watt amplifier. For random tests the signal from a white noise generator was filtered to simulate jet noise (pressure spectrum from 0 to 1 Kc/s) and then passed to the siren element again via the 100-watt amplifier. A compressed air supply was required for the siren at a pressure of 25 lb/in^2.

3.2.5 Instrumentation

The two quantities to be measured during the tests were the

pressure at the panel centre (behind strain gauge 1) and the strains at the three positions mentioned previously.

To measure the pressure a Bruel and Kjaer condenser microphone was mounted inside the tunnel and adjacent to the panel surface at the panel centre. It was assumed that the mean square pressure was the same at all positions on the plate and that the panel was being excited by grazing plane waves so that measurement was required at only one microphone position. This microphone was connected to a Bruel and Kjaer third-octave spectrum analyser which was switched to measure overall sound intensity. The monitoring socket of this instrument was connected to a tape recorder.

The three strain gauges were connected to a standard a.c. Wheatstone bridge, which was energised by a 24 volt battery, via a switching box. The output from the strain gauge switching box (which was the out-of-balance a.c. voltage) was taken to an a.c. voltmeter. A resolved component indicator was also used for a 'vector plot' analysis of the panel motion. The reference signal used for this instrument was the microphone output voltage. Against this reference the phases of the strain gauge signals were measured.

3.3 Harmonic Excitation of the Panel

3.3.1 The First Series of Tests

The panel was excited harmonically, at a fixed pressure intensity of 133.5 dB, at various frequencies. The pressure intensity at the microphone was maintained at a constant value by varying the input to the amplifier. Readings were taken of the output of each strain gauge

using the a.c. valve voltmeter. The response curve of each strain gauge was plotted as millivolts output against frequency, in order to find the modal natural frequencies and modal damping ratios. A typical example of one of these curves is shown in Figure 18. It is clearly impossible to derive damping ratios for the 'in vacuo' modes of the panel from these curves because other resonances of the panel were occurring due to acoustic cavity and support structure effects. The modes of vibration of the panel which are predicted in chapter one are 'in vacuo' modes. A more perceptive method of analysis therefore becomes necessary. The method due to Kennedy and Pancu[27] and known as 'vector plot' analysis was used to derive the damping ratios and natural frequencies of the 'in vacuo' panel modes.

3.3.2 The Second Series of Tests: Vector Analysis

The Resolved Component Indicator was connected to the microphone and to the strain gauges. For each modal resonance the strain gauge which measured most strain in that mode was switched on. Readings of in-phase and quadrature components of the strain were taken with reference to the microphone pressure. Vector response diagrams were plotted for each mode. A typical vector response diagram is shown in Figure 19 for the fourth mode. At each peak of the response a pencil was run along the panel to detect the nodes of the panel mode shape. Each of the four panel modes was positively identified in this way. However, the same nodal pattern was detectable at all of the frequencies given on Figure 19. The vector response diagram is only shown for the fourth mode.

3.4 Random Excitation of the Panel

The siren driving equipment was set up as described in § 3.2.4 for random excitation of the panels by plane waves at grazing incidence. The panel was excited at a noise intensity of 143.5 dB measured at the microphone. A tape recording was made of the noise pressures at the microphone. This tape recording was subsequently used to obtain the Power Spectrum of the pressure using a Hewlett-Packard wave analyser. At this time readings were also taken of the mean square voltage output from the strain gauge bridge for each strain gauge.

3.5 Experimental Results

3.5.1 Direct Results

From the second series of harmonic tests data were obtained which enabled vector response diagrams to be plotted for each mode. The natural frequencies and damping ratios of each mode were derived from these diagrams (see the next section). A typical example of the diagram obtained is shown in Figures 19 and 20 for mode 4.

From the random tests on the panel we have (i) a pressure power spectrum, without a scale, as an output of the wave analyser, and (ii) values of mean square strain at each strain gauge, as follows:

Strain Gauge	r.m.s. Strain
1	6.29×10^{-5}
2	10.68×10^{-5}
3	10.29×10^{-5}

3.5.2 Derived Results

From the vector response diagrams the following dynamic parameters of the plate in each mode were derived: The last column shows computed values of the modal natural frequency using the theory of chapter one.

Mode	Damping Ratio	Natural Frequency c/s	Computed Natural Frequency c/s
1	0.015	204	219
2	0.028	370	367
3	0.005	579	596
4	0.020	937	888

From the dynamic parameters given above and from a scaled pressure power spectrum theoretical values of the r.m.s. strains were evaluated (for the details, see the next section) using the theory of Appendix A.3.1. These results are shown in the table below:

Strain Gauge	r.m.s. Strain
1	6.11×10^{-5}
2	4.53×10^{-5}
3	5.75×10^{-5}

3.6 The Derivation of Results given in § 3.5.2

3.6.1 Derivation of Plate Modal Characteristics from the Vector Response Diagram

The vector response diagram was plotted from experimental

readings. In the case of the fourth mode (Figure 19) there were three almost circular curves running into each other. It was assumed (rightly or wrongly) that any acoustic resonance would be more highly damped than a panel resonance. Therefore the circular curve was chosen which gave rise to the largest damping. The nearest circle was drawn to this curve (dashed curve in Figure 20). The resonant frequency is the point at which $dS/d(\omega^2)$ is a maximum (where S is the distance along the curve). It was judged to be at 937 c/s for this diagram. The damping ratio is found, as follows:

(i) Draw the radius vector to the point on the curve corresponding to the natural frequency

(ii) Draw the diameter normal to this radius vector.

The points at the end of this diameter correspond to two frequencies whose difference is equal to $2\delta_r \omega_r$. Thus, for the fourth mode, $\delta_4 = 0.020$. Results of these analyses and also of the computations for natural frequency using the theory of chapter one are given in the first table in § 3.5.2.

It was necessary to determine values of ω_r and δ_r from this harmonic experiment for 'in vacuo' panel modes so that these values could be used in the theoretical calculation of bond strains in the panel when it was excited by random waves (see the next section). Indeed, the modal damping ratios could be determined in no other way although an estimate for the 'in vacuo' natural frequencies can and has been made.

3.6.2 Derivation of the Theoretical Values of r.m.s. Strain

The theoretical bond strain has been calculated under the assumption that only four modes of vibration contribute to the motion of the panel. These four modes are the four theoretical panel modes whose natural frequencies are less than 1 Kc/s. These modes are four of those which could occur if the panel were vibrating in vacuo. Other modes of vibration of practical panels due to acoustic and structural effects are not included in the theoretical analysis as they will complicate the prediction of strain. 'In vacuo' theoretical modes of a higher order, whose natural frequencies are greater than 1 Kc/s, are not included in this analysis because their contribution to the strain was found to be insignificantly small: The computer was used to evaluate the theoretical strain incorporating eight 'in vacuo' modes of the panel, four of which had one half-wave in the y-direction, the other four having three half-waves in the y-direction (these were the eight lowest order modes of the panel). It was found that the contribution to the mean square strain from the modes with three half-waves in the y-direction was less than one-hundredth of the total mean square strain.

The pressure power spectrum, as found in the random experiments was unscaled. It was found that a correction to this spectrum to take account of the tape recorder characteristic was unnecessary. It was known that the noise intensity was 143.5 dB corresponding to 0.043 lb/in^2 r.m.s. pressure. Thus, scaling of the spectrum was carried out by integrating the given spectrum using the method of counting squares.

Values of the scaled pressure spectrum at 20 c/s intervals, are given in the second column of Table 5. Values of the function $C(\omega,s')$ were then computed, also at 20 c/s intervals, for each strain gauge position using the derived values for the damping ratio and natural frequency of each 'in vacuo' mode. $C(\omega,s')$ is the factor by which the pressure spectrum must be multiplied to give the strain spectrum at the point s'. $C(\omega,s')$ is an infinite series involving the generalised impedances of the various modes and the joint acceptance between the modes and the sound field. If the infinite series is truncated to include effects from the first four 'in vacuo' modes only, $C(\omega,s')$ can be computed for the three strain gauge positions using the values of ω_r and δ_r derived from the harmonic tests. This was carried out and the values obtain for $C(\omega,s')$ are shown in Table 4. The power spectrum of strain was then calculated by multiplying the pressure spectrum by the function $C(\omega,s')$ at each frequency. The mean square strain was then calculated by integrating the power spectrum of strain. This integration was carried out by adding the values of the spectrum of strain at 20 c/s intervals and multiplying by $20 \times 2\pi$ rads/sec. Table 5 shows the progression of this calculation for strain gauge 1. Values of the r.m.s. strain at each strain gauge thus obtained, using the theory of appendix A.3.1, are shown as the second table in § 3.5.2.

3.7 Discussion of Results

The shim supports, which were evolved for the panel described in this chapter, provided an excellent model of simple supports.

No failures of the shims occurred during the tests made. The comparison of predicted and actual natural frequencies of the sandwich panel is shown in § 3.5.2. From these results we can conclude that the natural frequency theory of chapter one, for flat plates, has predicted accurate values for the first four modal frequencies of the panel used in these experiments.

More than four resonant frequencies of the panel were found to occur in the frequency range from 0 to 1 Kc/s for the reasons already stated. Close to the resonant frequency of the fourth theoretical mode three resonant peaks (i.e. three partial circles in the vector plot) were observed and the mode of vibration corresponding to each was of the same form with four half waves along the panel. A different value of damping ratio was measured from each circle. The actual value used in the theoretical estimation of the mean square stress was the largest of the set of three. This choice gave rise to the theoretical frequency response curves which were most similar in magnitude to the actual response curves and therefore gave the most accurate results.

The differences between predicted and actual values of the r.m.s. surface strain of the panel, shown in the tables in §'s 3.5.2 and 3.5.1 respectively, could have been caused by some or all of the following factors:

(i) Cumulative errors in the arithmetical manipulation and methods of integration.

(ii) The assumption of travelling plane waves as a spatial pressure distribution.

(iii) The truncation of the theoretical infinite series $C(\omega, s')$ and the neglect of cross terms.

and,

(iv) The effect of the acoustic cavity behind the panel and the supporting structure on the panel impedance characteristics.

The major errors involved in arithmetical manipulation are a result of the crude integration methods used. The frequency step length in these integrations was 20 c/s and was larger than the bandwidth of some of the peaks. However, the order of error here is considered to be similar to that incurred in the measurement of the pressure power spectrum so that improvement of the integration methods is unnecessary. These errors, in any case, are considered to be a small part of the total error, and they do not explain why the results for strain gauge 1 agree with the theory while the other two results do not.

The assumption that the siren tunnel generates random plane waves at a constant pressure intensity can explain, in part, why the readings of strain gauges 2 and 3 are high, compared with the theoretical values. Calibration of the siren tunnel[28] indicated that, for higher frequency components of the siren noise, the noise intensity at the panel centre was up to 3 dB lower than the intensities at the edges. This effect becomes more acute as the frequency rises up to 1 Kc/s. Thus, gauges measuring strain in the fourth mode would detect the extra power at the higher frequency which is not being detected by the microphone. Strain gauge 1 is at a node of the fourth mode and will therefore not detect motion in this mode.

The truncation of the series for $C(\omega,s')$ by using only four of the infinite set of theoretical modes is thought to have little effect even on the results from the third strain gauge which would tend to be most sensitive to signals from higher modes (as a percentage of its total reading). The neglect of cross terms in the series is almost certainly a satisfactory assumption because of the wide separation of natural frequencies for these lower modes and their low damping.

The major part of the error is thought to lie in the computed function $C(\omega,s')$, the error arising as a result of the acoustic cavity behind the panel and as a result of the flexibility of the support structure. These effects introduce further resonances of the system whose peaks are not taken account of by the theoretical series for $C(\omega,s')$. The effects of these resonances could be included in the series for $C(\omega,s')$ by introducing further terms but the simplicity of the normal mode analysis would be lost. It therefore remains to judge whether or not the simple normal mode analysis gives sufficiently accurate results. These extra resonances are centred around the theoretical natural frequencies of the third and fourth modes and would tend to give a generally larger value of $C(\omega,s')$ in the region of these resonances. This is borne out by the large values of experimental strain at gauges 2 and 3 compared with the predicted values. Gauge 1 only measures strain in the first and third modes and therefore one would expect the error to be less. In fact, the actual $C(\omega,s')$ will be similar in shape to the square of the frequency response curves of the strain gauges.

These results suggest that:

(i) The effect of the acoustic cavity is to create r.m.s. stresses which are greater than those predicted by an 'in vacuo' plate theory, because more plate resonances occur.

and,

(ii) that the accuracy of the Fourier type theory for stress is good for this panel because of the accuracy of the result for strain gauge 1.

This latter conclusion satisfies the first objective of the experiment viz. to verify the theory for strain in the faces of a sandwich. The fact that this theory has been verified indicates that the Fourier Analysis treats this type of problem in an adequate manner. It therefore, indicates that the analysis of chapter two for normal bond stress has used a method which should give results of the correct order of magnitude.

The conclusion (i) above indicates that further researches could well be carried out on a simplified model, both in theory and practice, to gauge the effect of acoustic cavities on the structural response of sandwich plates with control surface panels, and their associated cavities, in mind. If r.m.s. stress levels are to be predicted for a fatigue analysis then they will be required to be accurate to a factor better than the factor of two obtained in this experiment. It appears that the normal mode analysis will not make a sufficiently accurate estimate of the stress for fatigue work if the panel has associated cavities. The fatigue properties of sandwich bonds under

random loading are not yet known and perhaps this topic would be worthy of primary investigation.

Appendix A.3.1 An Analysis of the Surface Strain of a Sandwich Panel Excited by Grazing Incidence Random Plane Waves

The bending strain in the x-direction (see Figure 17) in one of the face plates of a sandwich panel at some point S' on the panel in the rth mode is given by

$$\varepsilon_r = a_r h_1 q_r \frac{\partial^2 f_r(s')}{\partial x^2} \qquad \ldots(3.1)$$

where q_r is the generalised co-ordinate of the rth mode and a_r is the core shear alleviation factor used before in § 2.2.5.

The total strain at time t due to all modes of vibration is given by the sum:

$$\varepsilon = h_1 \sum_{r=1}^{\infty} a_r q_r \frac{\partial^2 f_r(s')}{\partial x^2} \qquad \ldots(3.2)$$

This is the same as equation 2.60.

Using the Fourier Transform notation we can write:

$$\mathcal{F}_\varepsilon(\omega,s') = h_1 \sum_{r=1}^{\infty} a_r \frac{\partial^2 f_r(s')}{\partial x^2} \frac{\mathcal{F}_{F_r}(\omega)}{Z_r(\omega)} \qquad \ldots(3.3)$$

making use of equation 2.13.

Now
$$W_\varepsilon(\omega,s') = \lim_{T\to\infty} \frac{\pi}{T} \mathcal{F}_\varepsilon(\omega,s')\, \mathcal{F}_\varepsilon^*(\omega,s')$$
$$= h_1^2 \lim_{T\to\infty} \frac{\pi}{T} \sum_{r=1}^{\infty}\sum_{\Delta=1}^{\infty} a_r a_\Delta \frac{\partial^2 f_r(s')}{\partial x^2} \frac{\partial^2 f_\Delta(s')}{\partial x^2} \frac{\mathcal{F}_{F_r}(\omega)\, \mathcal{F}_{F_\Delta}^*(\omega)}{Z_r(\omega)\, Z_\Delta^*(\omega)} \qquad \ldots(3.4)$$

If we now assume that the cross-terms in this double series are small and if we can restrict modes to a singly-infinite set by writing, for a simply-supported plate, that:

$$f_r(s') = \sin\frac{r\pi x}{a}\sin\frac{\pi y}{b}$$

then equation 3.4 can be written:

$$W_\varepsilon(\omega,s') = h_1^2\sum_{r=1}^{\infty} a_r^2\left(\frac{r\pi}{a}\right)^4 f_r^2(s')\,\frac{W_{F_r}(\omega)}{|Z_r(\omega)|^2} \qquad \ldots(3.5)$$

These assumptions will hdd good for the experimental panel. Cross-terms will be small because of the wide frequency separation and the low damping of the significant modes. Restriction to a single set of modes is sufficiently accurate because of the excitation spectrum cut-off at 1000 c/s.

For plane waves, the power spectrum of the generalised force is given by the equation:

$$W_{F_r}(\omega) = W_p(\omega)\int_{S_1}\int_{S_2} f_r(s_1)f_r(s_2)\cos\left(\frac{\omega\xi\sin\theta}{c}\right)ds_1\,ds_2$$

and for plane waves travelling in the x direction at grazing incidence:

$$\frac{\xi\sin\theta}{c} = \frac{x_1 - x_2}{c}$$

The integral can then be evaluated, using the assumed mode shape, yielding:

$$W_{F_r}(\omega) = W_p(\omega)\,\frac{8a^2b^2}{r^2\pi^4}\,\frac{\left[1-\cos r\pi.\cos\left(\frac{a\omega}{c}\right).\right]}{\left[1-\left(\frac{a\omega}{r\pi c}\right)^2\right]^2} \qquad \ldots(3.6)$$

Now Powell's 'joint acceptance' is given by:

$$j_n = \frac{2}{n\pi^2} \frac{\left[2\left(1 - \cos n\pi . \cos\left(\frac{a\omega}{c}\right)\right)\right]^{1/2}}{\left[1 - \left(\frac{a\omega}{n\pi c}\right)^2\right]} \qquad \ldots(3.7)$$

so that equation 3.6 becomes:

$$W_{Fr}(\omega) = W_p(\omega)\, a^2 b^2 j_r^2 \qquad \ldots(3.8)$$

thus equation 3.5 becomes

$$W_\varepsilon(\omega, s') = W_p(\omega) \frac{b^2}{a^2} h_1^2 \pi^4 \sum_{r=1}^{\infty} \frac{j_r^2}{|Z_r(\omega)|^2} r^4 a_r^2 f_r^2(s') \qquad \ldots(3.9)$$

If we write:

$$C(\omega, s') = \frac{b^2}{a^2} h_1^2 \pi^4 \sum_{r=1}^{\infty} \frac{j_r^2}{|Z_r(\omega)|^2} r^4 a_r^2 f_r^2(s') \qquad \ldots(3.10)$$

then equation 3.9 can be rewritten:

$$W_\varepsilon(\omega, s') = C(\omega, s') W_p(\omega) \qquad \ldots(3.11)$$

This provides a convenient form of the relationship between strain spectrum and pressure spectrum. A computer programme has been written to evaluate $C(\omega, s')$ for a limited number of modes.

CHAPTER FOUR

Fatigue Tests on the Bond of Honeycomb Sandwich Plates

Summary

Experiments have been carried out on small specimens of sandwich plate to determine the fatigue characteristics of the bond. The specimens have been excited at albubbling mode resonance by an electromagnetic vibrator to induce large values of uniaxial stress. A gramophone pick-up has been used to measure strain after being calibrated with a special strain-gauged specimen. Measurements of bond stress and specimen life have been made and an S-n curve drawn. The fatigue limit has been estimated to be 1500 lb/in^2. Rapid failures have occurred at stresses of the order of 3000 lb/in^2.

4.1 Introduction

The fatigue failures which have occurred in the bonding of sandwich panels used on aircraft have been described in the Introduction to this Thesis. It was stated there that most fatigue failures of the debonding type occur at panel centres, thus suggesting that only direct stresses are significantly responsible for fatigue failures of this type. Analyses have therefore been carried out in chapter two to investigate the mean square values of the direct stresses in a sandwich panel bond when the panel is being excited by random noise pressures. These values of stress do not have much meaning, however, as far as failure is concerned, until something is known of the fatigue properties

of the bond. In the bond of a vibrating sandwich plate a triaxial stress system exists. Experimental fatigue analysis under this stress system is a good deal more complicated than fatigue analysis under a uniaxial stress system. For this reason the experiments which are described in this chapter have been carried out with a sandwich bond under uniaxial stress.

The objects of the experiment are to find the fatigue limit and to obtain the S-n curve for a sandwich bond under uniaxial stress. For our purpose the 'Fatigue Limit' has been arbitrarily regarded as being that stress below which failure will not take place before 10^9 stress cycles have elapsed. We cannot make an estimation on any other basis because tests have not been carried out with more than 10^9 stress cycles. It is quite possible that the S-n curve for Redux bonding continues downward in the same way as the S-n curve for aluminium without reaching a definite Fatigue Limit. Thus, when Fatigue Limit is mentioned in this chapter it means the stress at which failure occurs after 10^9 cycles.

To fulfil these objects small pieces of sandwich plate were excited electromagnetically in a zero-order bubbling mode to induce stresses normal to the face plate. The specimens were loaded to reduce the natural frequency of this mode. The system was excited at resonance. A calibrated gramophone pick-up was used to measure the core stress (which is almost the same as the maximum bond stress). The time to failure was plotted against the stress to produce an S-n curve, from which the fatigue limit was estimated. This method of fatigue testing the bond of a sandwich was suggested by Mead in reference 20.

4.2 The Experimental Equipment

4.2.1 The Test Specimens

Each sandwich specimen consisted of a piece cut from a sandwich beam and measuring one inch square. The honeycomb core of this sandwich was "Aeroweb" type 142, and was $\frac{1}{2}$" deep. Aluminium faces were attached to this core with Redux bonding type 775R. To one face of the sandwich specimen a steel cube, of side one inch, was attached by means of Araldite resin adhesive. This cube was attached to the sandwich in order to reduce the natural frequency of the zero-order bubbling mode. To the other face a steel plate, $\frac{1}{4}$" thick, and measuring two inches square, was attached, also by means of Araldite. This plate had four $\frac{1}{4}$" diameter holes cut at its corners. The composition of the specimen can be seen in Figure 22. The natural frequency of the system had to be reduced because the performance of the excitation equipment was not adequate at high frequencies.

A special specimen was made in the early stages of the experiment with strain gauges attached to the externally visible faces of the core material. This specimen (No. 4) was used to calibrate the gramophone pick-up. A photograph of the special specimen is seen in Figure 22. In order to fit the strain gauges into the small space available the paper backing had to be reduced in area until it was only a little larger than the area taken up by the strain gauge element. The sensitivity of the strain gauges may have thus been reduced. The strain gauges used were Tinsley type 6J which have a nominal resistance of 100 ohms and a nominal sensitivity factor of 2.2.

4.2.2 The Test Rig

Each sandwich specimen was attached to a heavy cast-iron block by four $\frac{1}{4}$" B.S.F. bolts which passed through the four holes mentioned above. This side of the sandwich is known as the 'earth' side, for ease of reference. To the one-inch steel cube a $\frac{1}{4}$" B.S.F. stud was attached. The other end of the stud was attached to the armature of a Goodman's electromagnetic vibrator type 390A. The body of this vibrator was also firmly attached to a rigid foundation. A sketch of the specimen, as it appears in the rig, is seen in Figure 21.

4.2.3 Vibrator Driving Equipment

This equipment consisted of a decade oscillator, an attenuator box, and a 50-watt amplifier. The signal from the oscillator was passed to the amplifier, after attenuation, and the output from the amplifier energised the Goodman vibrator.

4.2.4 Instrumentation

The stress in the bond was, in effect, measured by means of a calibrated gramophone pick-up. The voltage output from the pick-up cartridge was proportional to the stylus deflection so that a linear relationship existed between core strain and pick-up voltage. The pick-up stylus rested in a scratch which was cut in the inch cube of steel near the sandwich face (see Figure 21). The output from the pick-up, which was of the order of one volt, was measured by an a.c. voltmeter.

4.3 The Experimental Procedure

4.3.1 Detection of the Bubbling Mode Resonance and other Preliminary Tests

The first three specimens to be mounted in the rig were excited variously in order;

(a) to find the frequencies at which peaks occurred in the modal response curves and how these frequencies varied from specimen to specimen,

(b) to find the pick-up output levels at which rapid failure took place in order to be able to programme the stress levels for the fatigue tests described later (§ 4.3.3),

and

(c) to ensure that failures were occurring in the bond.

Using the output from the gramophone pick-up as a measure of response it was found for the first specimen, that resonances occurred at 2087 c/s, 2564 c/s, and 5040 c/s. The largest response was obtained at 2564 c/s. By transferring the stylus from its groove in the inch cube to the edge of the fixing plate (to which the sandwich was attached on the earth side) it was possible to detect whether each resonance was a bubbling resonance or not. At 2087 c/s and at 2564 c/s there was little response on the earth side of the sandwich with large response on the exciter side. This indicated that at both of these frequencies resonant bubbling motion was taking place and therefore that the pure bubbling mode was coupled to a mode of the fixing block. Response curves in the region of these two lower resonant frequencies indicated

that these modes had damping ratios of 0.0113 (at 2087 c/s) and 0.0088 (at 2564 c/s). These figures are probably inaccurate due to motion in other modes. No vector response diagrams were plotted. The choice of which peak was to be used for fatigue testing rested upon which peak produced the larger bond stress. The first three specimens were vibrated until complete decohesion of the bond occurred.

4.3.2 Calibration of the Gramophone Pick-up

To ascertain which of the resonant peaks found in the last section produced the larger bond stress per unit input current to the vibrator, and also to calibrate the pick-up in terms of bond or core stress (the maximum values are the same*) the special specimen mentioned previously was mounted in the rig.

Considerable difficulty had been experienced in attaching the strain gauges to the sandwich core of this special specimen and it was thought wise to make a static calibration of the strain gauges to find their exact sensitivity factors. To this end static loads of up to 200 lbs were applied at the vibrator side of the sandwich. A spring balance was attached at one of its ends to the exciter side of the sandwich. The other end of the balance was attached to a long threaded stud which was used to apply the loads. Each of the pair of strain

*The maximum normal stress in the bond is slightly lower than the core stress due to the fillet of adhesive which always forms where the core meets the bond.

gauges was calibrated separately using a Tinsley strain recorder. The values found for the sensitivity factors of the gauges were 1.70 and 0.92 instead of the nominal 2.2 each. The reason for this disparity is either than the gauges were not attached to the honeycomb satisfactorily or that the removal of most of the paper backing reduced the gauge sensitivity factor. The former reason is the more likely of the two.

The sensitivity factors were now known so that dynamic calibration of the gramophone pick-up could be performed, assuming that the static and dynamic characteristics of the strain gauges were the same (this is a reasonable assumption.) The two strain gauges were measuring strain in phase with each other so that a bridge circuit of the following form was used:

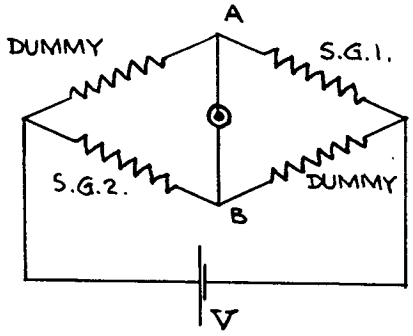

For this circuit it can quite simply be shown that the voltage difference across AB is given by V_o where:

$$V_o = (\rho_1 + \rho_2)\frac{e}{4}V$$

ρ is the gauge sensitivity factor, e is the strain and V is the battery voltage. This is true provided that the same actual strain is

occurring at both strain gauges.

The calibration of the pick-up was thus carried out by taking readings of bridge voltage difference and pick-up voltage for a series of frequencies over the likely range to be used. The bridge voltages were converted to actual strains in the core and thence to stress in the core. The r.m.s. stress per pick-up volt was then calculated from the gramophone pick-up voltage readings, and the calibration curve (Figure 23) was plotted. The bridge circuit was energised by a 6-volt battery. From the pick-up calibration curve it was deduced that the largest r.m.s. bond stress per unit input current to the vibrator occurred at the resonance in the region of 2,500 c/s so that the major part of subsequent fatigue testing was carried out at this resonance.

4.3.3 Fatigue Testing

The procedure for each fatigue test was:

(i) to mount the specimen squarely and securely in the rig

(ii) to tune the specimen to the natural frequency near 2500 c/s and

(iii) after consultation of the calibration curve, to run the specimen at the required stress level until failure. Failure was deemed to have occurred when the natural frequency had dropped by 100 c/s. Several tests were carried out at the resonance in the region of 2000 c/s.

Some of the tests had to be abandoned for various reasons. To quote an example, it was required that a certain test be run at a pick-up output of 1.5 volts. This output was maintained for three hours

but the resonant response dropped away so much that it was not possible to maintain this response with the equipment available. The tests were programmed to give failure times for a series of bond stresses up to 3,000 lb/in^2.

During these tests the crystal in the pick-up head fractured and there was not sufficient time available to recalibrate the new head, because the strain gauged specimen had been destroyed. The results after specimen 15 were therefore calculated from the calibration curve for the old head. These calculations should not be much in error because a pick-up head of the same type was used.

4.4 Experimental Results

Tests with the first three specimens showed that the frequencies at which peak response occurred were remarkably constant from specimen to specimen. Largest response occurred at the resonance around 2,500 c/s. Other peaks occurred at around 2,000 c/s and at around 5,000 c/s for all three specimens. Failures occurred in the bond on all occasions, sometimes on the 'earth' side of the sandwich and sometimes on the 'exciter' side of the sandwich (see Figure 22).

The fourth specimen which was used to calibrate the gramophone pick-up, produced the calibration curve shown in Figure 23. It will be noticed that this curve is quite peaky, due to the mechanical impedance characteristics of the pick-up arm.

The results of fatigue tests on the other specimens are shown in the table on the next page. From the results of these tests the S-n curve (Figure 24) has been drawn.

Specimen Number	Frequency of Excitation c/s	Bond Stress lb/in^2	Cycles to Failure $\times 10^7$	Comments
5	2,510	3,780	0.527	
6	2,055	2,355	0.679	
7	2,059	1,850	3.92	
8	2,067	830		9×10^8 cycles in 125 hours No Failure
9				Test abandoned
10				Test abandoned
11				Test abandoned
12	2,637	3,400	0.949	
13	2,670	2,520	9.26	
14	2,520	2,330	3.33	
15				Pick-up crystal fractured during test
16				Test abandoned
17	2,540	2,890	1.13	
18	2,060	1,680	16.3	
19	2,060	1,500		7.4×10^8 cycles in 100 hours No Failure
20	2,566	1,590		9.2×10^8 cycles in 100 hours No Failure

4.5 Concluding Remarks

The scatter of the results plotted on the S-n curve (Figure 24) is quite broad. This is a usual feature of S-n curves. At the same stress level outwardly identical specimens often fail after quite different times, unless the manufacture of these specimens is very strictly controlled. The manufacture of the specimens for the tests described here could not be strictly controlled because they were cut from sandwich beams which had been used for a previous experiment. Other factors also influenced the scatter. One factor was that some of the tests were carried out at different frequencies from others. It would seem that the calibration of the pick-up at one of these two frequencies was not accurate because the results of the tests carried out at the resonance in the region of 2000 c/s were generally lower than the results of the tests at around 2,500 c/s. The results of this experiment are only valid within a factor of two or so in any case, because of the small number of tests carried out.

The principal purpose of these tests has been to find the 'Fatigue Limit'. From Figure 24 the Fatigue Limit is conservatively estimated to be at a stress of 1500 lb/in^2. At stresses of the order of 3,000 lb/in^2 quite rapid failure has occurred. For example specimen 17 was excited at a bond stress of 2,890 lb/in^2, and failed in 73 minutes (at 2,540 c/s).

In Appendix A.4.1 the natural frequency of the zero-order bubbling mode of the experimental sandwich was calculated to be 3,150 c/s. In § 4.3.1 this natural frequency is seen to be 2,564 c/s (for the first specimen). This discrepancy is almost certainly due to the flexibility

of the block (the 'earth') to which the sandwich was attached.

The fatigue results of these tests could certainly be improved upon if a good calibration of the pick-up was obtained independently from two different sources. One of these two calibrations could be made by the method described in this chapter, after ensuring that the strain gauges were attached properly. A second confirmatory calibration could be obtained by measuring the vibration amplitude of face 'A' of the steel cube (Figure 21) using, say, a Wayne-Kerr vibration meter.

Once reasonable results have been obtained for the fatigue characteristics of the sandwich bond under uniaxial stress then design of a rig to measure triaxial stress fatigue properties should be undertaken.

Appendix A.4.1 Calculation of the Natural Frequency of the Zero-Order Bubbling Mode of the Sandwich Under Test

The natural frequency of the zero-order bubbling mode of a small piece of sandwich, when loaded on one face and fixed at the other face is extremely simple to calculate. The system is virtually a simple mass-spring system. The mass (M) here comprises the mass of the vibrator armature, the mass of the inch cube of steel, and the mass of the face plate. The core of the sandwich constitutes the spring (of rate K).

The natural frequency of such a system is, of course given by:

$$f = \frac{1}{2\pi}\sqrt{\frac{K}{M}}$$

The effective spring stiffness of the core is given by $EA/2h_1$ where A is the total cross-sectional area of the core material.

Measured (or given) values of these different quantities were:

$M = 0.477$ lbs

$E = 10^7$ lb/in^2 (Aluminium)

$A = 1/\lambda$ in^2 $= 0.02386$ in^2

$h_1 = 0.25$ in.

From which it was found that:

$f = 3{,}130$ c/s

CHAPTER 5

A Summary of Conclusions

5.1 Theoretical Work (Chapters One and Two)

The equations of motion of rectangular sandwich panels have been derived in chapter one. From these equations, the frequency equations for vibrations of simply-supported flat and cylindrically curved sandwich panels have been derived. A computer programme was written based on this theory to calculate natural frequencies of sandwich panels. A variation of the natural frequency of curved plates with circumferential wavelength was found which at first sight appeared to be anomalous. The natural frequency was rising as the wavelength increased. This effect, which has been found before for ordinary curved plates, is due to the predominance of the in-phase stretching strain energy of the curved plate when distorted in a vibration mode. The frequencies of vibration of the first four modes of the simply supported flat sandwich panel used in the experiments described in chapter three have been calculated using the theory of chapter one. A table comparing these values with the values found experimentally is shown in § 3.5.2 of chapter three. These experimental results confirm that the theory adequately predicts natural frequencies. The small differences between the predicted and experimental natural frequencies are probably derived from a shift of the natural frequencies due to the coupling of panel vibrations with acoustic vibrations in the siren tunnel. No experimental confirmation has been obtained for the natural frequency theory for curved sandwich plates.

In chapter two a full analysis has been presented of the bond stress in a sandwich panel in the plate normal direction when the panel is being excited by a general acoustic field. This chapter shows that the bending stress in the bond of the sandwich is of the same order of magnitude as the normal stress. In § 2.3 the excitation of aircraft sandwich panels by jet noise is discussed and it is concluded that the bond normal and bending stresses will be of the same order of magnitude for the typical case of a rudder panel. In this section it is also argued that, as far as bond fatigue falures are concerned, the normal stress in the bond is the more important of the two stresses because cracks due to this stress can propagate. Cracks due to the bending stress are not so likely to propagate because load carried by the bond is shed to the faces.

Largest values of stress occur, of course, when the panel is being excited in some resonant condition. Reference to equation 2.104 shows that the mean square stress due to inertia effects (this is the largest component of mean square stress under resonant conditions) is inversely proportional to the damping ratio, proportional to the modal natural frequency, and proportional to the panel length squared, when the panel is being excited by the coincidence effect. It can thus be seen that the length of panels between frames or ribs should be as short as possible and the maximum possible damping should be introduced in order to reduce resonant stresses. With a knowledge of noise field narrow band correlation wavelengths the coincidence effect should be avoidable by design.

5.2 Experimental Work (Chapters Three and Four)

The experimental work with a simply-supported sandwich panel which is described in chapter three was aimed specifically at verifying the theory of chapter two by confirming a similar Fourier Analysis for panel surface strain. The strain measured at the centre of the plate was almost exactly as predicted. The strains measured at the other two stations on the plate at which gauges were situated were twice as high as predicted. This discrepancy in the readings from strain gauges 2 and 3 was thought to be due to an acoustic standing wave system which was set up in the cavity behind the panel. It may also have been due to the effect of the flexibility of the plate supporting structure. Acoustic resonances of the tunnel cavity were known to occur at frequencies near the third and fourth modal resonant frequencies of the plate. The acoustic and structural effects modified the impedance characteristics of the panel considerably. The strain measured by gauge 1 was nearer to the predicted value than that measured by gauges 2 and 3 because gauge 1 measures strain in the first and third modes only. The other two strain gauges measure strain in more modes. These results indicate therefore, first, from the result obtained from strain gauge 1, that the type of theory used in chapter two gives results of the correct order of magnitude; and second, that the effect of a cavity behind sandwich panels is to modify the stresses in and the response of, these panels to a considerable extent. It would seem that the introduction of acoustic cavities behind panels raises the r.m.s. stress level. It is suggested that further research, both experimental and theoretical, should be carried out into the

response of sandwich panels with associated acoustic cavities, especially bearing in mind control surface panel-cavity-panel systems.

In chapter four fatigue tests are described which were carried out on the bonding of honeycomb sandwich panels by subjecting the cores of small specimens to high oscillatory stresses in a direction normal to the face-plates. From these experiments it has been concluded that the 'fatigue limit' stress (defined here as the stress at which failure occurs after 10^9 cycles) is 1500 lb/in^2. Rapid failures have occurred at stresses of twice this fatigue limit. These conclusions were somewhat tentative because of:

(i) the small number of tests carried out (16 fatigue tests)

(ii) the error involved in the calibration of the strain measuring equipment

and

(iii) the uniaxial nature of the applied stress.

It has been concluded in chapter four (and in chapter three) that more fatigue testing should be carried out in order to be able to predict the fatigue failures in aircraft sandwich panel bonds more accurately. Once reasonably consistent results have been obtained for uniaxial fatigue testing under harmonic loading, the tests should be extended to include triaxial bond stresses under both harmonic and random loading. However, results from uniaxial fatigue testing are quite useful provided that the limitations of these results are recognised.

In chapter two some calculations were carried out to find the

bond stresses in a typical sandwich panel (a panel with the same dimensions as that used for the experiments of chapter three) when it was being excited by random plane waves at normal incidence. At a noise level of 170 dB the bond r.m.s. bending stress was about 500 lb/in^2 and the r.m.s. normal stress was 125 lb/in^2. It can be seen that under these conditions the stresses do not reach the fatigue limit of 1500 lb/in^2 and failure is therefore quite unlikely. In order for failures to occur the bending stress must increase by a factor of three or the plate normal stress by a factor of twelve. It is unlikely that the acoustic coincidence effect will normally cause magnifications of this order (i.e. under random excitation conditions). Although the plate stresses due to high-order modes being excited by the coincidence effect may be very much greater than those due to the same modes being excited by plane waves of normal incidence (i.e. there exists a high degree of coincidence effect magnification) the stresses under the latter condition are very low, anyway, for the types of noise field usually met with in practice. A simple calculation has been carried out using equation 2.51 in conjunction with Figure 14. In this calculation it has been assumed that the configuration of the panel and noise field of the sample calculation in § 2.2.4 has been changed so that the plane wave noise field has been inclined at the correct angle for the coincidence effect to excite the second mode of the panel (i.e. two half-waves in the x-direction). Only the direct inertia term of equation 2.51 has been used (it is assumed that all other terms are small compared with it). The bond normal stress under this

condition (170 dB) is found to be 75 lb/in^2 (maximum) compared with the 125 lb/in^2 for the normal incidence case (sample calculation in § 2.2.4). The stress magnification here is 0.6. A similar calculation has been carried out for the case of the noise field inclined at the correct angle for coincidence excitation of the third mode. In this case the maximum bond normal stress is 173 lb/in^2; a magnification of 1.38. In both of these cases the magnification will be larger than the figures quoted because the effects of modes other than those being excited by the coincidence effect have been omitted. Especially will this be so if the incidence angle of the noise field for coincidence is similar for several modes. This is the case for the first four natural modes of the panel examined in this thesis because their natural frequencies are almost proportional to the number of half-waves of the modes in the x-direction (see the results of chapter three). It can thus be seen that magnifications of the overall stress due to coincidence effect excitation will not be great, although further magnification may take place if the modal damping ratios are smaller and if peaks occur in the Power Spectrum of the noise pressures at modal frequencies.

Failures have nevertheless occurred in practice at noise levels of the order of 170 dB (and probably lower). One reason may be that the estimate of the fatigue limit made in chapter four is too high. This figure of 1500 lb/in^2 does not apply anyway to the bonds of the sandwich plates which have been known to fail because these failures have occurred in bonding other than Redux 775R (on American aircraft). Other reasons, are that the structures which have failed have been somewhat different from the panel examined in this thesis and that the

practical panel environment was different also: The panel examined in this work has very light thin face plates. It is possible that the panels which have failed in practice have had faces with different thicknesses from those considered in our example causing the stresses in the bond due to inertia of the face-plates to be larger.

The predominant term in the expression for stress (equation 2.51) under coincidence excitation is the direct inertia term. This term has a factor of ω_r/β^2 . This factor is the only part of the term which is a function of the face-plate thickness. As the face thickness increases ω_r remains approximately constant whereas β decreases, and therefore the value of mean square stress will increase. Under conditions when the direct inertia term is not the most significant term then stresses will be small anyway. Thus to reduce coincidence effect stresses it is desirable that the mass per unit area of the face-plate should be as small as possible: We have seen the effect which acoustic cavities have had in magnifying stresses in a practical sandwich panel surface. Bond stresses will be similarly magnified by cavities.

From the arguments outlined in this chapter some recommendations can be made which will help to reduce bond stresses in sandwich plates excited by random noise pressures. These are:

(i) keep the face-plate thickness to the minimum compatible with a satisfactory plate stiffness and handling requirements

(ii) keep the lengths of panels between ribs or supports to a minimum and

(iii) add the maximum damping to the panel.

Item (ii) above has considerable weight penalties and, in any case, somewhat defeats one of the objects of the stiff sandwich panels, viz. to reduce the need for stiffeners. Item (iii) above is the most promising method of reducing bond stresses. It is recommended that some simple method of adding damping to a sandwich plate be sought which is:

(i) effective

(ii) simple to manufacture

and which (iii) does not affect the structural integrity of the sandwich. Research is necessary into the optimum dispositions and amounts of this damping.

REFERENCES

1. Hemp, W.S. 'On a Theory of Sandwich Construction' R & M 2672, March 1948

2. Reissner, E. 'Small Bending and Stretching of Sandwich Type Shells' NACA 975, 1950

3. Hoff, N.J. 'Bending and Buckling of Rectangular Sandwich Plates' NACA TN 2225, November 1960

4. Eringen, A.C. 'Bending and Buckling of Rectangular Sandwich Plates' Proc. Ist U.S. Nat. Congress of App. Mech., 1951

5. Humter-Tod, J.H. 'The Elastic Stability of Sandwich Plates' R & M 2778, 1953

6. Mindlin, R.D. 'Flexural Vibrations of Elastic Sandwich Plates' Columbia University Tech Report 35, 1959

7. Timoshenko, S. 'On the Transverse Vibrations of Bars of Uniform Cross-Section' Phil. Mag., Vol.43, 1922. p.125 ff.

8. Ekstein, H. 'High Frequency Vibrations of Thin Crystal Plates' Phys. Rev., 1945, p.11 ff

9. Yu, Y. 'A New Theory of Elastic Sandwich Plates - One-Dimensional Case' Jour. App. Mech., 1959 p.415 ff

10. Yu. Y. 'Simple Thickness-Shear Modes of Vibration of Infinite Sandwich Plates' Jour. App. Mech., 1951, p.679 ff

11. Yu, Y. 'Flexural Vibrations of Elastic Sandwich Plates' Jour Aerospace Sci., April 1960

12. Yu , Y. 'Simplified Vibration Analysis of Elastic Sandwich Plates' Jour. Aerospace Sci., December 1960

13. Yu, Y. 'Forced Flexural Vibrations of Sandwich Plates in Plane Strain' Jour. App. Mech, 1960 p.535 ff

14. Yu, Y. 'Vibrations of Elastic Sandwich Cylindrical Shells' Jour. App. Mech. Paper No. 60 -WA-21

15. Mindlin, R.D. 'Influence of Rotatory Inertia and Shear on Flexural Motions of Isotropic Elastic Plates' Jour. App. Mech., 1951, p.31 ff

16. Timoshenko, S. Goodier, J.N. 'Theory of Elasticity' McGraw Hill 1953

17. Wang. C. 'Applied Elasticity' McGraw Hill 1953

18. Mindlin, R.D. Goodman, L.E. 'Beam Vibrations with Time-Dependent Boundary Conditions' Jour. App. Mech., 1960, p.477 ff

19. Arnold, R.N. Warburton, G.B. 'Flexural Vibrations of the Walls of Thin Cylindrical Shells having Freely Supported Ends' Proc. Roy. Soc. Vol.197(A), 1949

20. Mead, D.J. 'A Note on the Use of Sandwich Structures in Severe Acoustic Environments' U.S.A.A. Report 145

21. Williams, D. 'Displacements of a Linear System under a given Transient Load' Aero. Quarterly August 1949

22. Middleton, D. 'Near Field Noise Tests on RA26' Rolls-Royce internal report

23. Mead, D.J. Appendix to; 'The Effect of a Damping Compound on Jet-Efflux Excited Vibrations' Aircraft Engineering, 1960

24. Mangiarotty, R.A. 'The Acoustic Radiation Damping of Vibrating Panels' M.Sc. Thesis, University of Southampton 1960

25. Powell, A. 'On the Fatigue Failure of Structures due to Vibrations Excited by Random Pressure Fields'
Jour. Acous. Soc. Am. December 1958

26. Froud, R. 'Unpublished work at the University of Southampton'

27. Kennedy, C.C.
Pancu, C.D.P. 'Use of Vectors in Vibration Measurement and Analysis'
Jour. Aero. Sci., November 1947

28. Clarkson, B.L.
Pietrusewicz, S.A. 'The University of Southampton Random Siren Facility'
A.A.S.U. Report 204

TABLE 1: SIMPLIFIED FORM OF THE NON-DIMENSIONALISED CHARACTERISTIC DETERMINANT FOR CURVED PLATE NATURAL FREQUENCIES.

$\frac{\pi\bar{\psi}}{A_n}\left[\frac{\mu}{2}\sin\phi-\frac{1}{\phi}\cos\phi\right]$	$-\bar{\varepsilon}$	$-\frac{A_m}{A_n}\bar{\psi}$	$\frac{\hat{r}\pi}{A_n}\left[\nu\cos\phi-\frac{(3-\nu)}{2}\frac{\sin\phi}{\phi}\frac{\pi^2}{A_m^2}\right]$	$\frac{\hat{r}\pi^2}{A_nA_m}\left[\frac{3\delta}{2\phi^2}\left\{\nu-\frac{3-\nu}{2}\frac{\pi^2}{A_m^2}\right\}+\frac{1+\nu}{2}\right]$	$\hat{r}\left[\frac{\pi^2}{A_m^2}(1-\nu)-\frac{\pi^2}{A_n^2}\frac{(1+\nu)}{3}\right]$
0	$\frac{1-\nu}{2}\bar{\psi}\frac{A_n}{A_m}$	0	$\frac{\hat{r}\pi}{A_m}\left[\cos\phi\left\{\frac{3\delta}{2\mu\lambda}(1-\nu^2)+(1-\nu)-\frac{\mu^2\bar{\psi}}{12}\right\}-\frac{\sin\phi}{\phi}\left\{\frac{3\delta}{2\mu\lambda}(1-\nu^2)+2\mu\frac{\pi^2}{A_m^2}+\frac{1+\nu}{2}\frac{\pi^2}{A_n^2}-\frac{3-\nu}{2}\frac{\pi^2}{A_m^2}\right\}\right]$	$\hat{r}\left[\frac{3\delta}{2\phi^2}\frac{\pi^2}{A_m^2}\left\{(1-\nu)+\frac{\pi^2}{A_m^2}\left(\frac{3-\nu}{2}-2\mu\right)-\frac{1+\nu}{2}\frac{\pi^2}{A_n^2}-\frac{\mu^2\bar{\psi}}{12}\right\}+\frac{3\delta}{2\mu\lambda}(1-\nu^2)+\frac{\pi^2}{A_m^2}\left\{2\mu-\frac{1+\nu}{2}\right\}\right]$	$\frac{\hat{r}\pi^2}{A_nA_m}\left[\frac{5}{6}(1+\nu)-\frac{A_n^2}{A_m^2}(1-\nu)-\frac{2}{3}\left\{2\mu+\frac{3\delta}{2\mu\lambda}\frac{A_m^2}{\pi^2}(1-\nu^2)\right\}\right]$
$\sin\phi\left[\frac{\hat{r}\lambda\mu^3\bar{\psi}^2}{12(1-\nu^2)}-\lambda\mu\phi^2+\frac{\lambda\hat{r}^2\mu}{1-\nu^2}\right]+\phi\cos\phi$	0	0	$\hat{r}\left[\frac{\sin\phi}{\phi}\left\{\frac{\lambda\mu\bar{s}}{1-\nu^2}+\frac{\pi^2}{A_m^2}\left(\frac{3\mu\delta}{4}-\frac{\lambda\mu^3\bar{\psi}}{12(1-\nu^2)}\right)\right\}-\cos\phi\frac{\pi^2}{A_m^2}\left\{\frac{\lambda\mu^3\bar{\psi}}{4(1-\nu^2)}+\frac{3}{4}\mu\delta\right\}\right]$	$\frac{\hat{r}\mu\lambda\pi}{A_m(1-\nu^2)}\left[\frac{1}{\phi^2}\left\{\frac{3\delta\bar{s}}{2}-\frac{\bar{\psi}\mu^2\delta\pi^2}{2A_m^2}\right\}-1+\frac{\bar{\psi}\mu^2}{12}\right]-\hat{r}\frac{3\delta\mu\pi}{2A_m}$	$\frac{\hat{r}\lambda\mu\pi}{A_n(1-\nu^2)}\left[\frac{2}{3}\left\{1-\frac{\bar{\psi}\mu^2}{12}\right\}-\nu\right]-\hat{r}\delta\mu\frac{\pi}{A_n}$
$\frac{\pi\hat{r}}{A_n}\left[\cos\phi\frac{\pi^2}{\phi}\frac{(3-\nu)}{A_m^2}\frac{}{2}+\nu\sin\phi\right]$	$\hat{r}\frac{\pi^2}{A_m^2}(1-\nu)$	$\hat{r}\frac{(3-\nu)}{2}\frac{\pi^2}{A_nA_m}$	$\frac{\pi}{A_n}\bar{\psi}\left[\frac{\sin\phi}{\phi}+\frac{\mu}{2}\cos\phi\right]$	$\frac{\pi^2}{A_nA_m}\left[\frac{3\delta\bar{\psi}}{2\phi^2}\left(1+\frac{\mu}{2}\right)-\frac{1+\nu}{2}\right]$	$\frac{2}{3}\frac{\pi^2}{A_n^2}\frac{1+\nu}{2}-\bar{\varepsilon}-\frac{\delta(1-\nu^2)}{\mu\lambda}$
$\frac{\pi\hat{r}}{A_m}\left[\frac{\cos\phi}{\phi}\left\{\frac{3\delta}{2\mu\lambda}(1-\nu^2)+2\mu\frac{\pi^2}{A_m^2}+\frac{1+\nu}{2}\frac{\pi^2}{A_m^2}-\frac{3-\nu}{2}\frac{\pi^2}{A_m^2}\right\}+\sin\phi\left\{1-\nu+\frac{3\delta}{2\mu\lambda}(1-\nu^2)-\frac{\mu^2\bar{\psi}}{12}\right\}\right]$	$\frac{\hat{r}\pi^2}{A_nA_m}\left[\frac{1+\nu}{2}-(1-\nu)\frac{A_n^2}{A_m^2}\right]$	$\hat{r}\left[\frac{3\delta}{2\mu\lambda}(1-\nu^2)+\frac{\pi^2}{A_m^2}\left\{2\mu-\frac{3-\nu}{2}\right\}+\frac{\pi^2}{A_n^2}\frac{1+\nu}{2}\right]$	0	$\frac{\pi^2}{A_m^2}\frac{1+\nu}{2}-\bar{\varepsilon}^*-\frac{3}{2}\frac{\delta(1-\nu^2)}{\mu\lambda}$	$\frac{2}{3}\frac{A_m}{A_n}\left\{\bar{\varepsilon}^*+\frac{3}{2}\delta\frac{(1-\nu^2)}{\mu\lambda}\right\}+\frac{A_n}{A_m}\left\{\bar{\varepsilon}+\delta\frac{(1-\nu^2)}{\mu\lambda}\right\}-\frac{5}{3}\frac{\pi^2}{A_nA_m}\frac{1+\nu}{2}$
$\hat{r}\left[\frac{\cos\phi}{\phi}\left\{\frac{\bar{\psi}\pi^2\lambda\mu^3}{12A_m^2(1-\nu^2)}-\frac{3\delta\mu\pi^2}{4A_m^2}-\frac{\lambda\mu\bar{s}}{(1-\nu^2)}\right\}-\frac{\pi^2}{A_m^2}\sin\phi\left\{\frac{\lambda\bar{\psi}\mu^3}{4(1-\nu^2)}+\frac{3\mu\delta}{4}\right\}\right]$	$-\hat{r}\frac{\nu}{1-\nu^2}\lambda\mu\frac{\pi}{A_n}$	$\frac{\hat{r}\pi}{A_m}\left[\frac{\lambda\mu^3\bar{\psi}}{12(1-\nu^2)}-\frac{3\mu\delta}{4}-\frac{A_m^2\mu\lambda\bar{s}}{\pi^2(1-\nu^2)}\right]$	$\cos\phi\left[\frac{\lambda\mu^3\bar{\psi}^2}{12(1-\nu^2)}+\frac{\lambda\mu\hat{r}^2}{(1-\nu^2)}-\lambda\mu\phi^2\right]-\phi\sin\phi$	$\frac{3\delta}{2}\frac{\pi}{A_m}\left[\frac{\mu}{2}-\lambda\mu+\frac{1}{\phi^2}\frac{\lambda\mu}{(1-\nu^2)}\left\{\hat{r}^2+\mu^2\frac{\bar{\psi}^2}{12}\right\}\right]$	0

TABLE 2 CURVED HONEYCOMB SANDWICH PLATE NON-DIMENSIONAL NATURAL FREQUENCIES FOR FLEXURAL TYPE MODES

2.1 VALUES OF ϕ FOR $\mu = 0.05$

A_n	A_m	$\hat{r} = 0$	$\hat{r} = 0.002$	$\hat{r} = 0.005$	$\hat{r} = 0.008$	$\hat{r} = 0.020$
96	96	.001877	.002082	.002931	.004054	.008983
70	96	.002672	.002898	.003874	.005219	.011428
50	96	.004246	.004447	.005379	.006778	.013838
25	96	.012612	.012707	.013193	.014051	.019965
17	96	.022769	.022825	.023117	.023650	.027820
96	70	.002682	.002770	.003188	.003841	.007213
70	70	.003462	.003577	.004126	.004985	.009515
50	70	.005007	.005134	.005754	.006754	.012344
25	70	.013243	.013324	.013744	.014492	.019794
17	70	.023282	.023334	.023606	.024103	.028022
96	50	.004295	.004327	.004488	.004770	.006636
70	50	.005045	.005090	.005315	.005708	.008296
50	50	.006595	.006595	.006904	.007443	.011007
25	50	.014515	.014576	.014895	.015469	.019731
17	50	.024322	.024367	.024603	.025036	.028495
96	25	.013225	.013230	.013251	.013291	.013622
70	25	.013835	.013840	.013864	.013910	.014286
50	25	.015054	.015061	.015095	.015158	.015686
25	25	.021766	.021783	.021872	.022037	.023403
17	25	.030365	.030386	.030499	.030708	.032452
96	17	.024725	.024726	.024731	.024741	.024822
70	17	.025199	.025200	.025206	.025216	.025300
50	17	.026154	.026155	.026162	.026175	.026280
25	17	.031562	.031566	.031591	.031636	.032021
17	17	.038807	.038816	.038863	.038950	.039690

2.2 VALUES OF ϕ FOR $\mu = 0.10$

A_n	A_m	$\hat{r} = 0$	$\hat{r} = 0.002$	$\hat{r} = 0.005$	$\hat{r} = 0.008$	$\hat{r} = 0.020$
96	96	.002055	.002260	.003121	.004279	.009496
70	96	.002894	.003132	.004165	.005596	.012266
50	96	.004511	.004731	.005751	.007275	.014947
25	96	.012363	.012477	.013062	.014083	.020908
17	96	.020955	.021028	.021404	.022086	.027262
96	70	.002915	.002995	.003382	.004000	.007345
70	70	.003725	.003841	.004400	.005281	.010019
50	70	.005289	.005426	.006095	.007173	.013194
25	70	.012944	.013042	.013548	.014439	.020575
17	70	.021400	.021468	.021818	.022454	.027327
96	50	.004606	.004630	.004754	.004976	.006528
70	50	.005361	.005402	.005611	.005979	.008472
50	50	.006826	.006889	.007212	.007774	.011514
25	50	.014108	.014182	.014564	.015249	.020205
17	50	.022298	.022357	.022661	.023215	.027532
96	25	.013321	.013323	.013332	.013349	.013491
70	25	.013858	.013861	.013874	.013900	.014110
50	25	.014920	.014925	.014952	.015003	.015426
25	25	.020554	.020574	.020679	.020872	.022465
17	25	.027445	.027473	.027618	.027885	.030089
96	17	.023502	.023502	.023502	.023503	.023508
70	17	.023879	.023880	.023881	.023882	.023895
50	17	.024637	.024637	.024641	.024646	.024693
25	17	.028873	.028878	.028906	.028958	.029399
17	17	.034459	.034471	.034531	.034643	.035591

2.3 VALUES OF ϕ FOR $\mu = 0.15$

A_n	A_m	$\hat{r} = 0$	$\hat{r} = 0.002$	$\hat{r} = 0.005$	$\hat{r} = 0.008$	$\hat{r} = 0.020$
96	96	.002130	.002335	.003202	.004375	.009710
70	96	.002972	.003217	.004275	.005743	.012604
50	96	.004557	.004788	.005855	.007439	.015377
25	96	.011797	.011925	.012575	.013701	.021036
17	96	.019311	.019395	.019830	.020613	.026414
96	70	.003003	.003081	.003458	.004064	.007406
70	70	.003805	.003922	.004489	.005385	.010220
50	70	.005319	.005462	.006161	.007282	.013509
25	70	.012332	.012442	.013004	.013989	.020605
17	70	.019710	.019788	.020193	.020924	.026395
96	50	.004689	.004711	.004824	.005026	.006469
70	50	.005417	.005458	.005664	.006027	.008514
50	50	.006806	.006872	.007207	.007790	.011650
25	50	.013397	.013480	.013906	.014665	.020045
17	50	.020514	.020582	.020934	.021571	.026435
96	25	.012937	.012938	.012944	.012955	.013046
70	25	.013409	.013411	.013423	.013443	.013616
50	25	.014340	.014345	.014372	.014421	.014839
25	25	.019207	.019230	.019348	.019564	.021339
17	25	.025089	.025121	.025289	.025599	.028123
96	17	.022028	.022027	.022027	.022027	.022020
70	17	.022345	.022345	.022345	.022346	.022350
50	17	.022982	.022982	.022985	.022991	.023036
25	17	.026543	.026550	.026582	.026641	.027149
17	17	.031254	.031267	.031338	.031469	.032576

2.4 VALUES OF ϕ FOR $\mu = 0.20$

A_n	A_m	$\hat{r} = 0$	$\hat{r} = 0.002$	$\hat{r} = 0.005$	$\hat{r} = 0.008$	$\hat{r} = 0.020$
96	96	.002175	.002380	.003249	.004429	.009829
70	96	.003010	.003258	.004332	.005821	.012788
50	96	.004550	.004789	.005885	.007568	.015600
25	96	.011288	.011427	.012126	.013329	.021007
17	96	.018085	.018177	.018657	.019515	.025753
96	70	.003049	.003126	.003498	.004099	.007443
70	70	.003833	.003952	.004526	.005432	.010328
50	70	.005291	.005439	.006159	.007310	.013664
25	70	.011787	.011906	.012512	.013566	.020512
17	70	.018453	.018539	.018986	.019788	.025680
96	50	.004712	.004733	.004841	.005034	.006431
70	50	.005410	.005450	.005657	.006022	.008521
50	50	.006724	.006792	.007137	.007738	.011689
25	50	.012779	.012869	.013329	.014144	.019822
17	50	.019195	.019270	.019658	.020358	.025612
96	25	.012529	.012530	.012535	.012544	.012620
70	25	.012954	.012956	.012967	.012986	.013152
50	25	.013789	.013795	.013822	.013874	.014306
25	25	.018141	.018165	.018293	.018529	.020448
17	25	.023400	.023435	.023621	.023963	.026726
96	17	.020835	.020835	.020835	.020834	.020829
70	17	.021115	.021115	.021115	.021116	.021123
50	17	.021677	.021677	.021681	.021687	.021741
25	17	.024831	.024838	.024873	.024940	.025505
17	17	.029033	.029048	.029127	.029273	.030503

TABLE 3 CURVED HONEYCOMB SANDWICH PLATE NON-DIMENSIONAL NATURAL FREQUENCIES FOR BUBBLING TYPE MODES

(N.B. This natural frequency is almost independent of wavelength and curvature)

μ	ϕ
0.05	0.640-0.641
0.10	0.470
0.15	0.389
0.20	0.339

TABLE 4 Values of the Parameter $C(\omega, S')$ (ft^4/lb^2) at the Various Strain Gauge Positions

ω(c/s)	x/a = 0.5(S.G.1)	x/a = 0.25(S.G.2)	x/a = 0.125(S.G.3)
0	1.4105 -12	7.0526 -13	2.8988 -13
20	1.4221 -12	7.2690 -13	2.9761 -13
40	1.4597 -12	7.9348 -13	3.2156 -13
60	1.5336 -12	9.1052 -13	3.6401 -13
80	1.6647 -12	1.0895 -12	4.2948 -13
100	1.8957 -12	1.3534 -12	5.2637 -13
120	2.3196 -12	1.7513 -12	6.7140 -13
140	3.1786 -12	2.4094 -12	9.0441 -13
160	5.3144 -12	3.7560 -12	1.3549 -12
180	1.3861 -11	8.3707 -12	2.7835 -12
200	2.4840 -10	1.2607 -10	3.7361 -11
220	1.7959 -11	1.1391 -11	3.9179 -12
240	2.8785 -12	4.5837 -12	2.1245 -12
260	1.0930 -12	4.7383 -12	2.4564 -12
280	7.2962 -13	6.1926 -12	3.3156 -12
300	7.2920 -13	9.0947 -12	4.8902 -12
320	8.7844 -13	1.5431 -11	8.2006 -12
340	1.1195 -12	3.4538 -11	1.7926 -11
360	1.4380 -12	1.4230 -10	7.2018 -11
380	1.8379 -12	1.1558 -10	5.8920 -11
400	2.3363 -12	2.0434 -11	1.1675 -11
420	2.9670 -12	7.3831 -12	5.5627 -12
440	3.7918 -12	4.2051 -12	4.5369 -12
460	4.9281 -12	3.5320 -12	4.9098 -12
480	6.6170 -12	3.8208 -12	6.1299 -12
500	9.4199 -12	4.9603 -12	8.4546 -12
520	1.4924 -11	7.5829 -12	1.3156 -11
540	2.9354 -11	1.4733 -11	2.5513 -11
560	1.0200 -10	5.1026 -11	8.7582 -11
580	3.2659 - 9	1.6329 - 9	2.7882 - 9
600	5.3879 -11	2.6942 -11	4.6636 -11
620	1.0926 -11	5.4635 -12	1.0038 -11
640	3.6222 -12	1.8112 -12	3.8610 -12
660	1.4338 -12	7.1740 -13	2.0423 -12
680	6.0598 -13	3.0405 -13	1.3748 -12
700	2.5656 -13	1.2977 -13	1.1044 -12
720	1.0288 -13	5.3136 -14	9.8936 -13
740	3.6168 -14	1.9787 -14	9.3681 -13
760	9.4649 -15	6.2863 -15	9.0723 -13
780	9.7873 -16	1.8014 -15	8.8307 -13
800	2.2258 -16	1.1436 -15	8.3694 -13
820	2.1378 -15	1.8259 -15	8.2659 -13
840	4.3856 -15	2.7068 -15	7.9269 -13
860	6.0150 -15	3.3257 -15	7.5781 -13
880	6.7730 -15	3.5608 -15	7.2581 -13
900	6.7374 -15	3.4480 -15	6.9701 -13
920	6.1182 -15	3.0844 -15	6.0772 -13
940	5.1513 -15	2.5784 -15	1.2161 -13
960	4.0462 -15	2.0245 -15	2.7854 -14
980	2.9633 -15	1.4937 -15	8.9762 -14
1000	2.0091 -15	1.0319 -15	1.0351 -13

These numbers are given in decimal floating point form, thus + 1.4105 -12 is 1.4105×10^{-12}. The units are ft^4/lb^2.

TABLE 5 Showing the Development of $W_\varepsilon(\omega)$ and $\overline{\varepsilon^2(t)}$ for the Face at Strain Gauge 1 (x/a = 0.5) Overall Noise Pressure Intensity = 143.5 dB

ω c/s	$W_p(\omega)$ lb^2 sec/ft^4 rad.	$C(\omega)$ ft^4/lb^2	$W_\varepsilon(\omega)$ sec/rad.
0	0.0025 -2	1.4105 -12	0.0035 -14
20	0.0025 -2	1.4221 -12	0.0036 -14
40	0.0025 -2	1.4597 -12	0.0036 -14
60	0.0025 -2	1.5336 -12	0.0038 -14
80	0.0025 -2	1.6647 -12	0.0042 -14
100	0.0025 -2	1.8957 -12	0.0047 -14
120	0.0025 -2	2.3196 -12	0.0058 -14
140	0.0025 -2	3.1786 -12	0.0079 -14
160	0.0025 -2	5.3144 -12	0.0133 -14
180	0.0025 -2	1.3861 -11	0.0347 -14
200	0.0025 -2	2.4840 -10	0.621 -14
220	0.0025 -2	1.7959 -11	0.045 -14
240	0.0023 -2	2.8785 -12	0.0072 -14
260	0.021 -2	1.0930 -12	0.0229 -14
280	0.109 -2	7.2962 -13	0.0795 -14
300	0.408 -2	7.2920 -13	0.298 -14
320	1.367 -2	8.7844 -13	1.200 -14
340	0.452 -2	1.1195 -12	0.506 -14
360	0.261 -2	1.4380 -12	0.375 -14
380	0.425 -2	1.8379 -12	0.780 -14
400	0.543 -2	2.3363 -12	1.270 -14
420	1.130 -2	2.9670 -12	3.36 -14
440	0.978 -2	3.7918 -12	3.70 -14
460	0.628 -2	4.9281 -12	3.09 -14
480	0.472 -2	6.6170 -12	3.13 -14
500	1.330 -2	9.4199 -12	1.253 -13
520	1.872 -2	1.4924 -11	2.79 -13
540	2.63 -2	2.9354 -11	7.72 -13
560	1.112 -2	1.0200 -10	1.135 -12
580	0.798 -2	3.2659 - 9	2.605 -11
600	1.702 -2	5.3879 -11	9.16 -13
620	1.57 -2	1.0926 -11	1.713 -13
640	0.880 -2	3.6222 -12	3.19 -14
660	0.336 -2	1.4338 -12	0.483 -14
680	2.41 -2	6.0598 -13	1.46 -14
700	1.112 -2	2.5656 -13	0.285 -14
720	1.728 -2	1.0288 -13	0.178 -14
740	1.079 -2	3.6168 -14	0.039 -14
760	0.226 -2	9.4649 -15	0.007 -14
780	0.399 -2	9.7873 -16	0.001 -14
800	0.726 -2	2.2258 -16	0.001 -14
820	0.958 -2	2.1378 -15	0.002 -14
840	1.354 -2	4.3856 -15	0.006 -14
860	0.629 -2	6.0150 -15	0.004 -14
880	0.544 -2	6.7730 -15	0.004 -14
900	0.241 -2	6.7374 -15	0.002 -14
920	0.232 -2	6.1182 -15	0.001 -14
940	0.1292 -2	5.1513 -15	0.001 -14
960	0.078 -2	4.0462 -15	0.000 -14
980	0.062 -2	2.9633 -15	0.000 -14
1000	0.040 -2	2.0091 -15	0.000 -14

$\sum = [2.969 \quad -11]$

r.m.s. $\varepsilon = [6.11 \quad -5]$

FIGURE 1 : FIRST ORDER MODE SHAPES OF A SIMPLY-SUPPORTED SANDWICH PLATE.

(a) ANTI-SYMMETRIC MODES

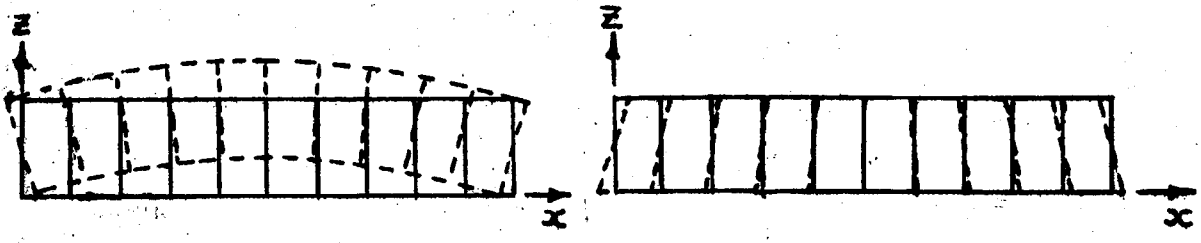

FLEXURAL MODE

THICKNESS-SHEAR MODE

(b) SYMMETRIC MODES

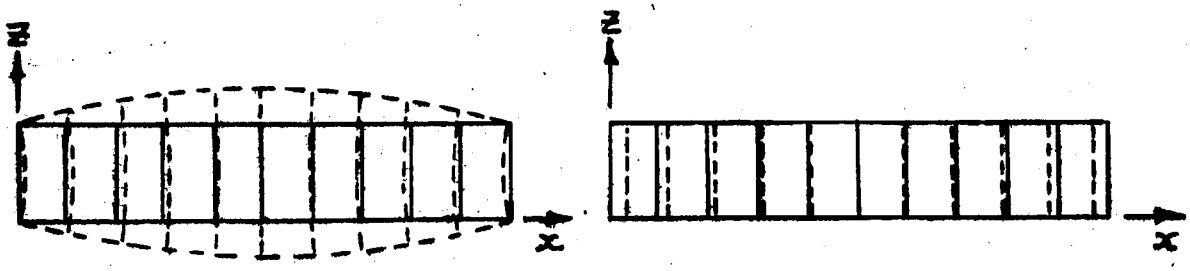

BUBBLING MODE

LONGITUDINAL MODE

FIGURE 2: SKETCH SHOWING PLATE AND SKIN CONVENTIONS.

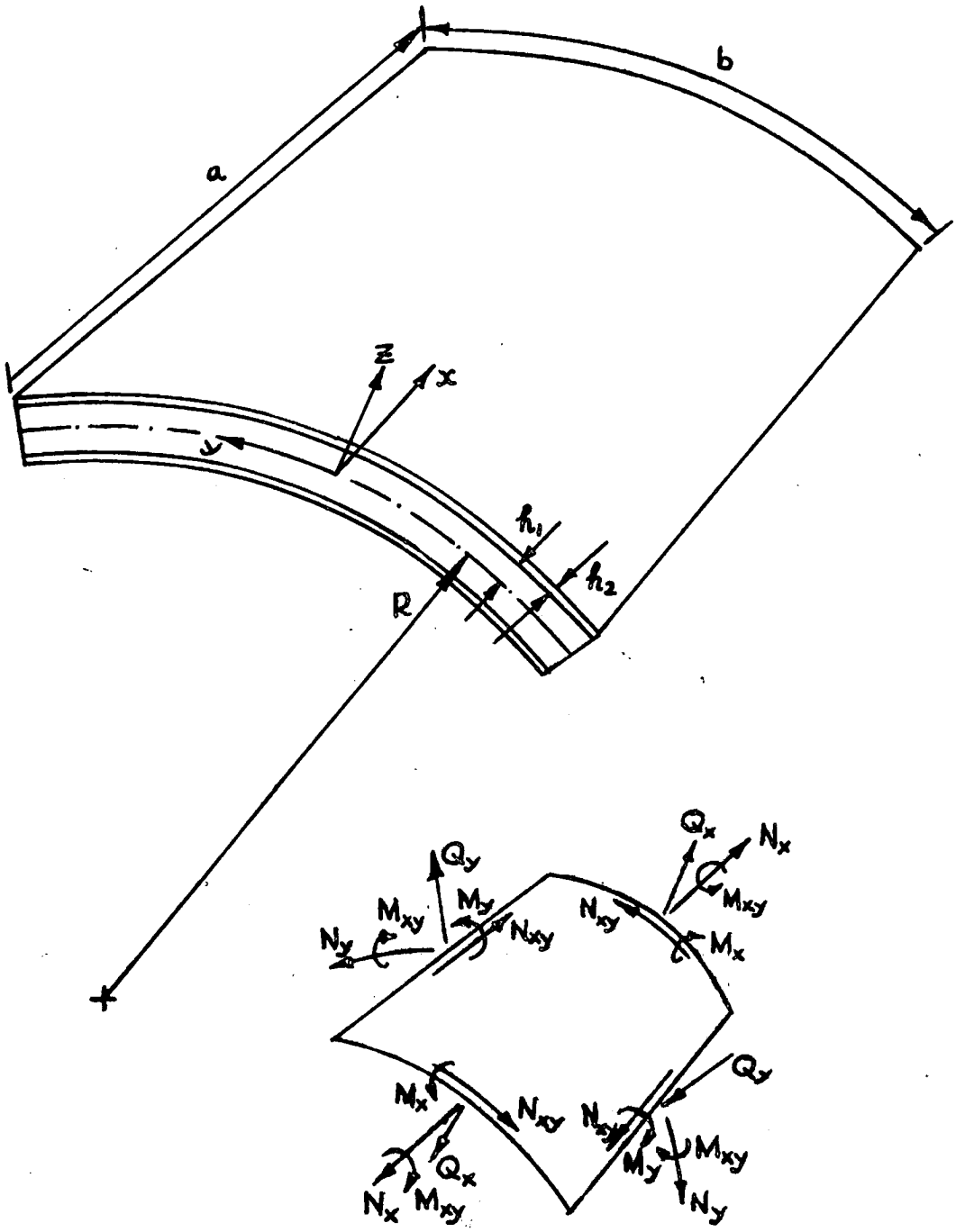

FIGURE 3A : FLAT PLATE FLEXURAL MODE FREQUENCIES (NON-DIMENSIONAL) : $\mu = 0{\cdot}05$.

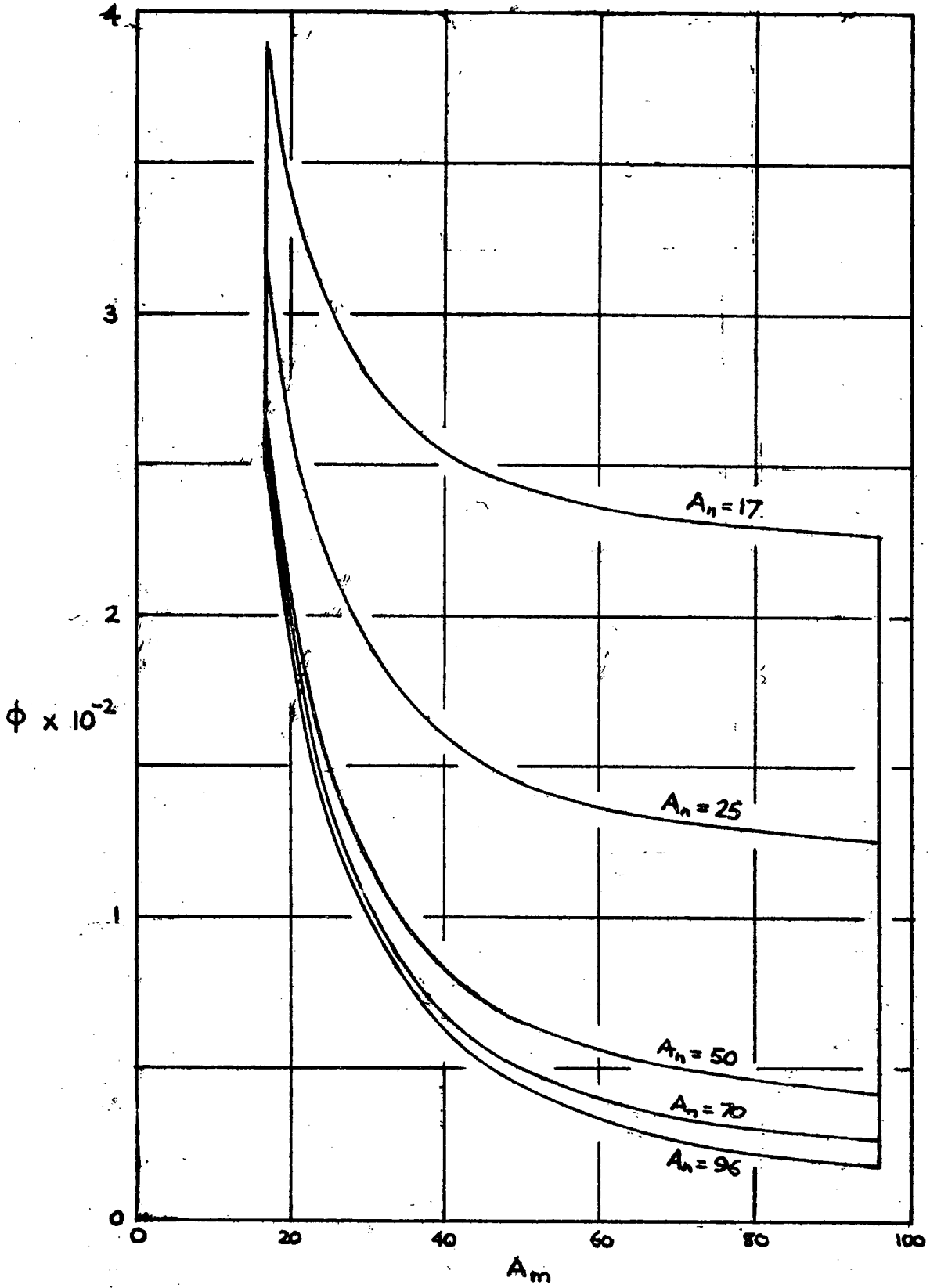

FIGURE 3B: FLAT PLATE FLEXURAL MODE FREQUENCIES (NON-DIMENSIONAL): $\mu = 0{\cdot}10$.

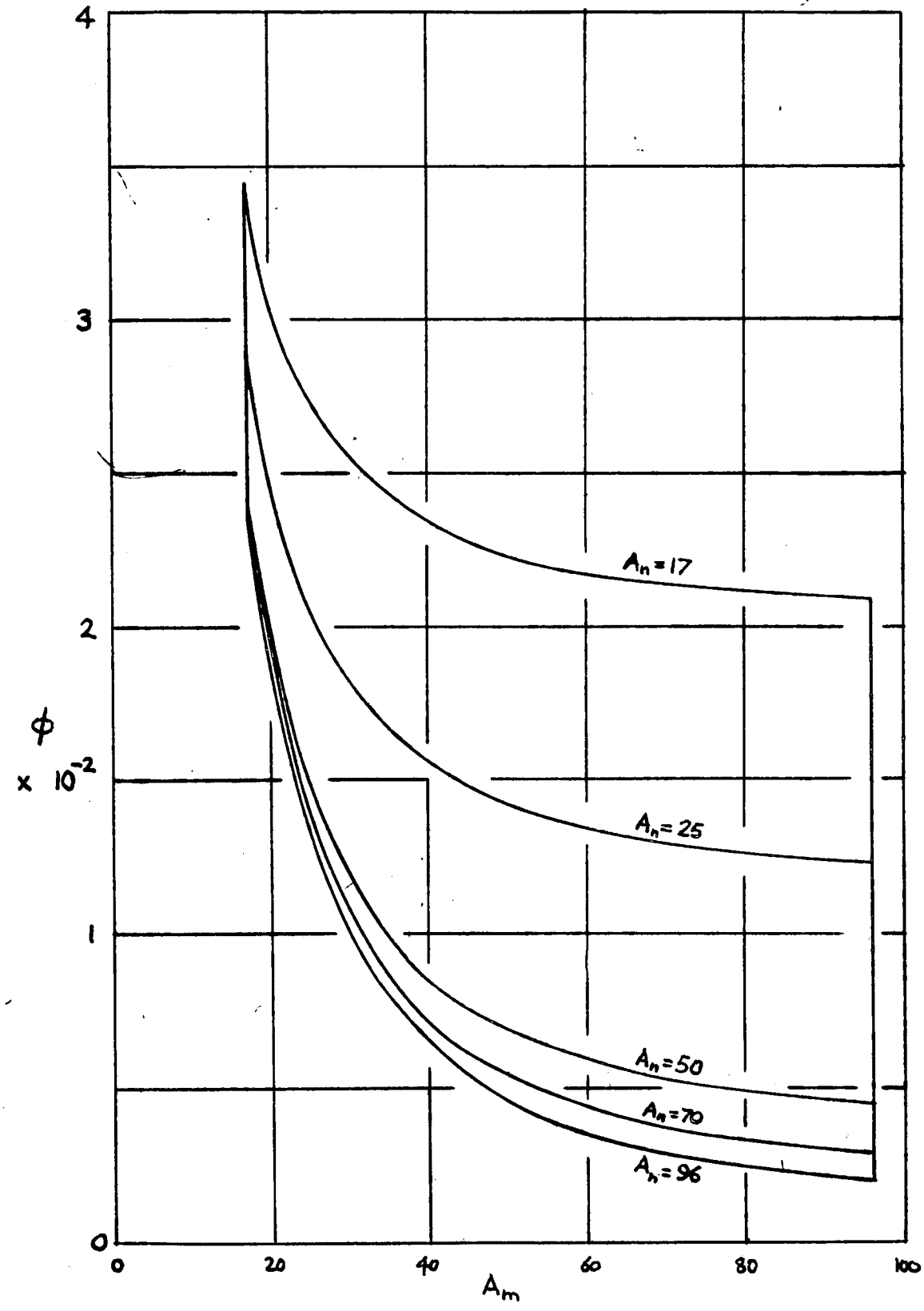

FIGURE 3c: FLAT PLATE FLEXURAL MODE FREQUENCIES (NON-DIMENSIONAL): $\mu = 0.15$.

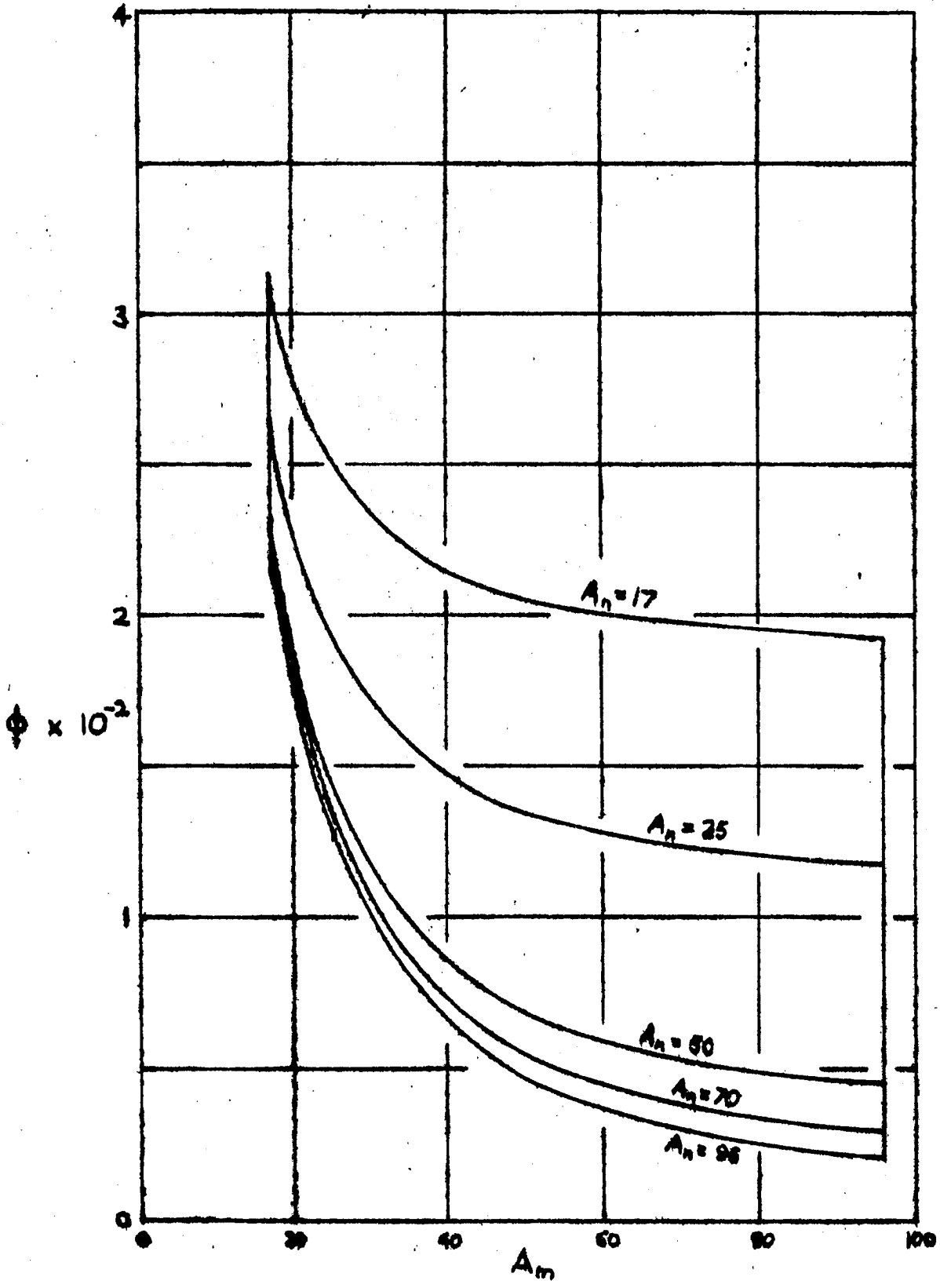

FIGURE 3D: FLAT PLATE FLEXURAL MODE FREQUENCIES (NON-DIMENSIONAL) : $\mu = 0.20$.

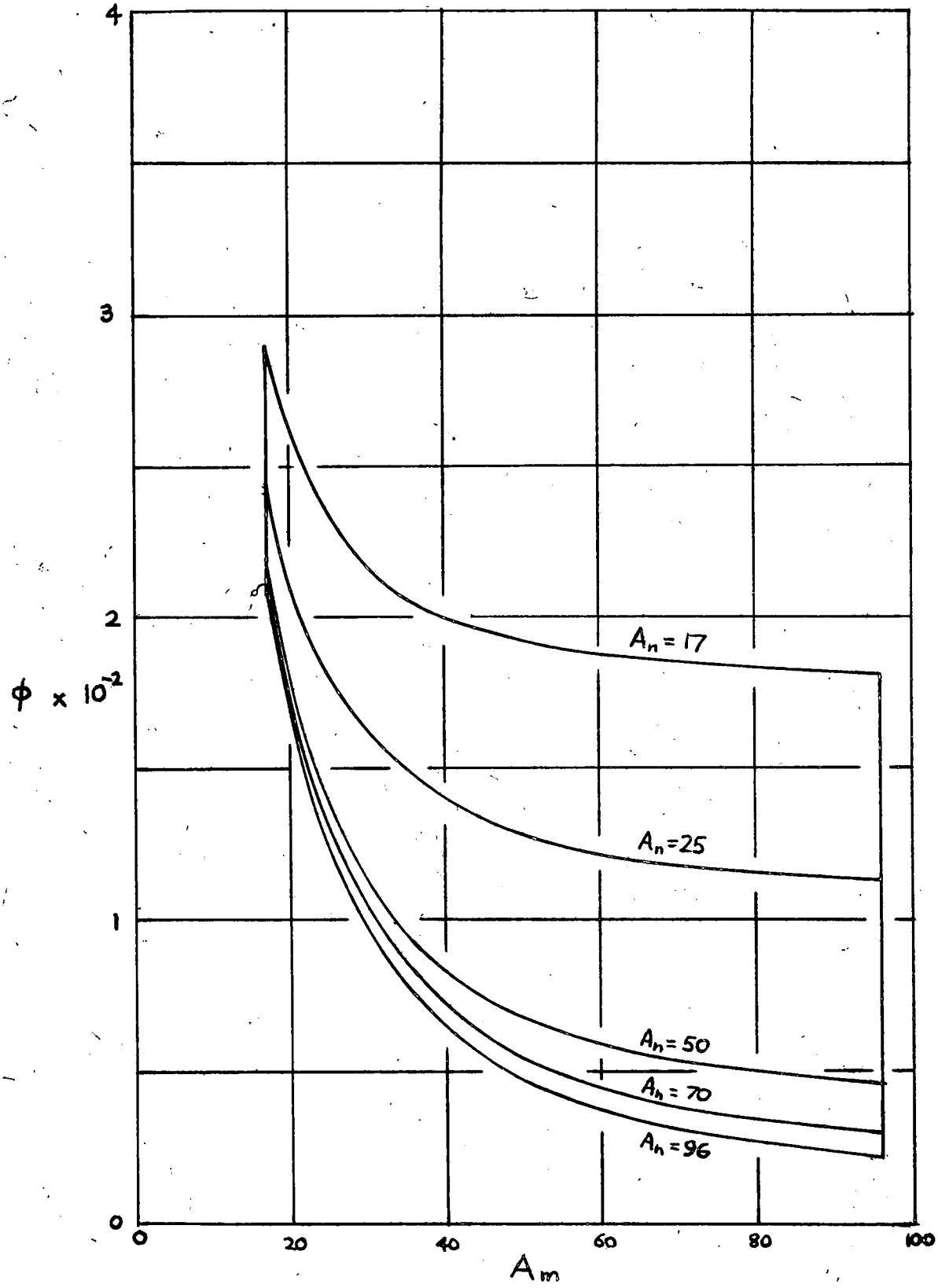

FIGURE 4: NON-DIMENSIONAL FREQUENCY vs. FREQUENCY IN KC/S

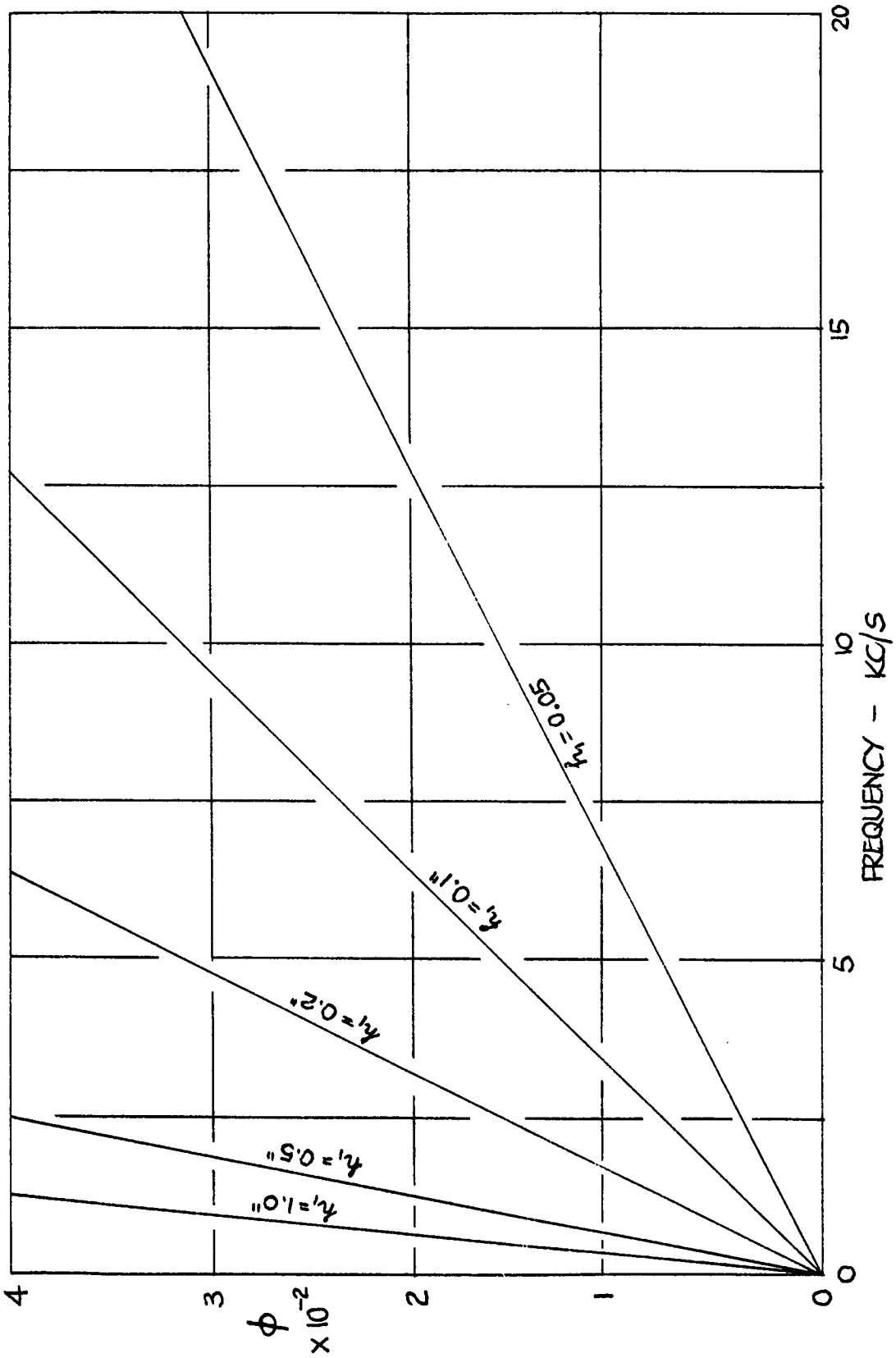

FIGURE 5 : FLAT PLATE FLEXURAL MODE
MASS RATIO FREQUENCY CORRECTION.

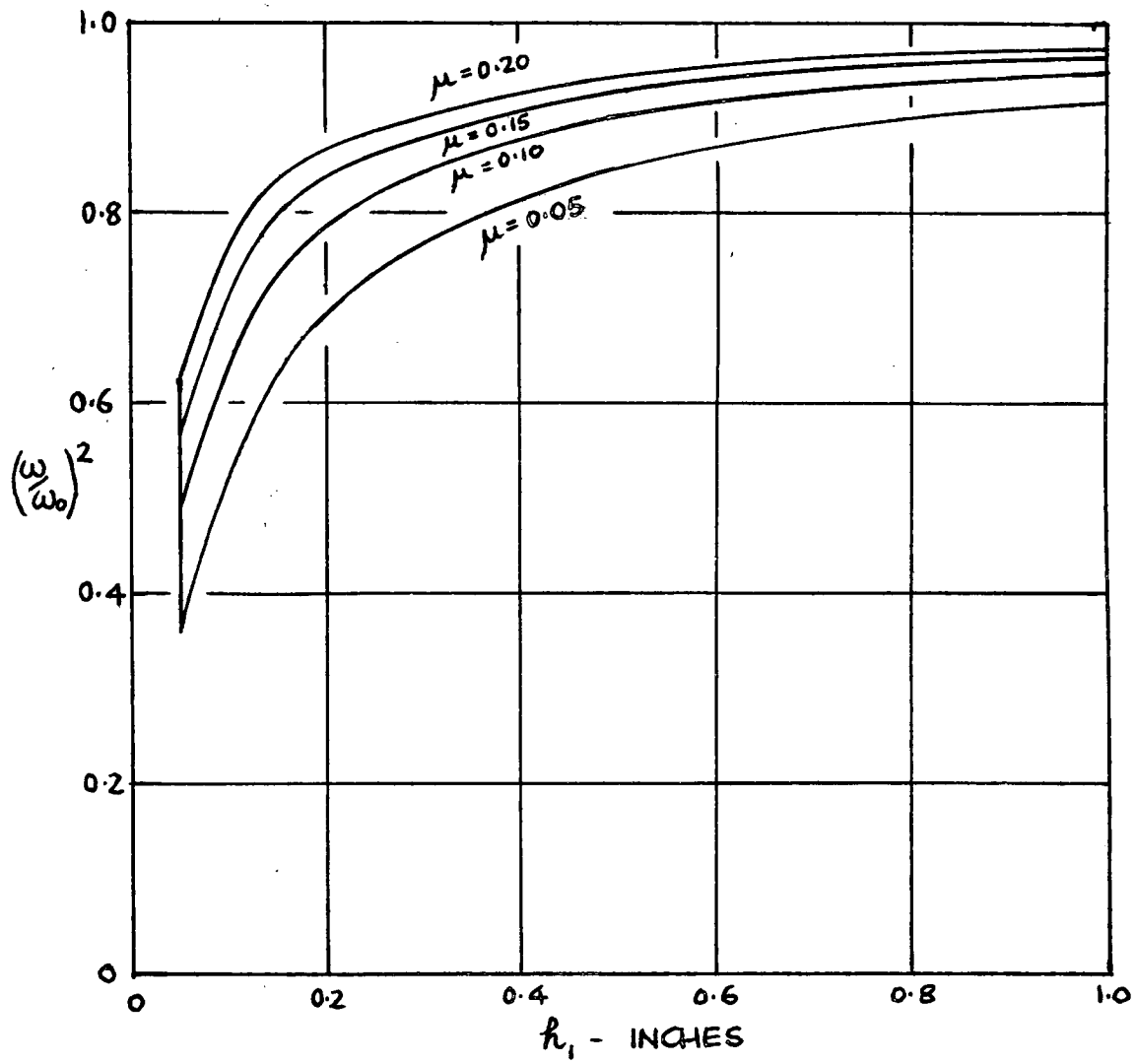

FIGURE 6 : FLAT PLATE BUBBLING MODE FREQUENCIES (NON-DIMENSIONAL)

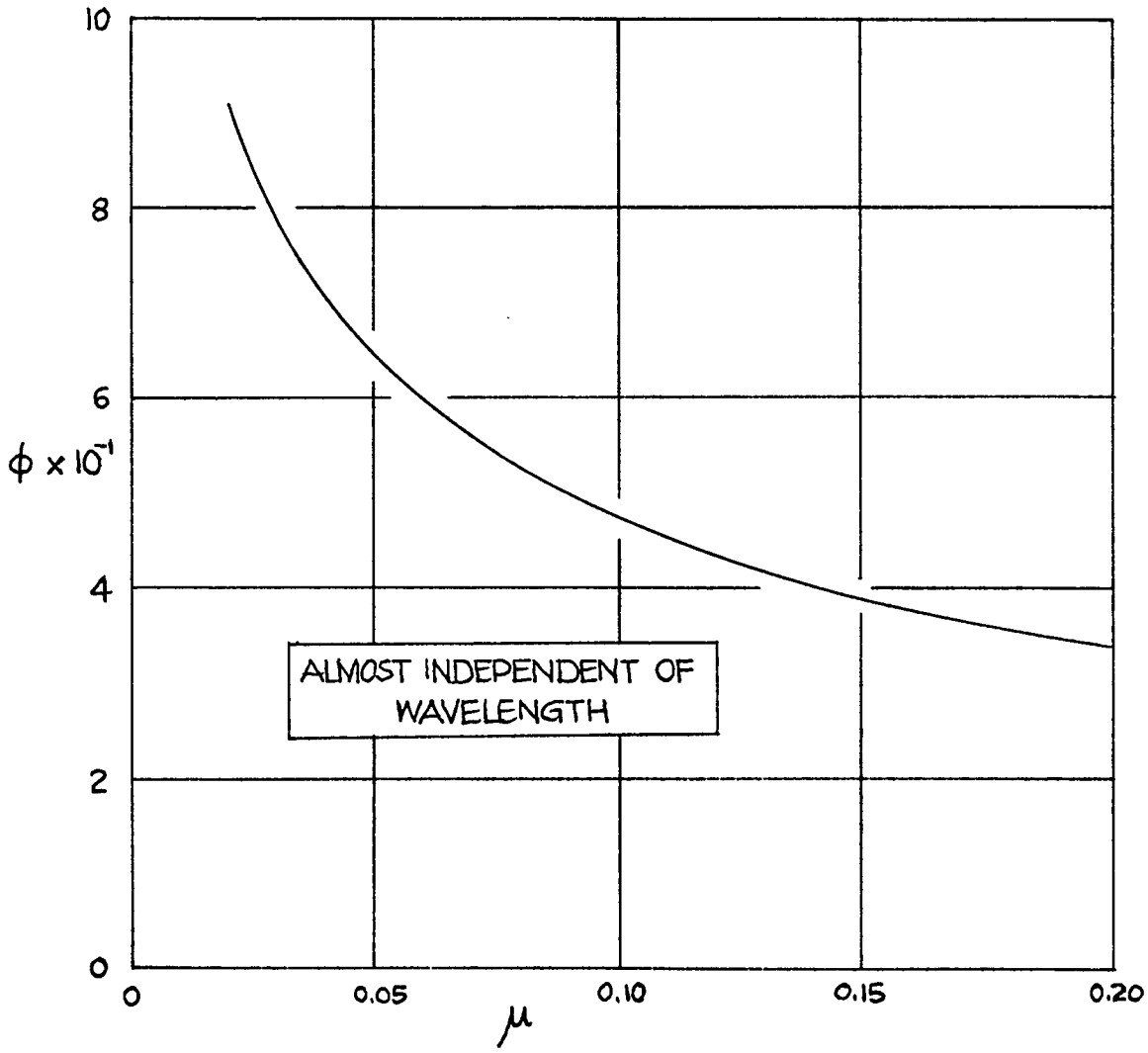

FIGURE 7: FLAT PLATE BUBBLING MODE

MASS RATIO FREQUENCY CORRECTION

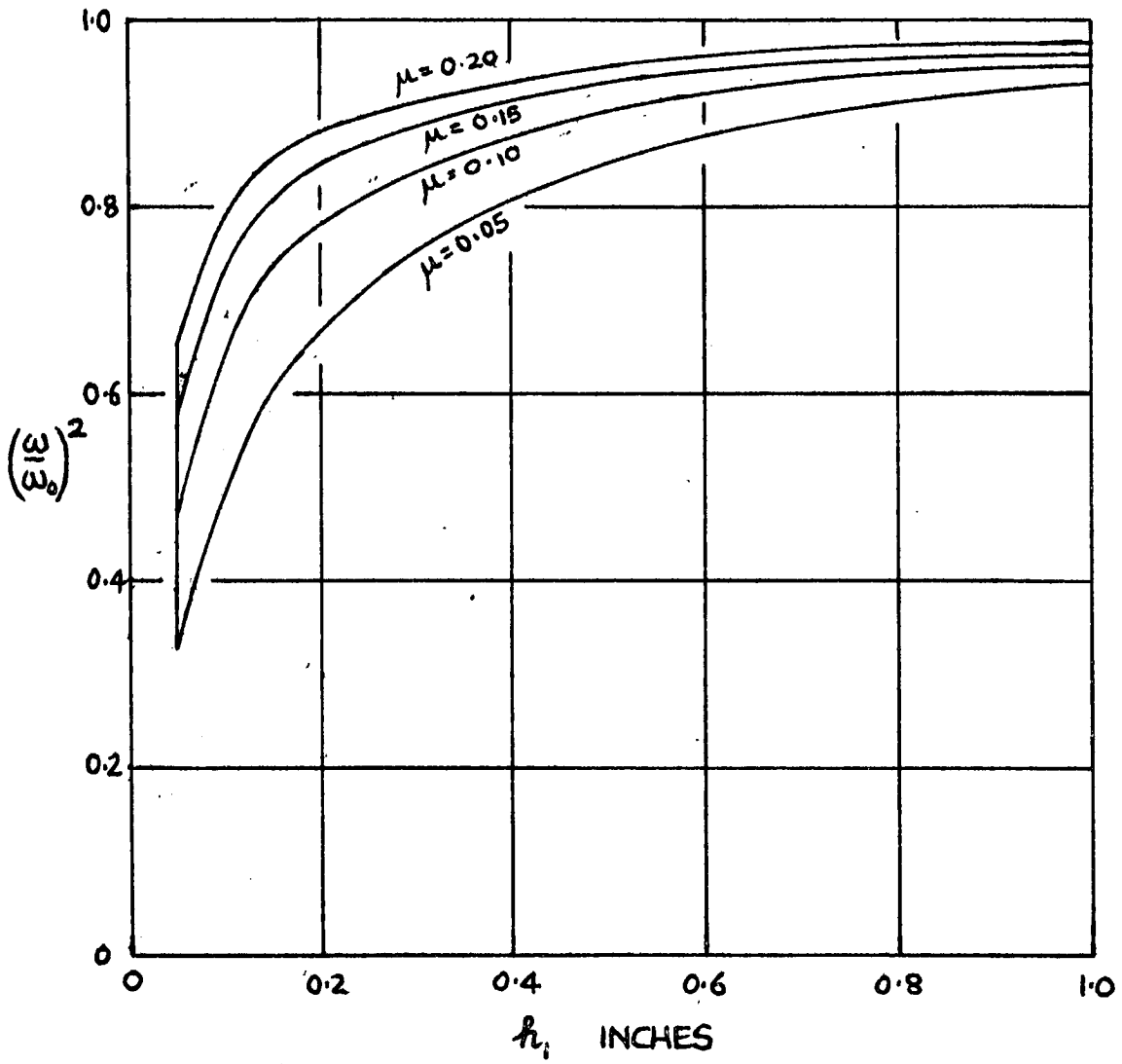

FIGURE 8A: FLAT PLATE FLEXURAL MODE FREQUENCIES WITH INCIDENCE ANGLES FOR THE COINCIDENCE EFFECT; $\mu = 0.05$

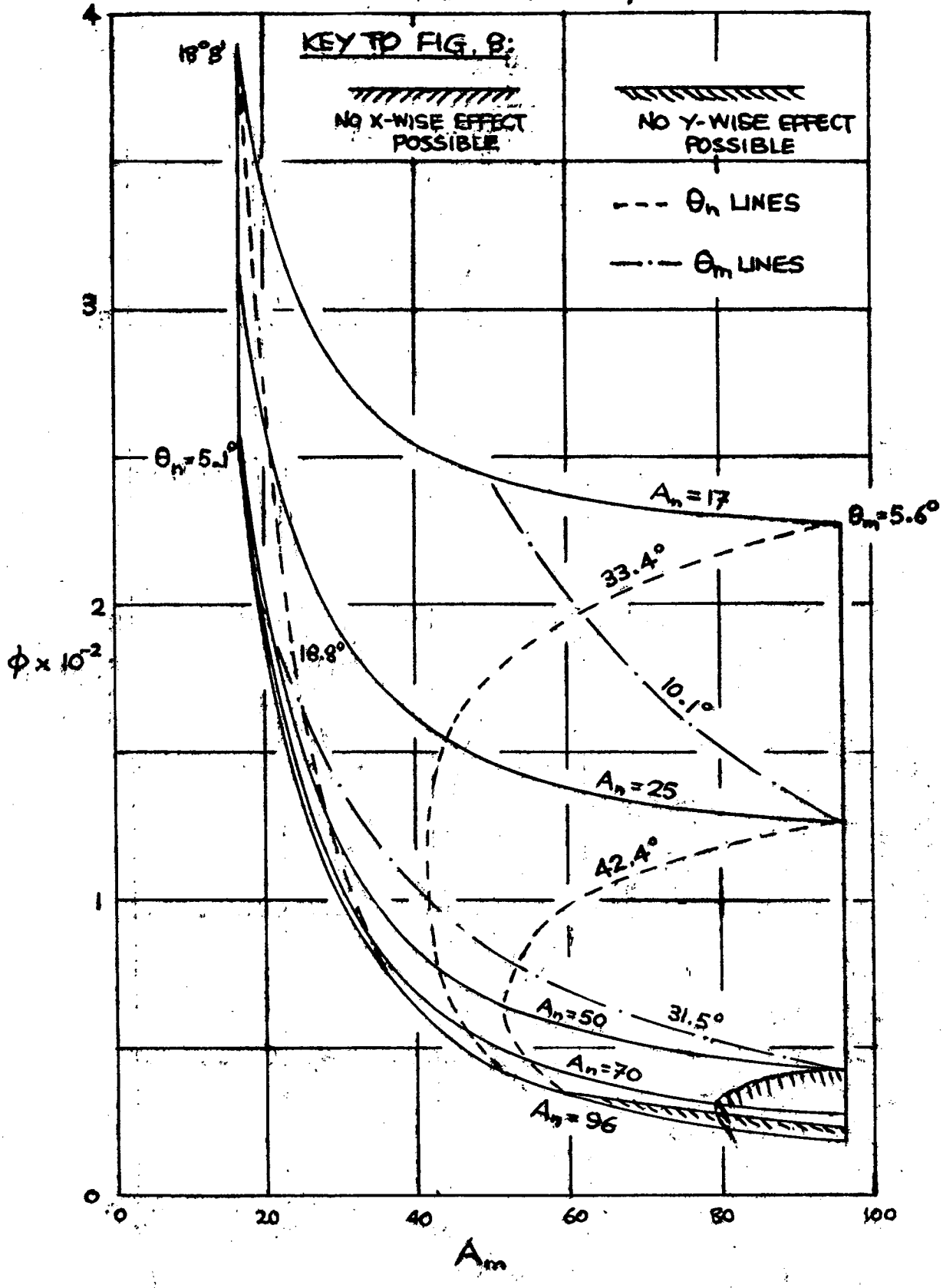

FIG 88 : FLAT PLATE FLEXURAL MODE FREQUENCIES WITH INCIDENCE ANGLES FOR THE COINCIDENCE EFFECT : $\mu = 0.10$.

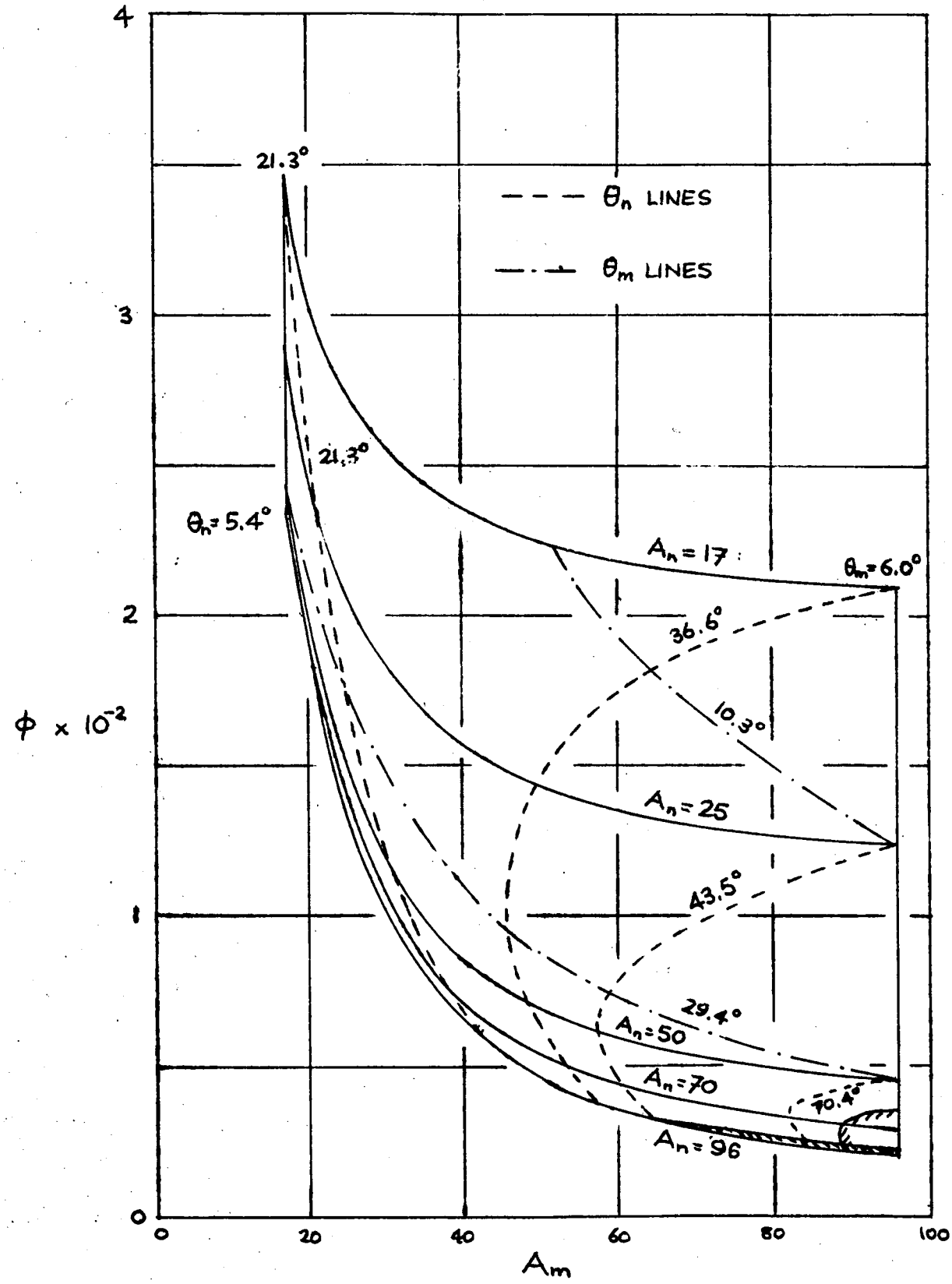

FIGURE 8C : FLAT PLATE FLEXURAL MODE FREQUENCIES WITH INCIDENCE ANGLE FOR THE COINCIDENCE EFFECT : $\mu = 0.3$

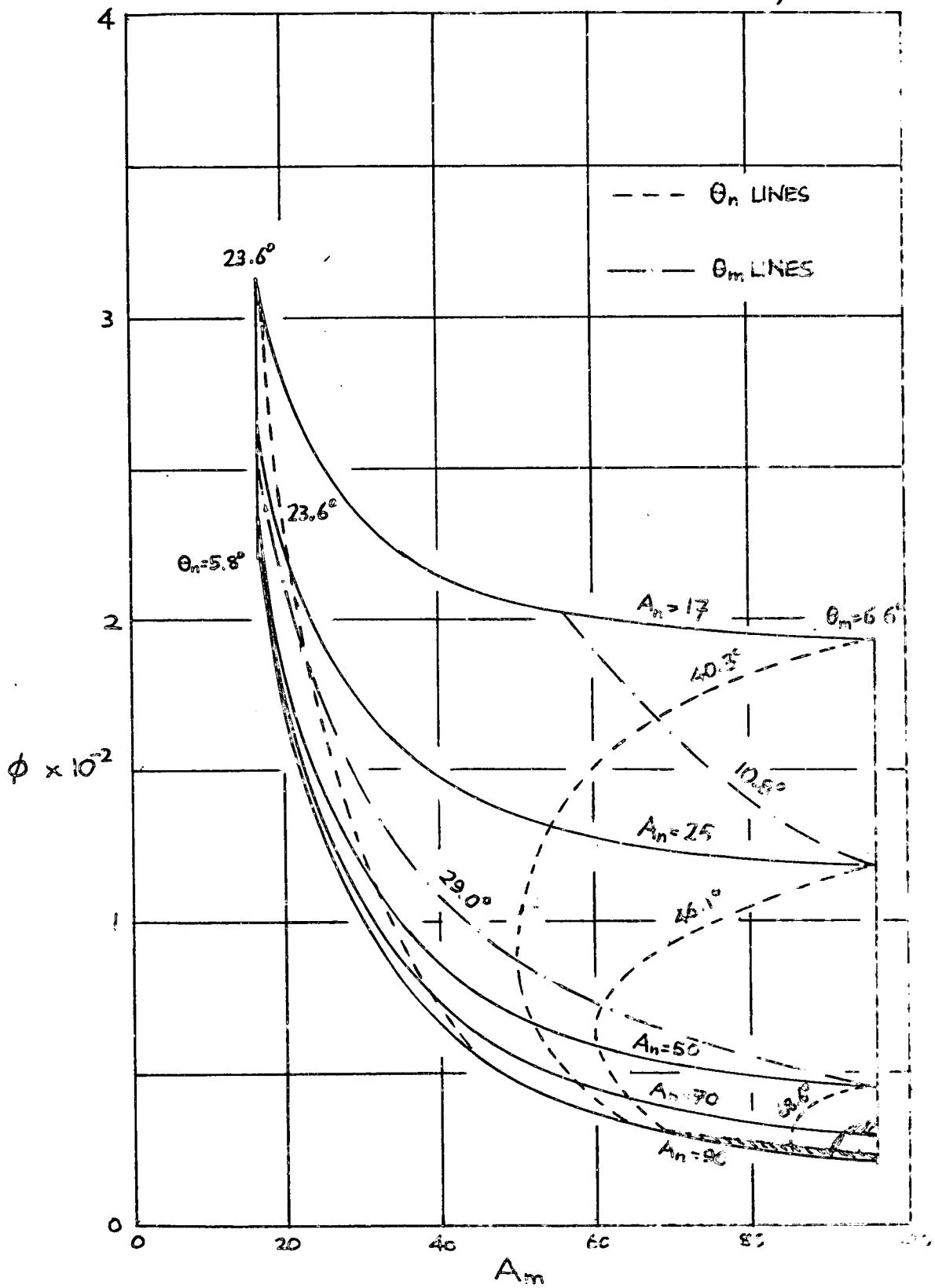

FIGURE 8D: FLAT PLATE FLEXURAL MODE FREQUENCIES WITH INCIDENCE ANGLE FOR THE COINCIDENCE EFFECT : $\mu = 0.20$

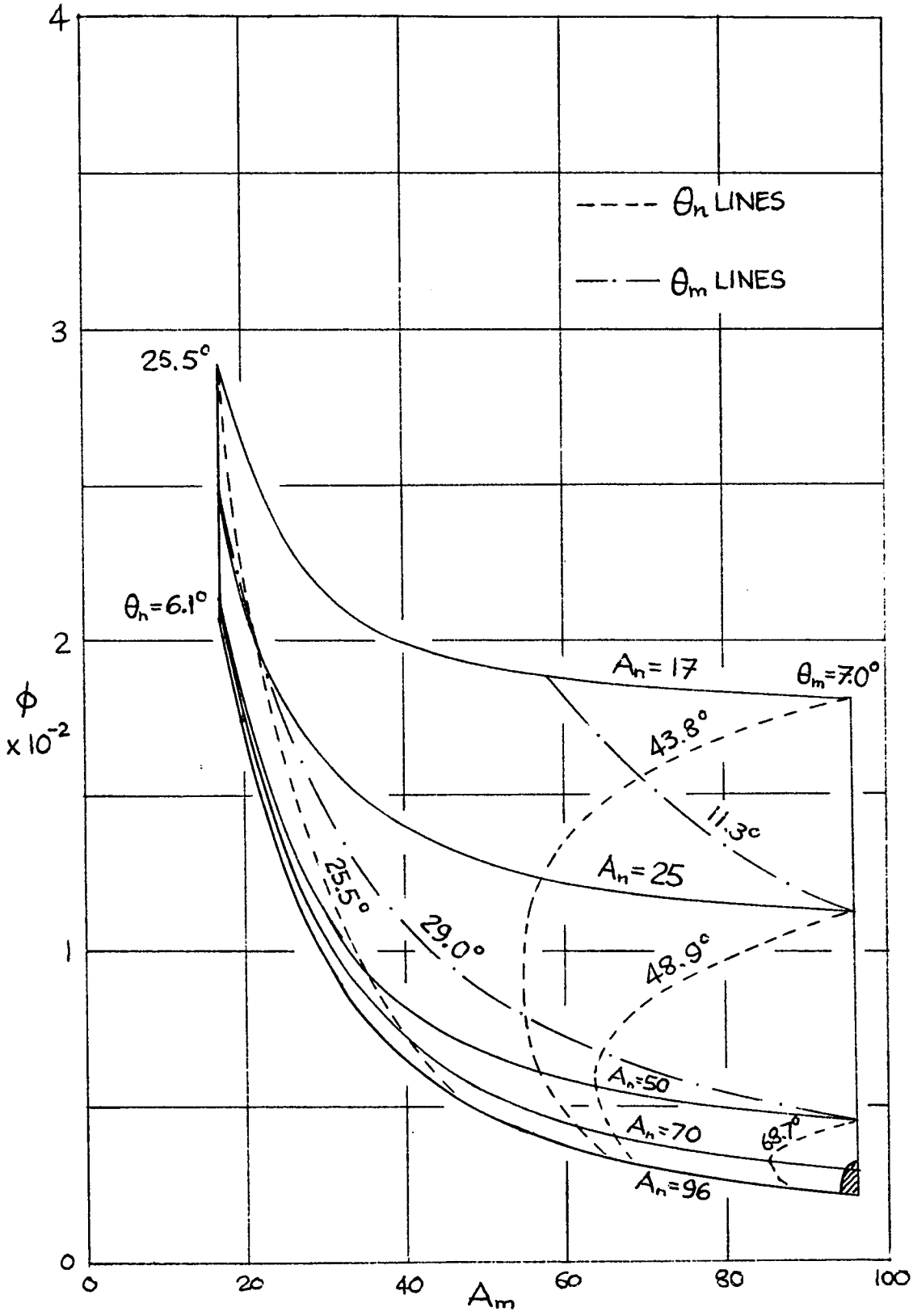

FIGURE 9 : CURVED PLATE FLEXURAL MODE FREQUENCIES vs. CIRCUMFERENTIAL WAVELENGTH : $\mu = 0.05$, $\hat{f} = 0.020$.

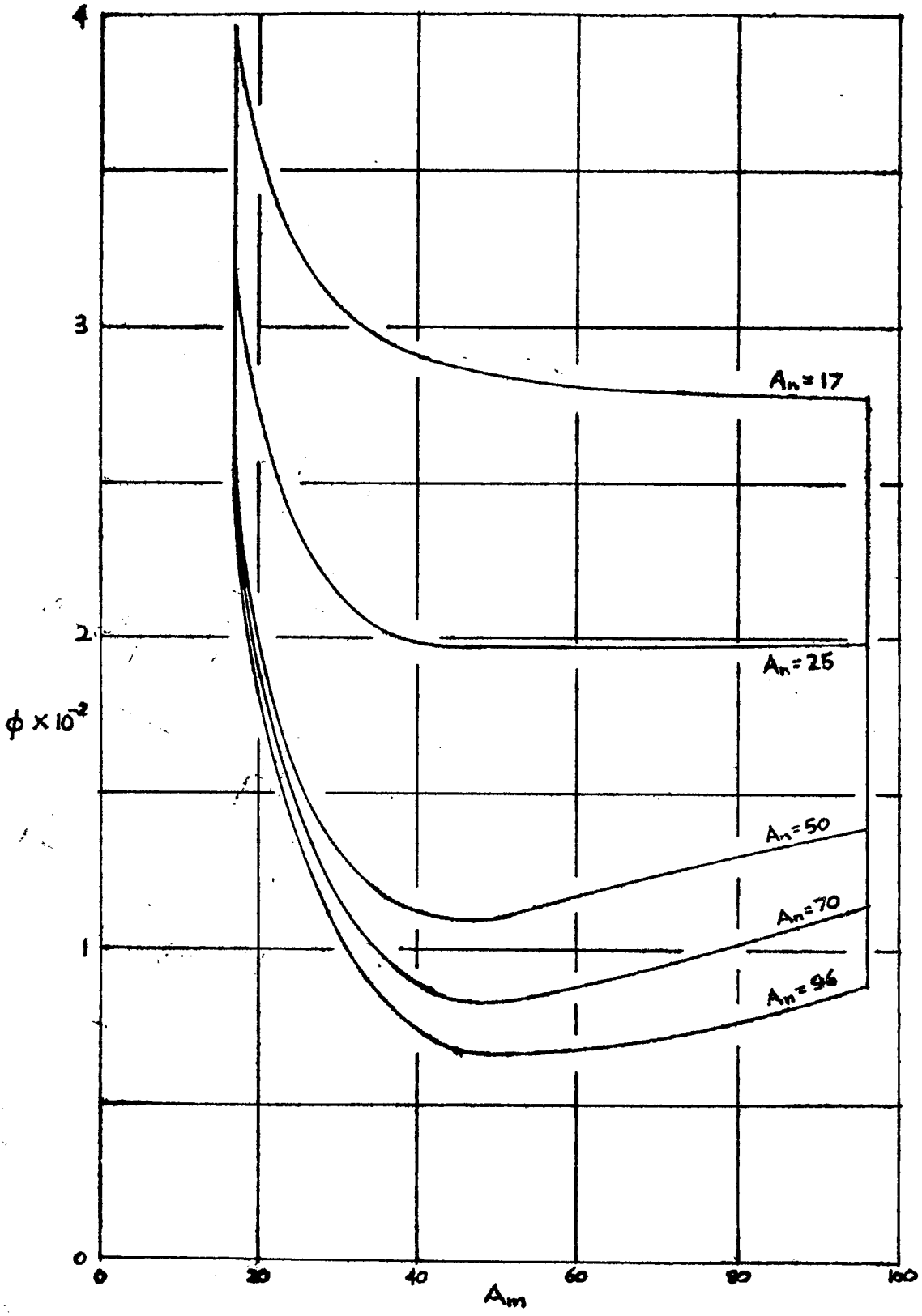

FIGURE 10: CURVED PLATE FLEXURAL MODE FREQUENCIES vs AXIAL WAVELENGTH : $\mu = 0.05$, $\hat{f} = 0.020$.

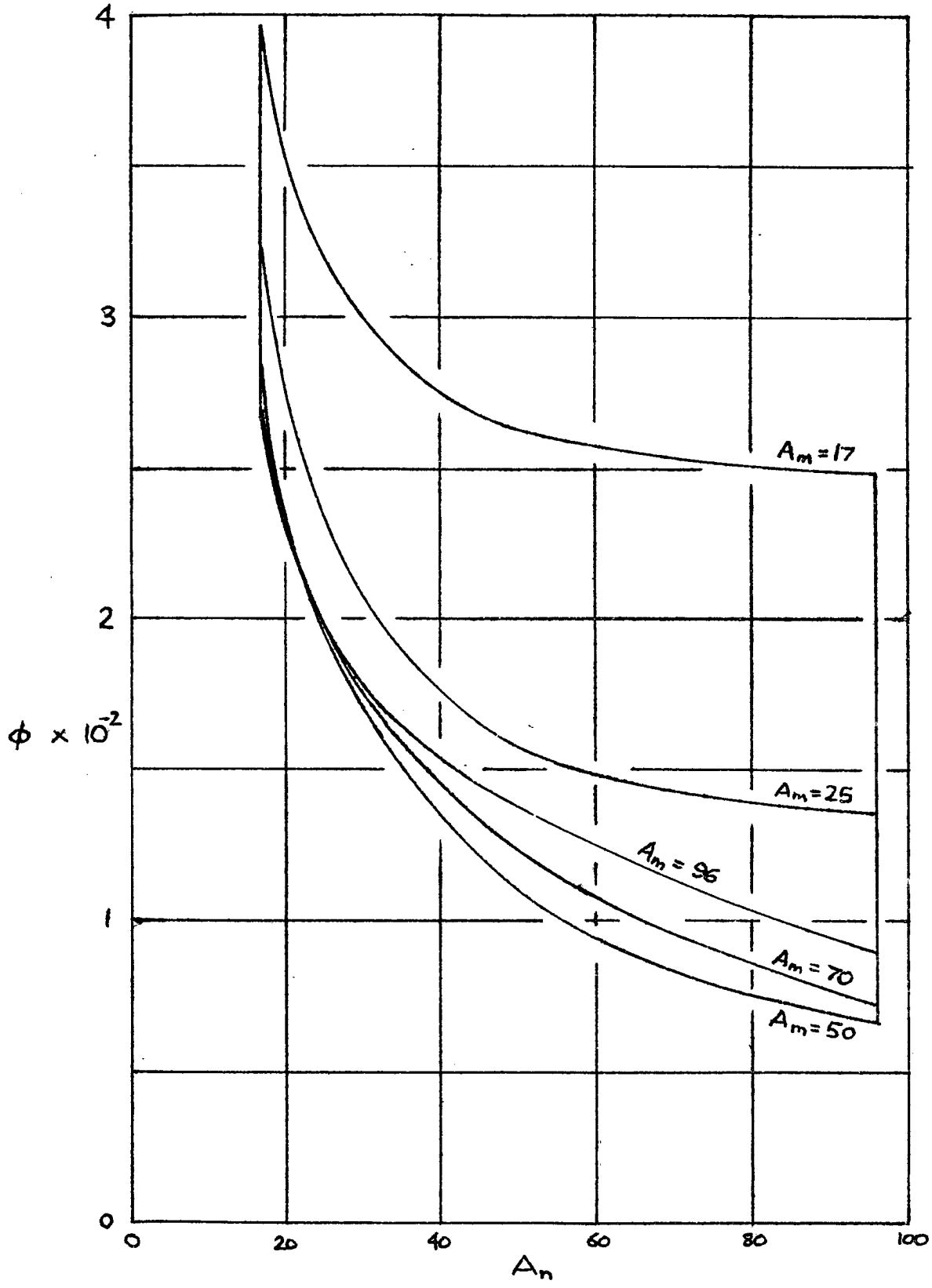

FIGURE 11 : CURVED PLATE FLEXURAL MODE FREQUENCIES vs μ : $\hat{\Phi} = 0.020$

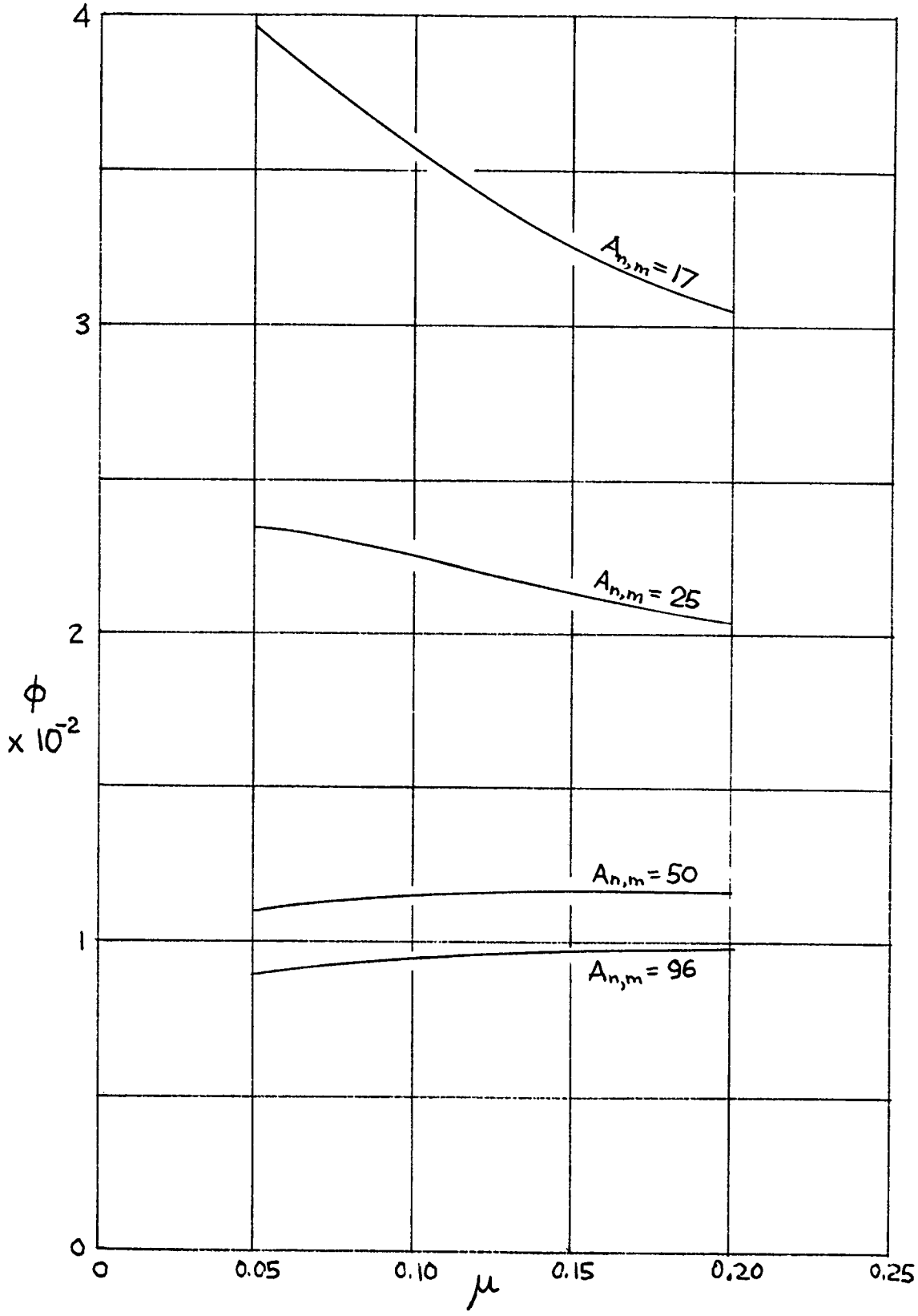

FIGURE 12: CURVED PLATE FLEXURAL MODE FREQUENCIES vs. CURVATURE ($\hat{f}$): $\mu = 0.05$.

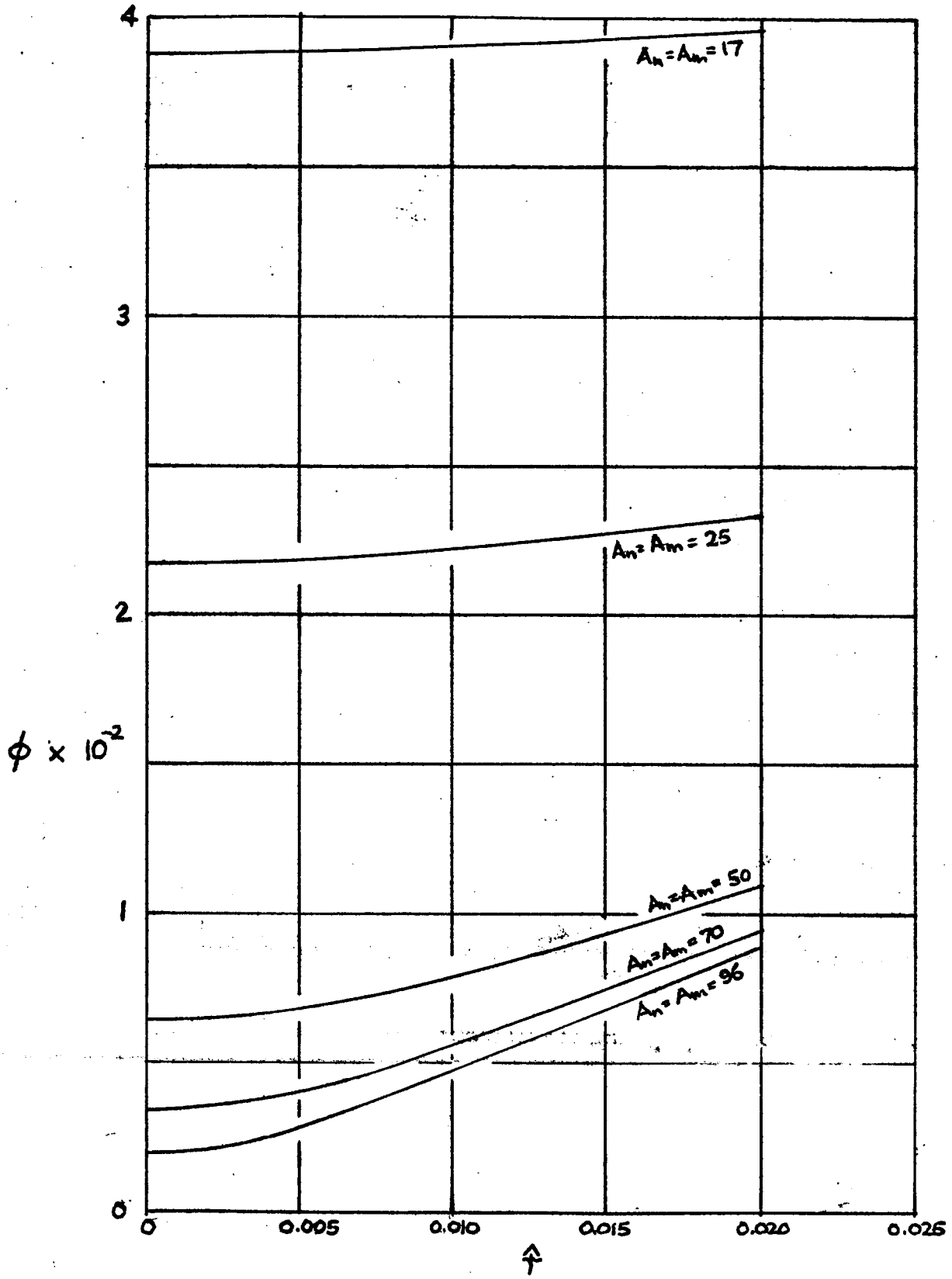

FIGURE 13: CURVED PLATE BUBBLING MODE FREQUENCIES vs. μ. (ALMOST INDEPENDENT OF WAVELENGTH & $\hat{\gamma}$)

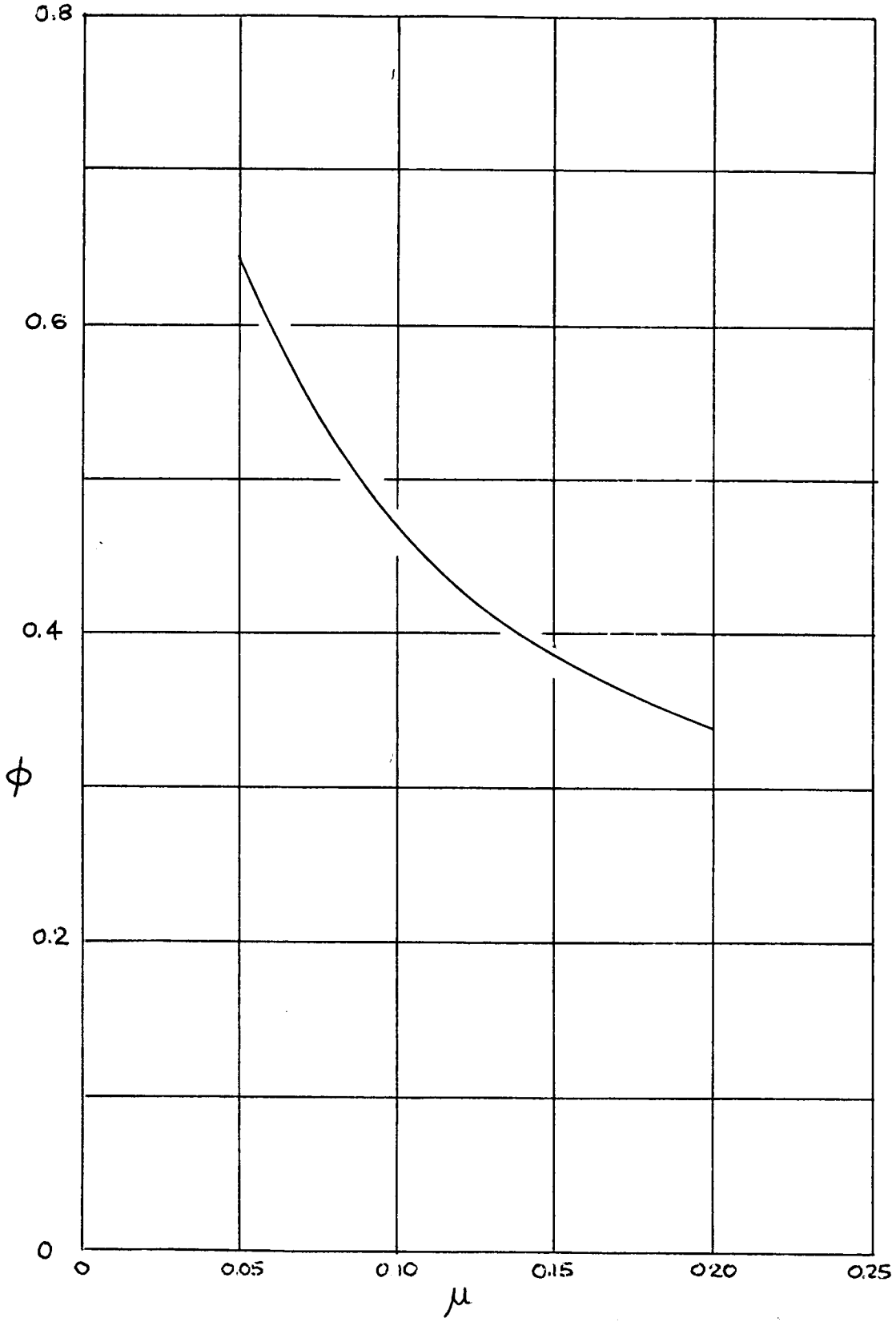

FIGURE 14: PARAMETER $\phi(\omega)$ vs FREQUENCY; FOR ROLLS-ROYCE AVON R.A.26 WITH 20.8" DIA. CONICAL NOZZLE (AFTER REF. 21).

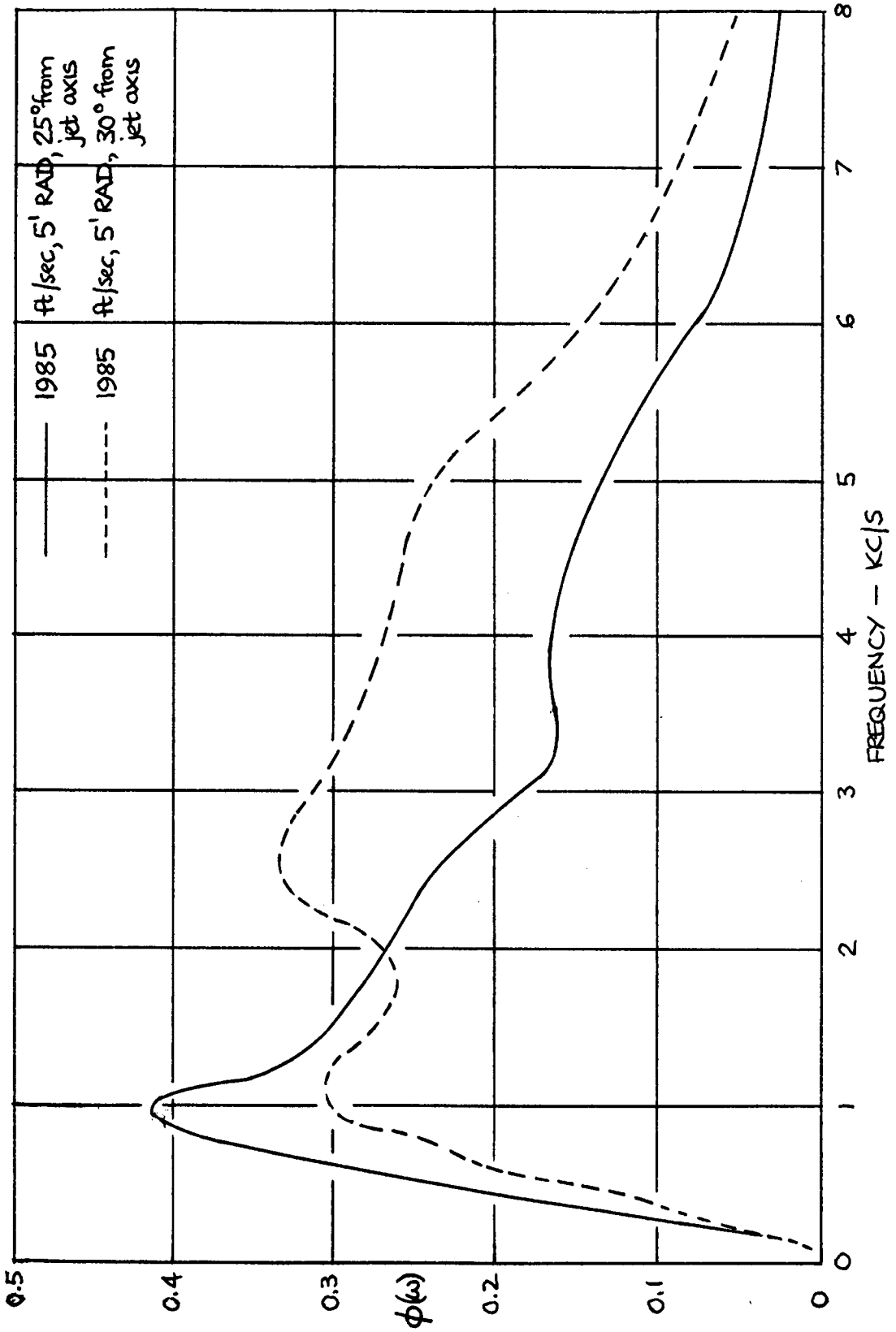

FIGURE 15: JOINT MAGNIFICATION FACTOR L_5 VS λ_m/λ_T

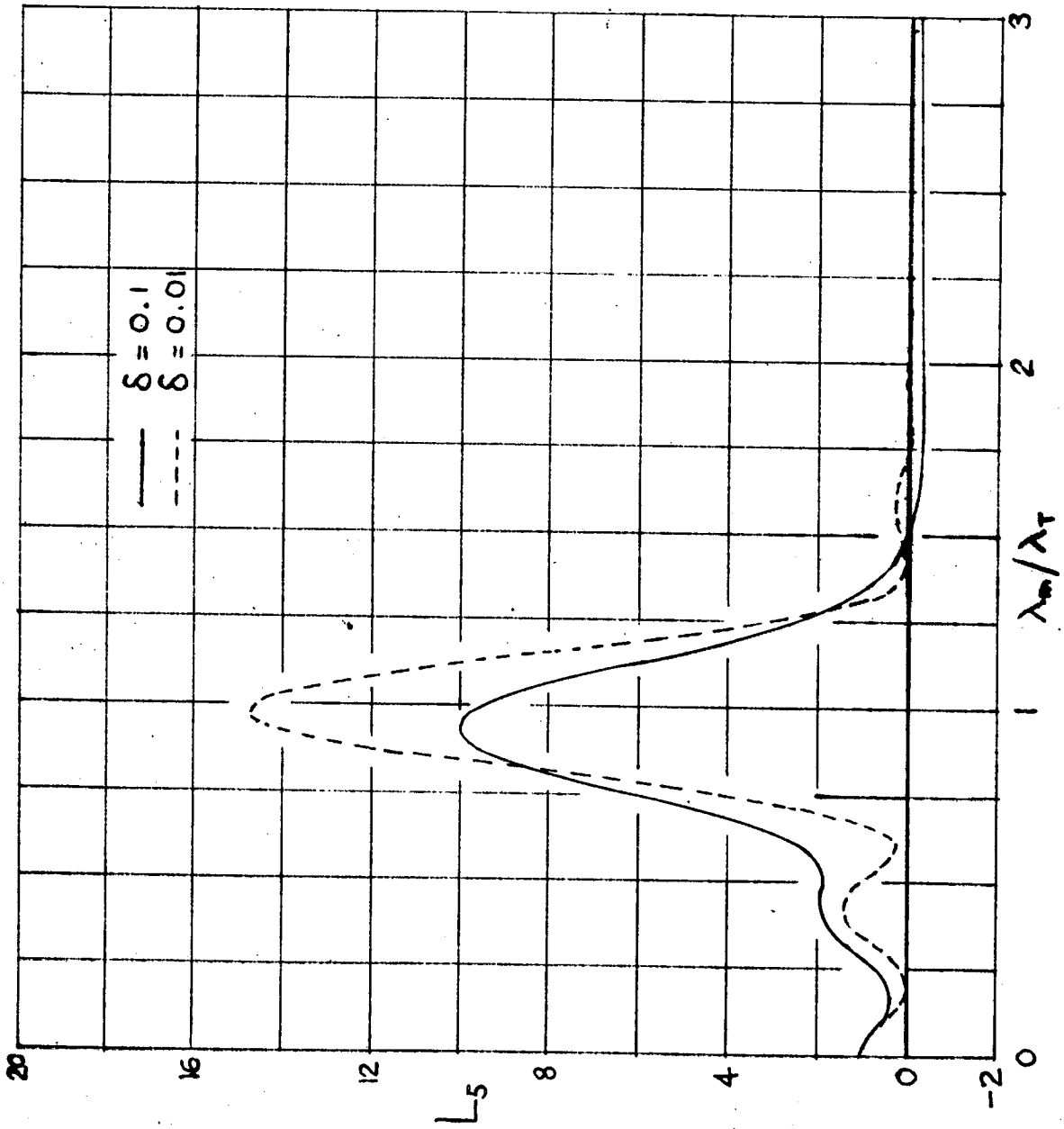

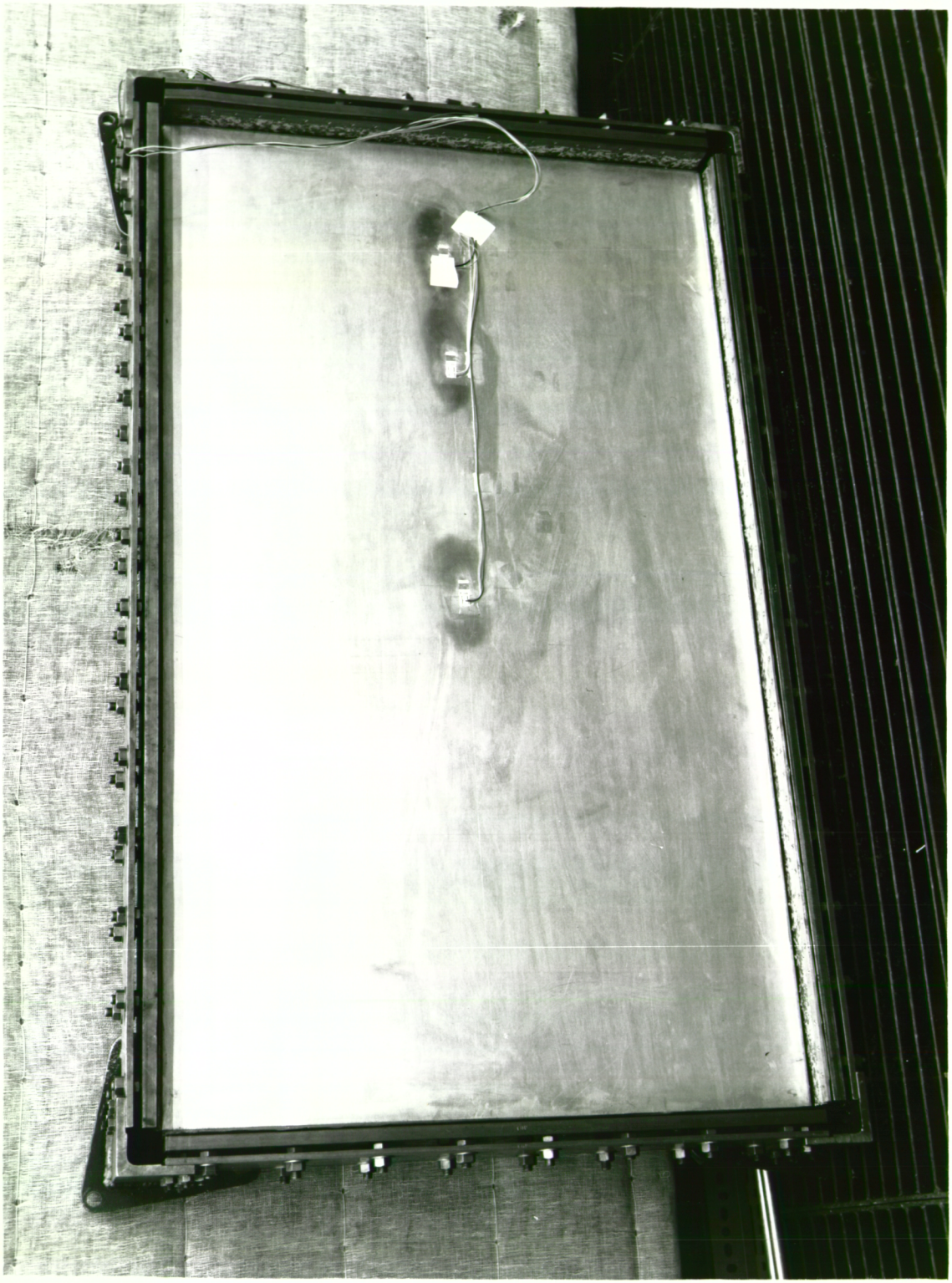

FIGURE 16 : PHOTOGRAPH OF THE SANDWICH PANEL OF CHAPTER THREE SHOWING THE STRAIN GAUGES.

FIGURE 17 :

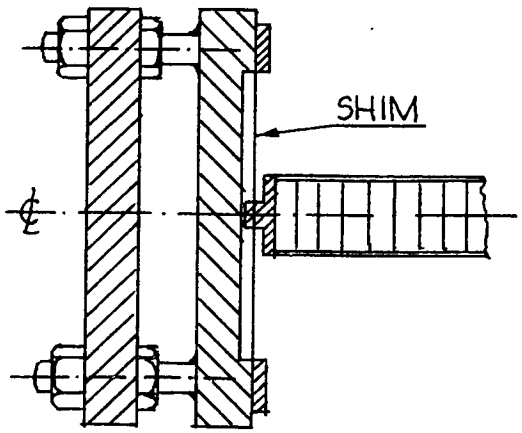

SKETCH OF PANEL SUPPORT SYSTEM

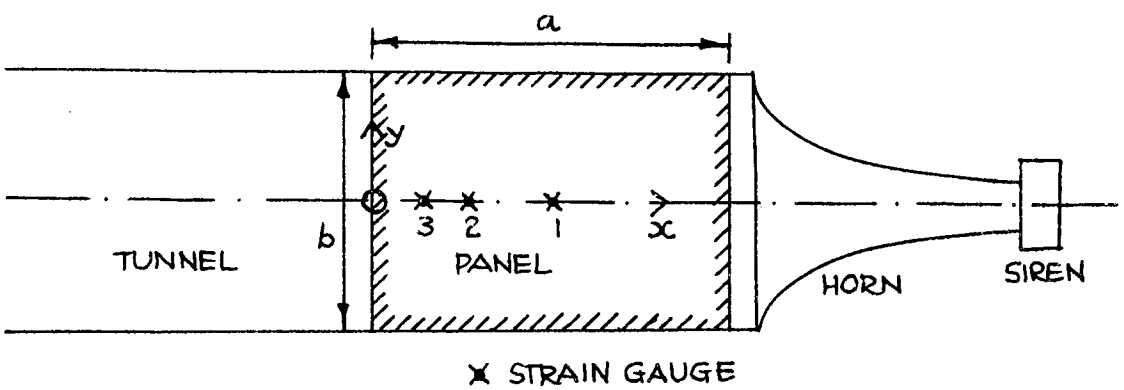

SKETCH OF THE SANDWICH PANEL IN THE SIREN TUNNEL SHOWING AXIS SYSTEM AND STRAIN GAUGE POSITIONS

FIGURE 18: HARMONIC RESPONSE CURVE FOR STRAIN GAUGE 3 AT AN INPUT PRESSURE INTENSITY OF 133.5 dB.

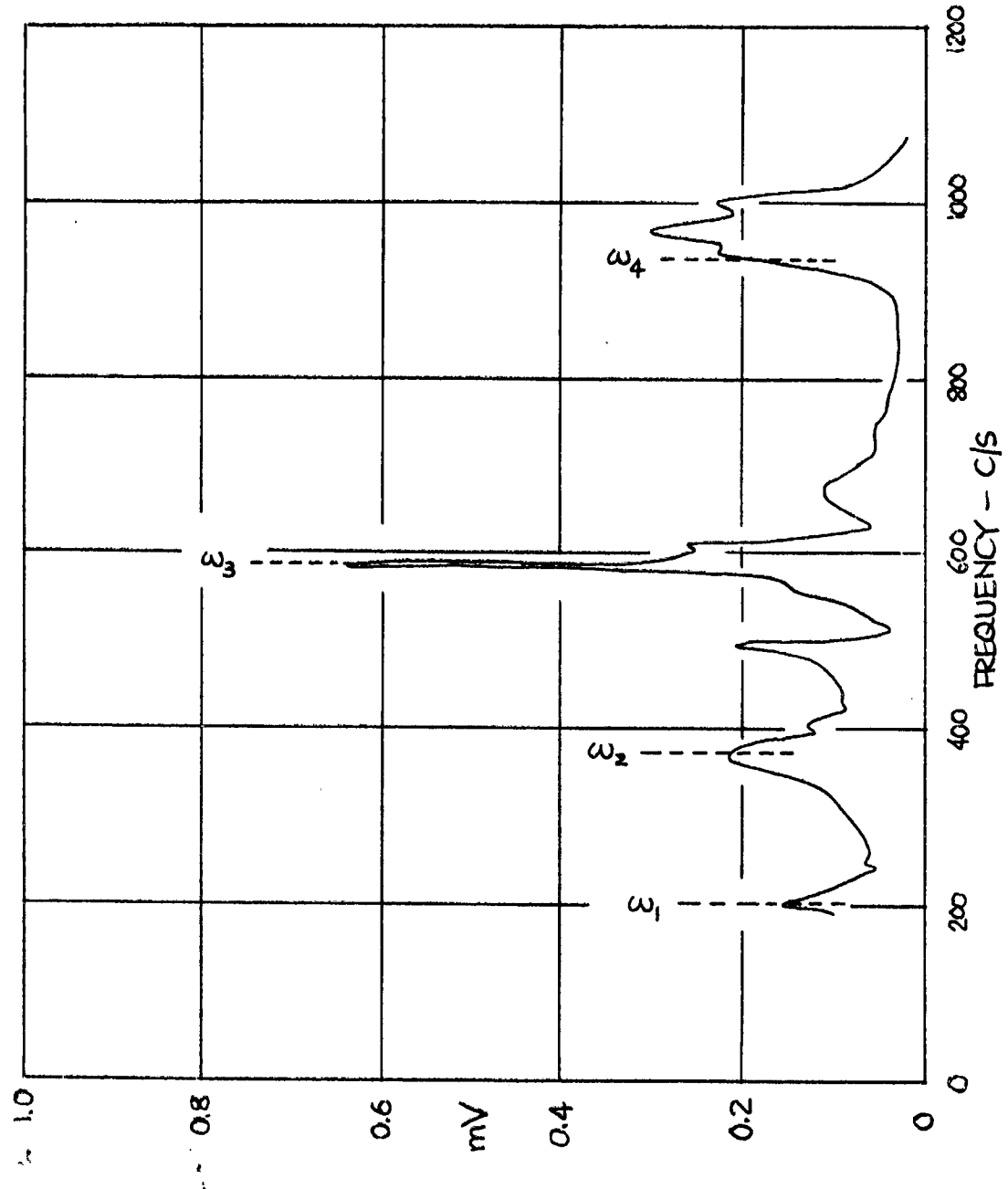

FIGURE 19: PHASE DIAGRAM OF THE RESPONSE OF STRAIN GAUGE 3 IN THE REGION OF THE FOURTH NATURAL FREQUENCY (937 C/S).

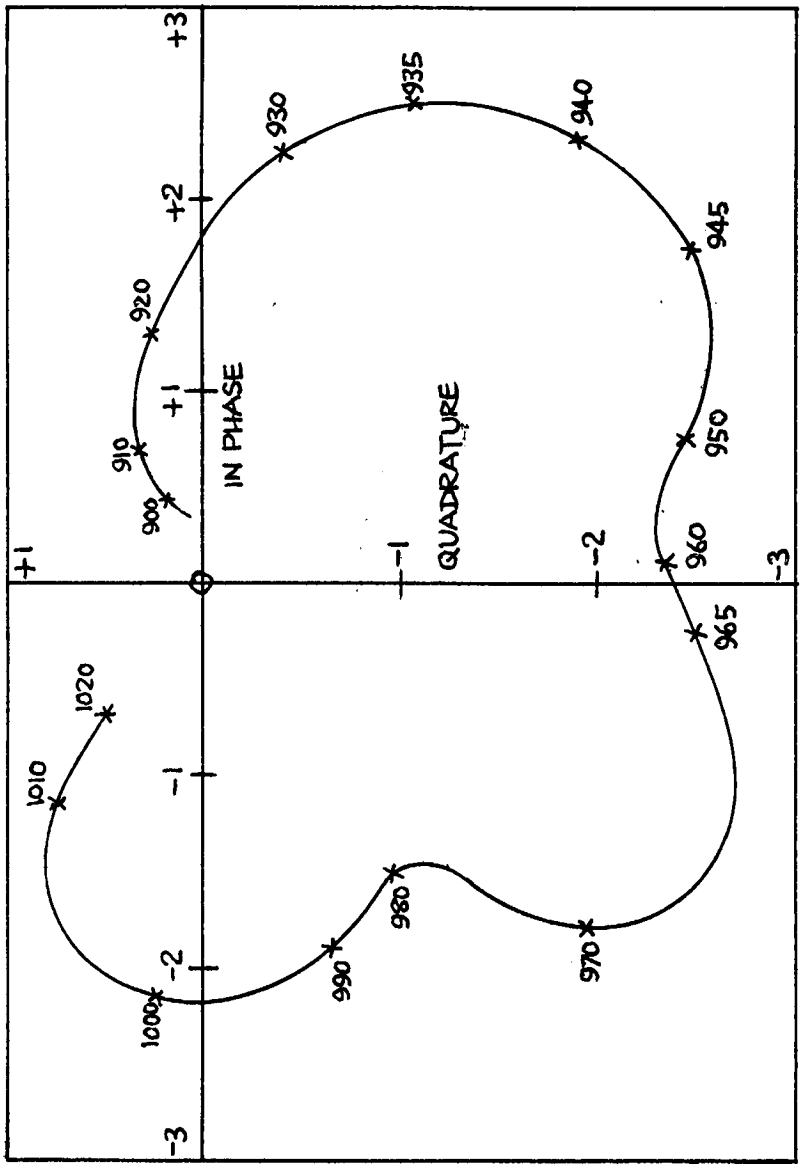

FIGURE 20: A MORE DETAILED PHASE DIAGRAM, AS FIG. 19, SHOWING THE DERIVATION OF ω_4 AND δ_4.

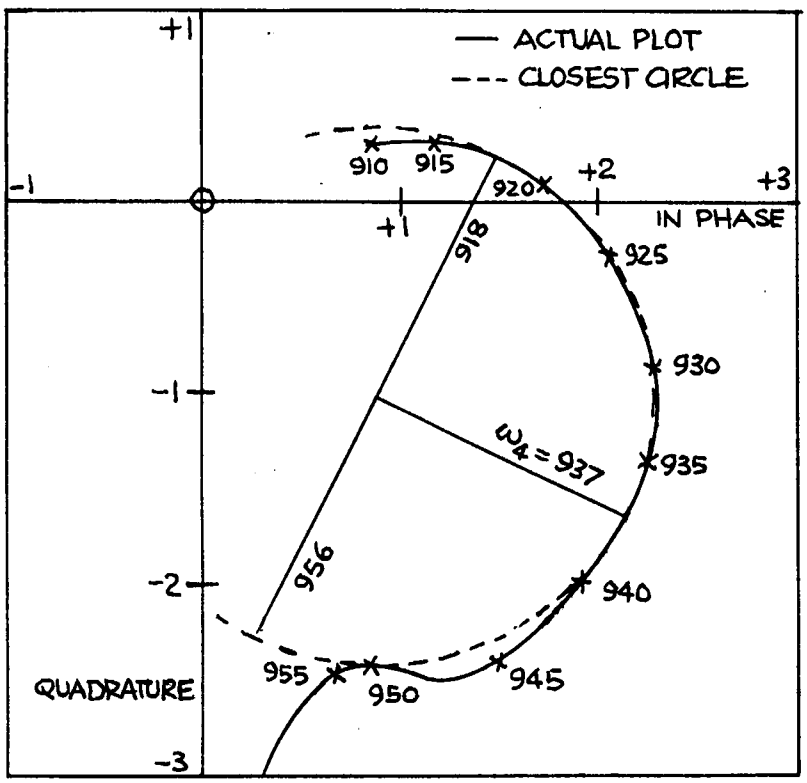

$$2\delta\omega_n = 956 - 918$$

$$\delta_4 = 0.020$$

FIGURE 21 : A SKETCH OF THE EXPERIMENTAL SANDWICH VIEWED FROM ABOVE.

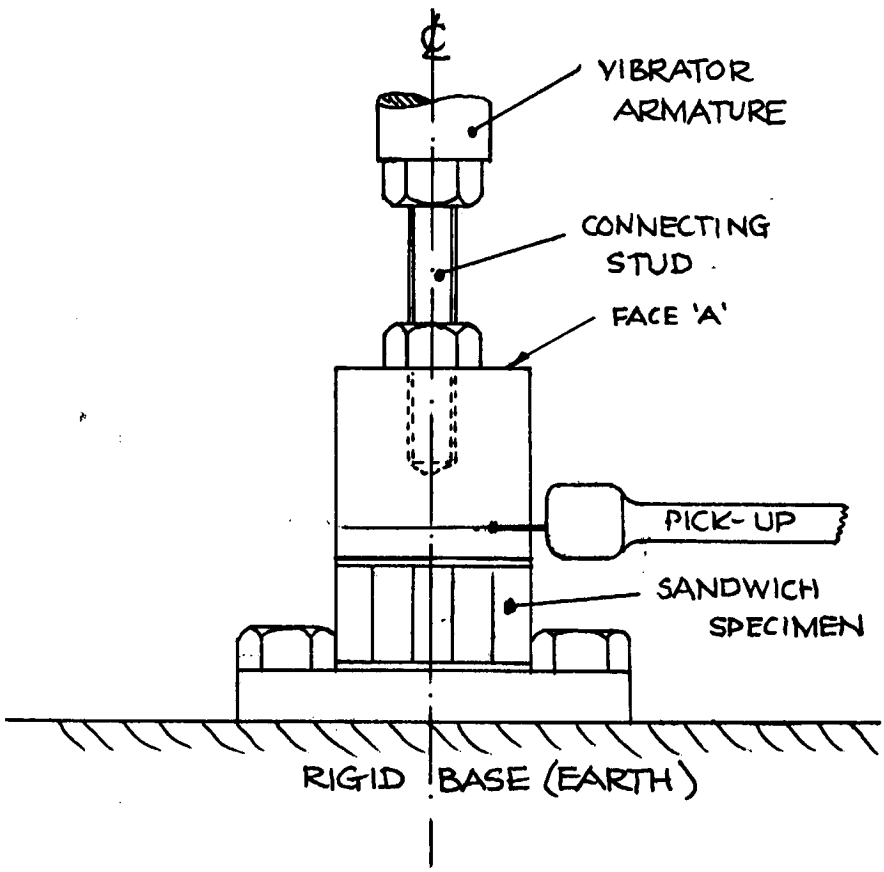

Figure 22 Photographs of typical bond failures and of the strain-gauged specimen

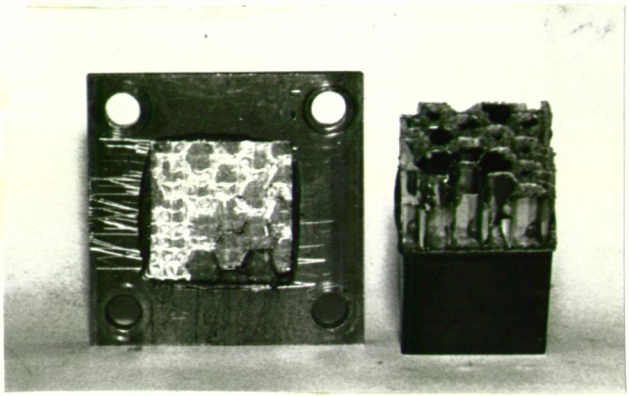

1. Earth side bond failure

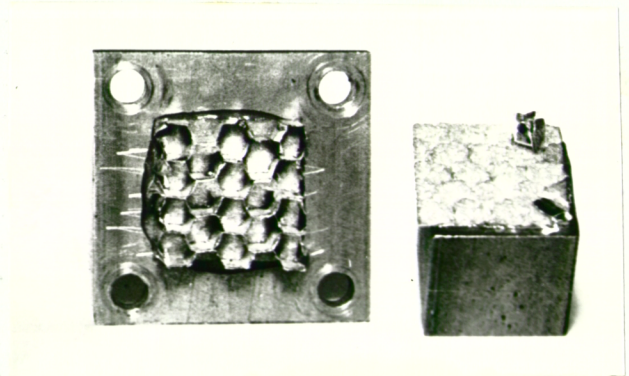

2. Exciter side bond failure

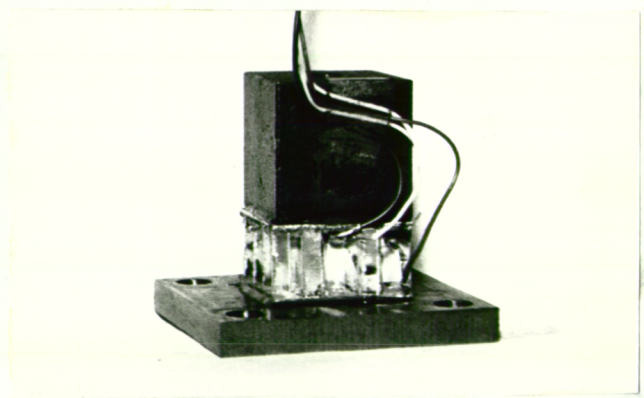

3. Strain-gauged specimen

FIGURE 23 : THE CALIBRATION OF THE GRAMOPHONE PICK-UP. CORE STRESS PER VOLT vs. FREQUENCY

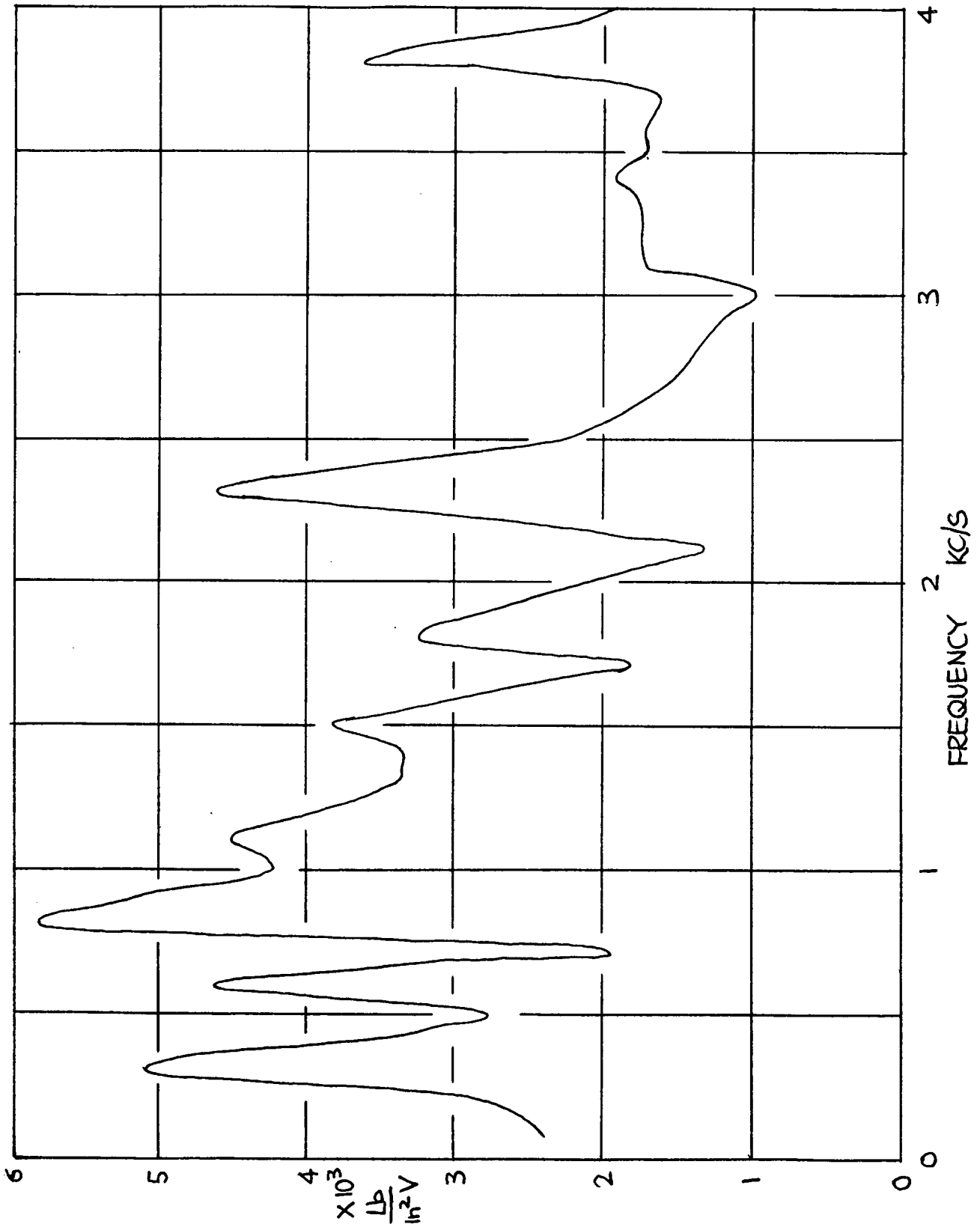

FIGURE 24: AN S-n CURVE FOR THE UNIAXIAL FATIGUE OF HONEYCOMB SANDWICH BOND TYPE REDUX 775R.